Constitutive Model for Rubber like Materials

A THESIS

submitted by

Maboo Subhani Pathan

for the award of the degree of

Master of Science

(By Research)

Machine Design Section

Department Of Mechanical Engineering

Indian Institute of Technology Madras, Chennai

October, 2008

THESIS CERTIFICATE

This is to certify that the thesis entitled **"CONSTITUTIVE MODEL FOR RUBBER LIKE MATERIALS"** submitted by **MABOO SUBHANI P** to the Indian Institute of Technology Madras, Chennai for the award of the degree of Master of Science (By Research) is a bonafide record of research work carried out by him under our supervision. The contents of this thesis, in full or in parts, have not been submitted and will not be submitted to any other Institute or University for the award of any degree or diploma.

Research Guide

DR. R. KRISHNA KUMAR
Professor & HOD

Department of Engineering Design

Indian Institute of Technology Madras

Chennai – 600 036

India

TABLE OF CONTENTS

ABSTRACT

Constitutive modelling of material plays an important role in the numerical analysis of products. Typical behaviour of rubber is viscoelastic with equilibrium hysteresis. Experimental data of rubber shows the loading and unloading paths are depending upon the maximum strain occurred in history of material, called as Mullins effect. Though, elastomers are capable of stretching to more than 500 %, many applications like tyres require accurate representation at relatively low strains of 50 %. In the present work the existing stored energy functions are evaluated for such strains (<50%). NeoHookean, Mooney-Rivlin, Ogden, Yeoh, Arruda-Boyce and Vander Waals models are evaluated for these strains by using the uniaxial tension and compression data. A new stored energy function is proposed for small strains which is a logarithmic function of first and second invariants. The new stored energy function is compared with the existing models. Uniaxial tension experiments with various strain rates and quasistatic test were carried out to determine the rate dependent and rate independent behaviour of rubber. Finite strain linear and nonlinear viscoelastic models available in the literature have been used to explain the behaviour. It is observed that in Maxwell model, hysteresis increases upto a certain strain rate. Further increase in the strain rate results in decrease of hysteresis. A new formulation for generalized Kelvin model has been developed using the dual variable concept which is consistent with the Second law of thermodynamics. Though, finite strain nonlinear Kelvin and Maxwell models give the same result in loading, they are different during unloading. The results show that the delay in response of dashpot while unloading causes sharp edges in the hysteresis loop.

Chapter1

INTRODUCTION

Mechanical properties of rubber are important designing rubber products. Rubber has good elastic characteristic along with damping properties. To improve the rubber properties filler material such as carbon black, sulpher etc. are added. Rubber withstands for large strain without failure. Typical applications of rubber are tyres, vibration absorbers etc. many applications rubber products will go large strains compression and tension together. Unlike metals, rubber is different mode the properties depends on previous history of material such as time dependent (viscoelastic) and maximum strain undergone so called as Mullins effect (Mullins et al,1957). Typically behaviour of rubber is thermo viscoelastic with equilibrium hysteresis (Lion, 1997) which exhibits stress softening characteristics.

Constitutive modeling of rubber is important to design and development stage of rubber products. It predicts the behaviour of component in application using idealized data such as uniaxial tension and compression. Rubber undergoes large deformations, to predict the elastic behaviour hyperelastic material models are developed, where constitutive equations are derived from stored energy functions (Haupt, 2000). Rate dependent behaviour of rubber is captured using the finite strain viscoelastic material models (Lion, 1996; Lin et al, 2003; Reese and Govindjee, 1998a). Rubber also exhibits the rate independent dissipation which is characterized using endochronic theory of plasticity (Valanis, 1980). Dissipated energy converted into heat it increases the temperature of material, increase temperature degrades the elastic properties of material to predict the behaviour themoelastic material models are available in literature (Reese and Govinjee, 1998b).

1.1. Experimental Work:

This section describes the experimental data considered in this study. The significance of the Mullins effect is demonstrated. Uniaxial tension and compression tests have been conducted on rubber with

different strain rates, relaxation and quasistatic tests. Dumbbell test samples are prepared as per ASTM-D412 standards for tension tests. Button type test sample are prepared for compression. The temperature of 25^0C is maintained through out the testing.

Mechanical properties (stiffness) of filled rubber change drastically during the initial cycles, when material experiencing strain. This behavior is commonly referred to as the Mullin's effect. Specimen is loaded to a particular percentage of strain followed by unloading upto zero stress, and then loaded again, it follows another loading and unloading path, like that it change the loading paths in first few cycles (approximately 8 to 12 cycles) after that, it is stabilize . Once the material stabilized it will not change the loading path below maximum strain where it stabilized. If the specimen is loaded new maximum percentage of strain above the previous maximum strain, it again change the loading graph, if loaded repeatedly it stabilizes to another loading path. So stress-strain relation of rubber depends upon the maximum strain undergone in previous history of the material.

In order to stabilize the material, first twelve strain controlled loading and unloading cycles are given continuously to stabilize the material behaviour. After this process one hour relaxation time is allowed to remove the rate dependent hysteresis. Then the test is conducted at a strain rate of 0.00066 sec^{-1} (Lion, 1996). Fig.1.1 shows the loading and unloading graph of the stress softened to different percentage of strains (i.e. 50%, 120%, 200%, and 300%). It can be seen that the reduction of stiffness of the material is a function of the maximum strain at which stress softening occurred. The same kind of behavior is observed in literature (Kurt Miller, 2000).

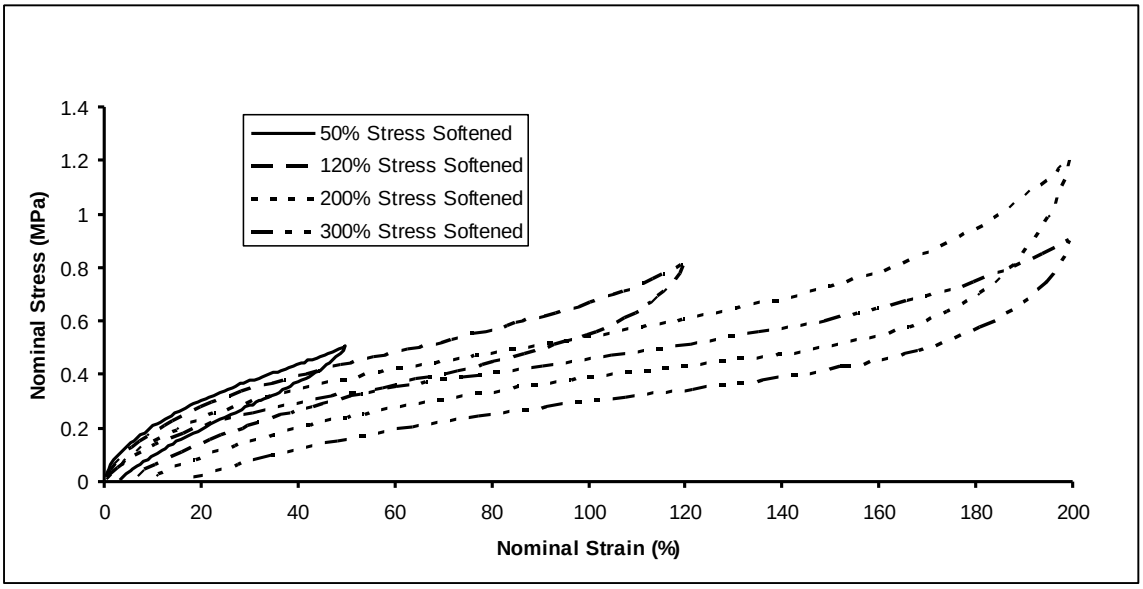

Fig.1.1. Variation in loading and unloading of stress softened upto 50%, 120%, 200% and 300% percentage of strain.

Many applications such as tyre, rubber may not undergo large strains, one may interest to do experiments upto 40-50% of strain to predict the constitutive models. This study considers maximum 50% strain tension and 30% of in compression. Once Mullins effect removed upto 50% of strains and kept the samples one hour to relax the material and test conducted different strain rates 0.00066, 0.0066, 0.066 and 0.155 sec^{-1} (which is equal to 4%/min, 40%/min, 400%/min, 1000%/min). Note that each strain rate new sample has been used. Experimental results are shown in fig.1.2 it can be observed that with strain rate increases stress are increasing. If calculate the area under loading and unloading curves each strain rate, it can be observed that it is increasing with strain rate shown in fig.1.3.similar kind of behaviour observed in Dalrymple et.al (2007).

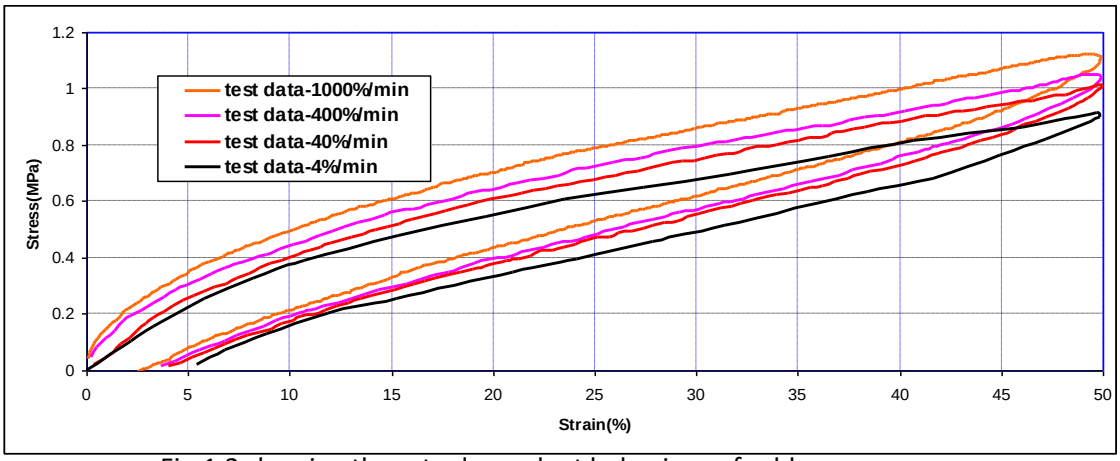

Fig.1.2 showing the rate dependent behaviour of rubber

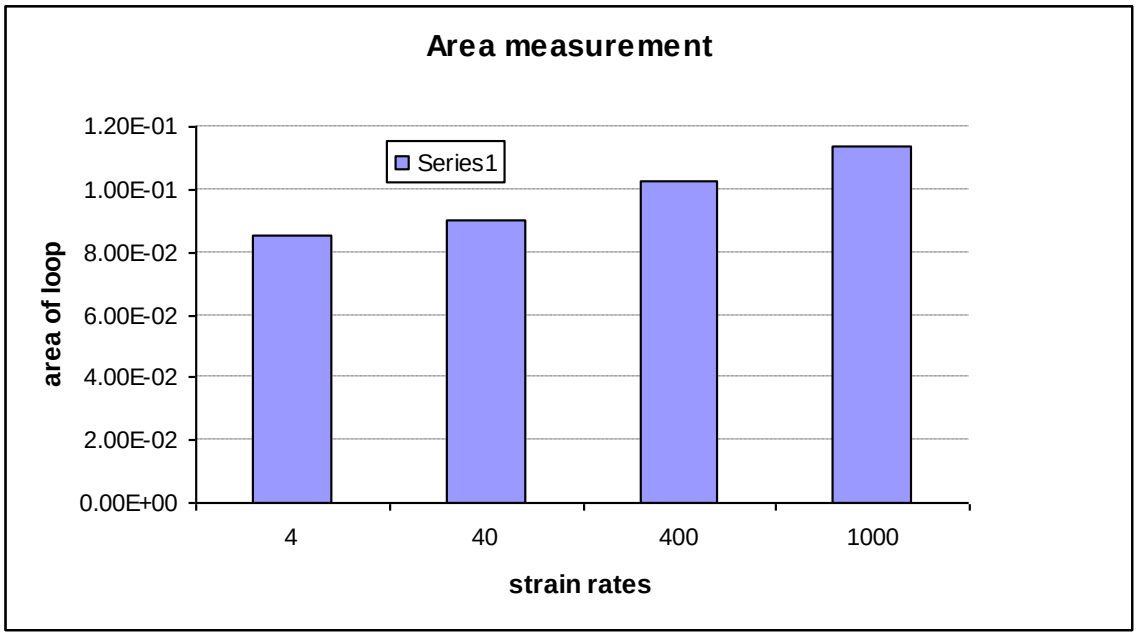

Fig.1.3 shows area increases with strain rate

Compression test has been conducted with the same material. Similar procedure has been followed. Button type sample is of 29 mm diameter and 13mm thickness used. Silicone lubricant used to reduce the friction effect. Mullins effect is removed upto 35% of nominal strain. Test is conducted different strain rates of 0.00066, 0.0066, 0.066, and 0.155 sec^{-1} upto 30% of nominal strain. Test results are shown in fig.1.4

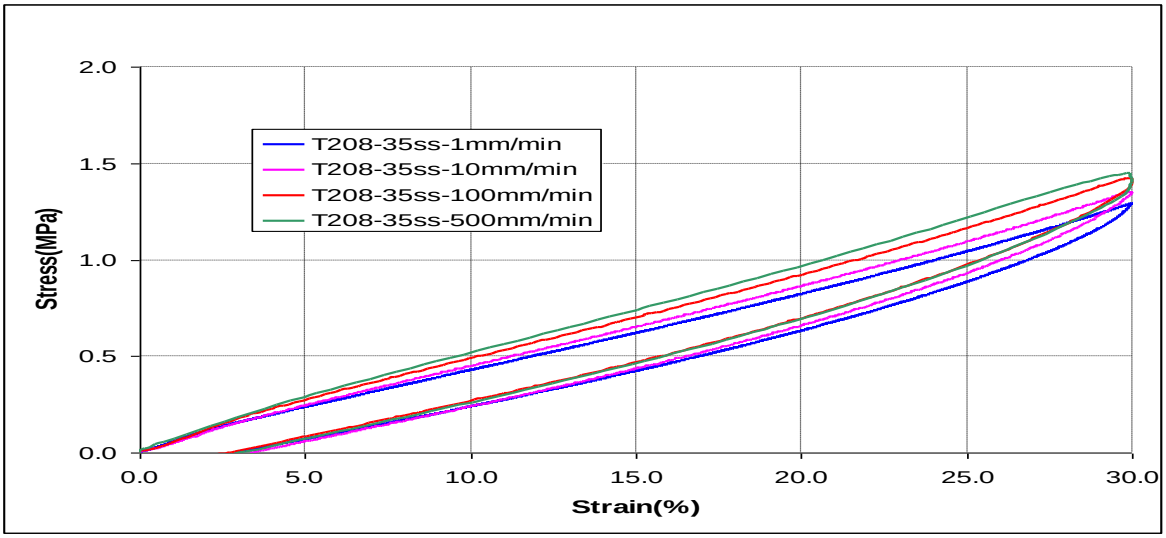

Fig.1.4. shows strain rate dependent behaviour in compression

1.2. Quasistatic test:

Rate independent hysteresis can be captured by quasistastic test. After removing the Mullins effect, stepped strain in loading and unloading given as input to specimen is shown in fig.1.5, 1.6 respectively. Relaxation kept one hour for each step. Fig.1.7, 1.8 is the response is measured force versus time in loading and in unloading . It can be observed from fig.1.7,.18 that stress is dropping exponentially and material is completely relaxed at 60 min (1hour).once material is relaxed the time dependent stresses are disappear, the stress at which material is relaxed is summation elastic and plastic (rate independent hysteresis) behaviour. To get the rate independent hysteresis, force is measured each step at end of relaxation time and converted into nominal stress versus nominal strain plotted in fig.1.9 along with different strain rates. Loading path of quasistatic result is used to fit the hyperelastic material models. Fig.1.10 shows the area under each loading and unloading path. It is clear that hysteresis increases with stain rate and even at quasistatic test, material has the hysteresis with is called as equilibrium hysteresis (Haupt ,2000)

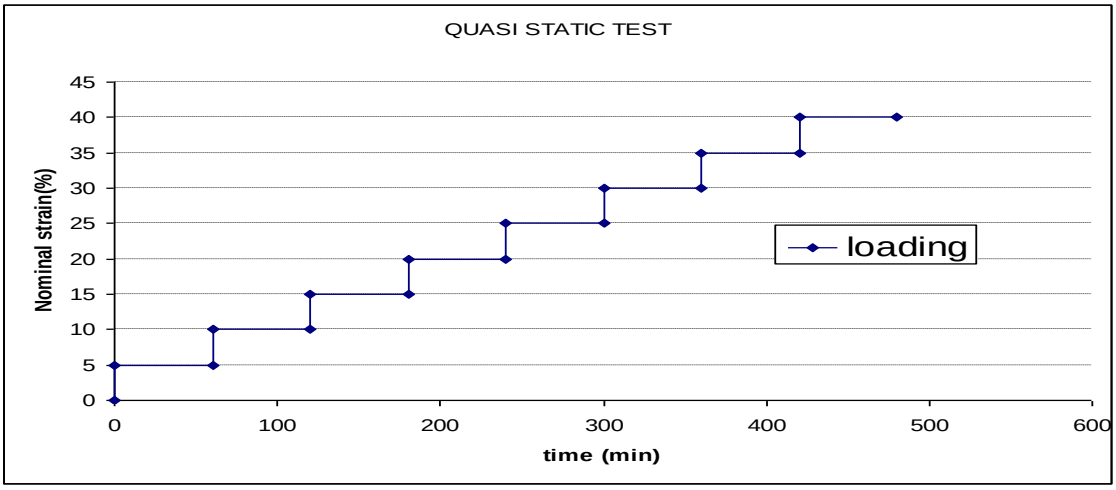

Fig.1.5.strain input to the quasistatic test

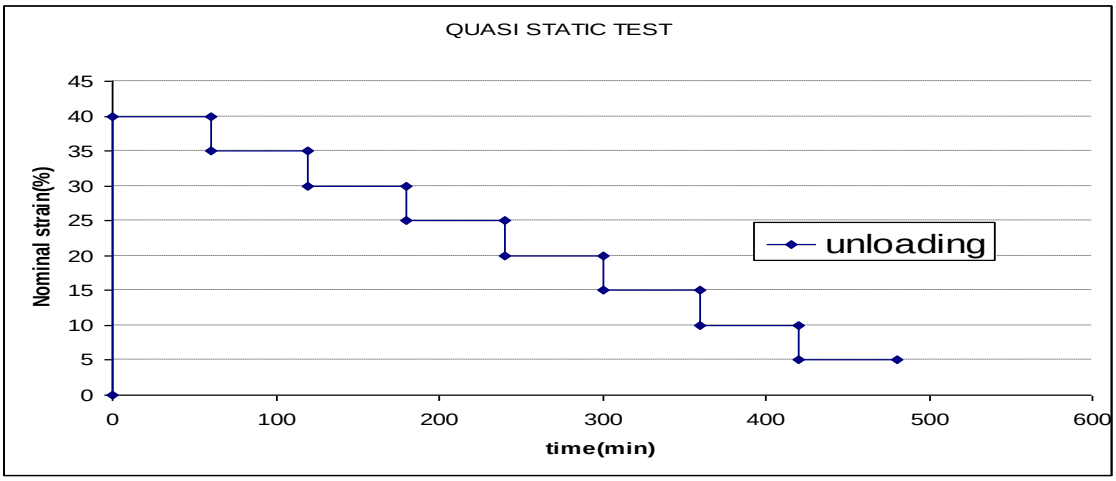

Fig.1.6.strain input to the quasistatic test

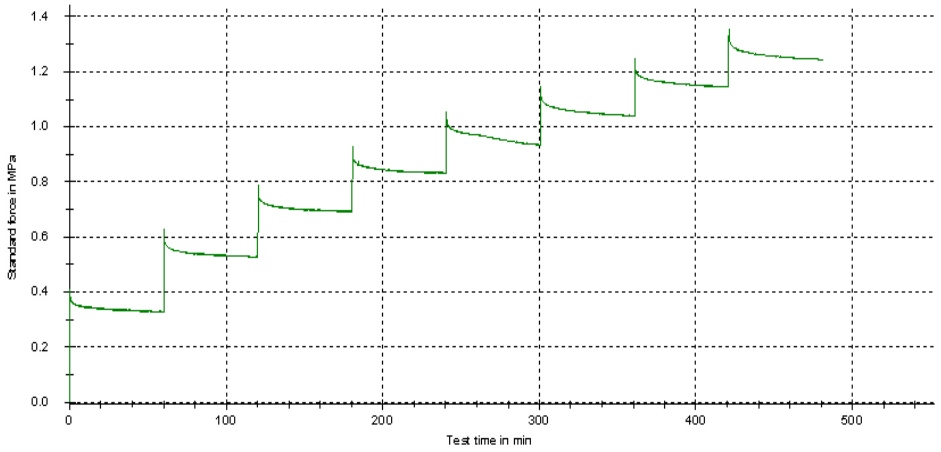

Fig.1.7. Response measured force in the quasistatic test (Loading)

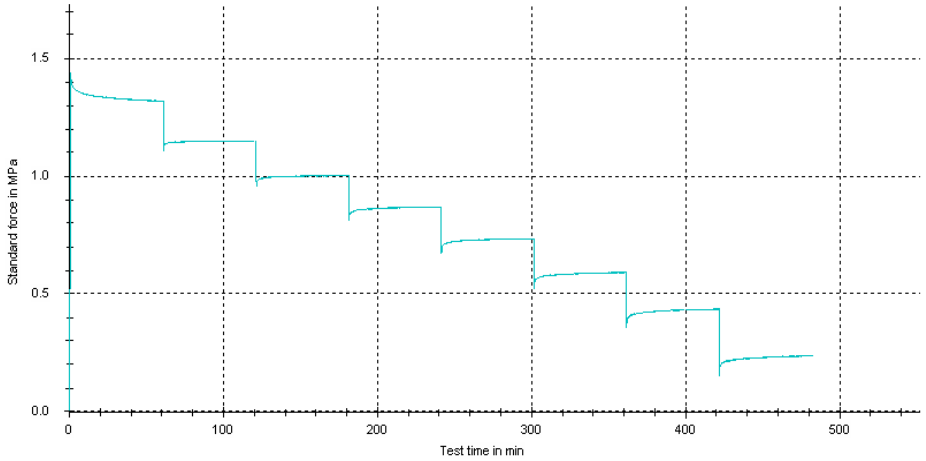

Fig.1.8. Response measured force in the quasistatic test (unloading)

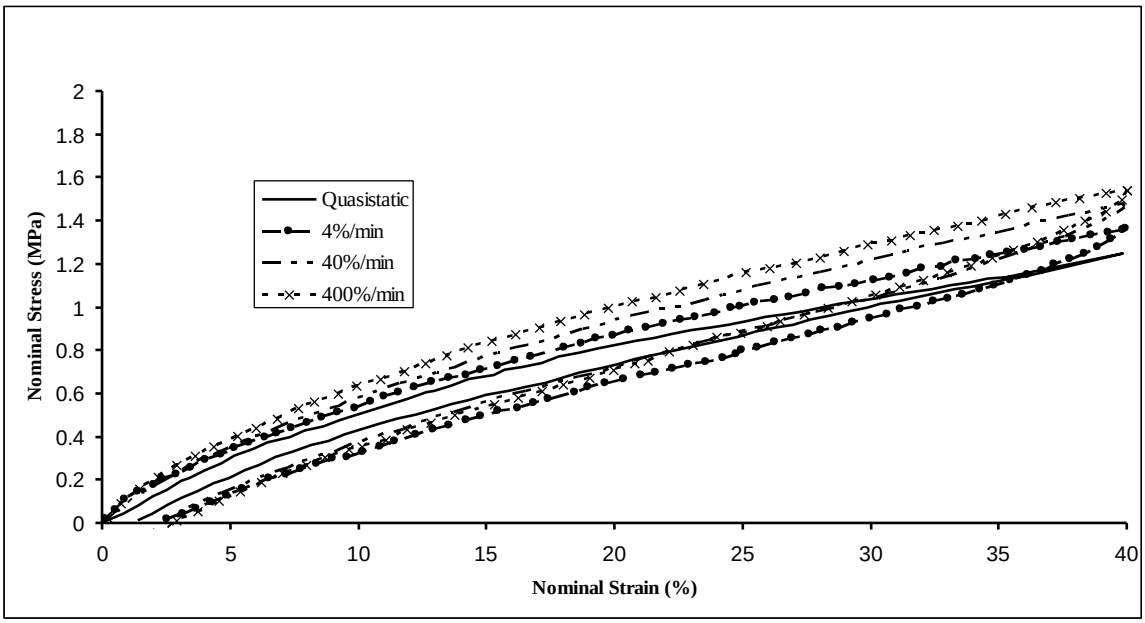

Fig.1.9. shows the rate dependent behaviour of rubber

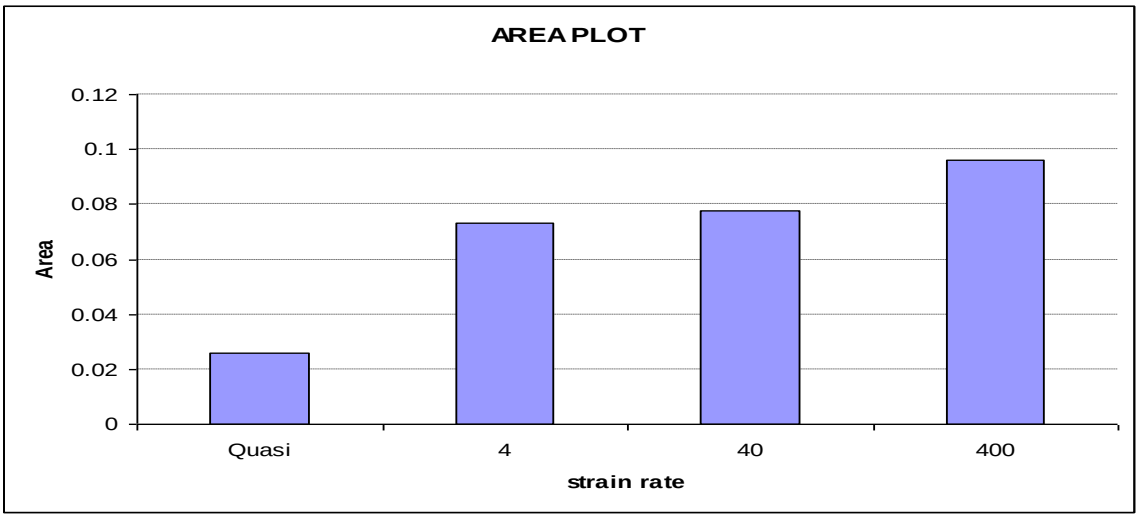

Fig.1.10. shows the rate dependent and rate independent hysteresis

1.3. Literature survey

Constitutive models for rubber have attracted the attention of researchers for the past seven decades. In the literature, a number of stored energy functions have been reported. The models that are popular in the numerical community are the once proposed by Ogden (1972), Yeoh (1993), Mooney and Rivlin, Arruda and Boyce (1993), Vander Waals (Kilian, 1981) to name a few. Of these models, Arruda and Boyce and Vander Waals are based on a statistical mechanics approach and the rest are based on a phenomenological approach. Rubber also exhibits Mullins effect, which is represented by models like Ogden-Roxburgh (1999) and Qi-Boyce (2004). These models are integrated with the stored

energy function. These models are still evolving. In the available literature all hyperelastic models are evaluated at much higher strains. The efficiency and accuracy of hyperelastic models for chloroprene rubber have been documented (Bergstrom). Though the material itself can withstand strains over 500 %, many applications require accurate description of its behaviour at low strains, upto 50 %. It is also the practice in industries to use tensile data to predict the behaviour of rubber components under multiaxial loading. This work also explores the problems with such a practice.

Experimental data of rubber shows the rate dependent behaviour, it is represented using viscoelastic material models. The fundamental models are Maxwell and kelvin-voigt model used to represents the viscoelastic behaviour. Basic linear viscoelastic models are valid only in linear range and small perturbation away from thermodynamic equilibrium. Many applications require the model to be predicting finite strains. Number of viscoelastic models is proposed which are suitable to rubber. e.g. Lubliner (1985) , Le Tallec et al (1993) and Bergstorm and Boyce (1998). Lubiner (1985) proposed the viscoelastic constitutive equations for kelvin by extending the small linear viscoelastic evolution equations in terms of strain to finite strain tensors and also proposed Maxwell model by additively decomposition of strain energy into elastic and inelastic part. Reese and Govindjee (1998a) extended this approach to finite strain viscoelasticity and developed a finite strain viscoelastic constitutive model for large deformations and large deviations away from thermodynamic equilibrium which is consistent with the second law of thermodynamics. Bonet (2001) assumed evolution equation in terms of second Piola kirchoff stress tensor instead of strain to introduce the nonlinearity in evolution equation. Bergstorm and Boyce (1998) conducted experiments on filled and natural rubber and proposed a constitutive model based on the multiplicative decomposition of the deformation gradient with an assumed nonlinear relation between stress and strain rate. Drozdov (1997) employed fractional derivative tensors. Reese and Govindjee (1998b) have proposed a thermo-viscoelastic constitutive model using an evolution law to include thermal effects. The computational setting is also addressed and they have used predictor-corrector algorithm to integrate the evolution equations. Recently models proposed by Haupt and Sedlan (2001), Lion (1996, 1997), Lin and Schomburg (2003),

Nedjar (2002a,2002b) consider viscoelastic-elastoplasticity which include rate dependent and the so called rate independent hysteresis. Lion (1996) has suggested a viscoelastic-elastoplastic constitutive model using an additive decomposition of the total stress into a rate independent equilibrium stress and a rate dependent overstress. He assumed that the rate dependent stress is a nonlinear function of strain rate using the viscoelastic coefficient in an exponential form. Lin and Schomburg (2003) have proposed a finite viscoelastic-elastoplastic constitutive model for rubber like materials including Mullins effect. Their model is based on the multiplicative decomposition of the deformation gradient and is derived using objective rates for calculating time derivatives. Simo (1992) studied in detail the return mapping algorithm for finite elasto-plasticity from a computational point of view and his work uses principle of maximum dissipation.

1.4. Motivation and Objectives:

Experimental data shows that huge variation in rubber loading and unloading depending upon the history of material. Because of the complexity of the Mullins effect, if one is interested in data upto to 50 percentages of strains. In the literature all the hyperelastic models are evaluated at much higher strains. These models do not seem to be accurate for moderate strains. The objective is to evaluate the existing hyperelastic models upto 50 percent of strain and propose a new stored energy function for moderate strains (<50%) to capture both tension and compression in one equation.

The Finite strain viscoelastic models are developed in literature captures the experimental data during loading, and it is not clear how these models behave during unloading with different strain rates. Objective is to bring the issues with existing models while predicting the experimental data of rubber in loading and unloading. And a new formulation for finite strain Kelvin model developed to address these issues.

1.5. Organization of thesis:

This thesis deals with hyperelastic and viscoelastic material models used to predict the rubber behaviour.

Chapter 1 gives the introduction rubber characteristic such as Mullins effect, rate dependent and rate independent hysteresis. The importance of constitutive modeling of rubber is discussed and followed by experiment conducted as stress softening dependent, rate dependent experiments with different strain rates, quasistatic test, and compression test, Followed by literature survey, motivation and objectives.

Chapter 2 starts with popular stored energy functions which are available in literature and discussed with issues with the existing models while fit the low stains.

Chapter 3 starts with the deformation gradient and followed by conditions should satisfy the stored energy function. A new stored energy proposed and comparison has done with existing models using r-square method. Finite element implementation of proposed model is discussed in detail fashion.

Chapter 4 starts with concept of internal variables and decomposition of deformation gradient. Derivation Maxwell model and new formation for kelvin-vigot model is discussed. Followed by finite element implementation of these models are discussed.

Chapter 5, the results of implanted Maxwell and developed kelvin models are discussed while fitting the rubber loading and unloading test data.

Chapter 6, conclusions based on current work is presented. Scope of future work discussed.

Chapter 2

HYPERELASTIC MATERIAL MODELS

2.1. Introduction

Typical mechanical behaviour of rubber is nonlinear viscoelastic with weak equilibrium hysteresis (Lion, 1997). The type of behaviour invoked for analysis depends on the particular application. In many instance rubber is treated as hyperelastic, defined by a stored energy function. The determination of the coefficients in these functions generally require uniaxial, biaxial and shear test data. The range of strain and strain rate has a bearing on the accuracy of the results (Kurt Miller, 2000). It is also important that the coefficients obtained by the laboratory tests should represent the three dimensional state of stress accurately. Because of the complexity of the Mullins effect, if one is interested in data upto to 50%, then one is forced to remove the effect only upto that strain and test the data for elastic properties. This chapter evaluates the existing models with tensile test data upto 50% of strain.

2.2. Stored energy functions

Stored energy function (ψ) is a scalar valued function which is objective (Holzafel, 1990) and for a homogeneous isotropic materials, stored energy function is a function of invariants of C, given by the following equation

$$\psi(C) = \psi(I_1, I_2, J) \tag{2.1}$$

In the eq. (2.1) I_1, I_2, and J are defined as follows

$$I_1 = \lambda_1^2 + \lambda_2^2 + \lambda_3^2 \tag{2.2a}$$

$$I_2 = \lambda_2^2\lambda_3^2 + \lambda_3^2\lambda_1^2 + \lambda_1^2\lambda_2^2 \tag{2.2b}$$

$$J = \lambda_1 \lambda_2 \lambda_3 \qquad (2.2c)$$

Where, $\lambda_1^2, \lambda_2^2, \lambda_3^2$ are the eigen values of $\mathbf{C}$ and $\lambda_1, \lambda_2, \lambda_3$ are the principal stretches of deformation gradient ($\mathbf{F}$). In order to compare the stored energy function with experimental data eq. (2.1) is reduced into Cauchy stress given by the following eq. (2.3)

$$\sigma_i = \lambda_i \frac{\partial \psi}{\partial \lambda_i} - p \quad \text{(no summation over i)} \qquad (2.3)$$

2.3. Calculations:

2.3.1. Uniaxial:

For incompressible material the principal stretches are as follows

$$\lambda_1 = \lambda; \quad \lambda_2 = \lambda_3 = 1/\sqrt{\lambda} \qquad (2.4)$$

Stress tensor is given by

$$\sigma_1 = \sigma_u; \quad \sigma_2 = \sigma_3 = 0 \qquad (2.5)$$

$$\sigma_u = \lambda_1 \frac{\partial \psi}{\partial \lambda_1} - \lambda_3 \frac{\partial \psi}{\partial \lambda_3} \qquad (2.6)$$

First and second invariants in terms of these stretches

$$I_1 = \lambda^2 + \frac{2}{\lambda} = e^{2\ln\lambda} + 2e^{-\ln\lambda} \qquad (2.7)$$

$$I_2 = \frac{1}{\lambda^2} + 2\lambda = e^{-2\ln\lambda} + 2e^{\ln\lambda} \qquad (2.8)$$

2.3.2. Biaxial:

The stretches in two directions are equal in biaxial and due to incompressibility constraint the third direction stretches are given by

$$\lambda_1 = \lambda_2 = \lambda; \quad \lambda_3 = 1/\lambda^2 \tag{2.9}$$

Cauchy stresses are

$$\sigma_1 = \sigma_2 = \sigma_b; \quad \sigma_3 = 0 \tag{2.10}$$

$$\sigma_b = \lambda_1 \frac{\partial \psi}{\partial \lambda_1} - \lambda_3 \frac{\partial \psi}{\partial \lambda_3} \tag{2.11}$$

First and second invariants in terms of these stretches

$$I_1 = 2\lambda^2 + \frac{1}{\lambda^4} = 2e^{2\ln\lambda} + e^{-4\ln\lambda} \tag{2.12}$$

$$I_2 = \frac{2}{\lambda^2} + \lambda^4 = 2e^{-2\ln\lambda} + e^{4\ln\lambda} \tag{2.13}$$

As it can be seen from equations (2.7), (2.8), (2.12) and (2.13) first invariant and second invariants are symmetry with respect origin of true stress-strain plane.

2.4. NeoHookean form (NH form):

The neoHookean form of stored energy function is given by the following equation (Treloar, 1978)

$$\psi = C_{10}(I_1 - 3) \tag{2.14}$$

Combining eq. (2.4) and eq.(2.3), the following equations are obtained

$$\sigma_u = 2C_{10}\left(\lambda^2 - \frac{1}{\lambda}\right) \tag{2.15}$$

$$\sigma_b = 2C_{10}\left(\lambda^2 - \frac{1}{\lambda^4}\right) \tag{2.16}$$

$$\sigma_s = 2C_{10}\left(\lambda^2 - \frac{1}{\lambda^2}\right) \tag{2.17}$$

Eq. (2.15), eq. (2.16) and eq. (2.17) show that the uniaxial tension, biaxial tension and shear behaviour are function of λ^2 ($1/\lambda$,$1/\lambda^4$ and $1/\lambda^2$ values are small compared to λ^2 in tension). In the case of uniaxial compression $1/\lambda$ dominates the λ^2 term and in biaxial compression $1/\lambda^4$ dominates. The result is that, any Stored Energy function which depends on the first invariant always predicts a lower uniaxial compression value than uniaxial tension. The biaxial compression is greater than the biaxial tension, which is not the case for a function which depends on the second invariant. On the otherhand the function which depends on the second invariant behaves in an opposite fashion.

The fig.2.1 and fig. 2.2 shows the NeoHookean model fitted with uniaxial tension and compression. NH model gives better fit in uniaxial tension and in uniaxial compression, when the coefficients are determined using the uniaxial tension data. the error in the fit in uniaxial tension increases when coefficients are determined using uniaxial compression data. This model gives same fit when the coefficients predicted from uniaxial tension and both tension and compression. So the uniaxial tension data alone gives the best fit for this model. This is because of the difference in the order of the dominant terms in the two modes of deformation.

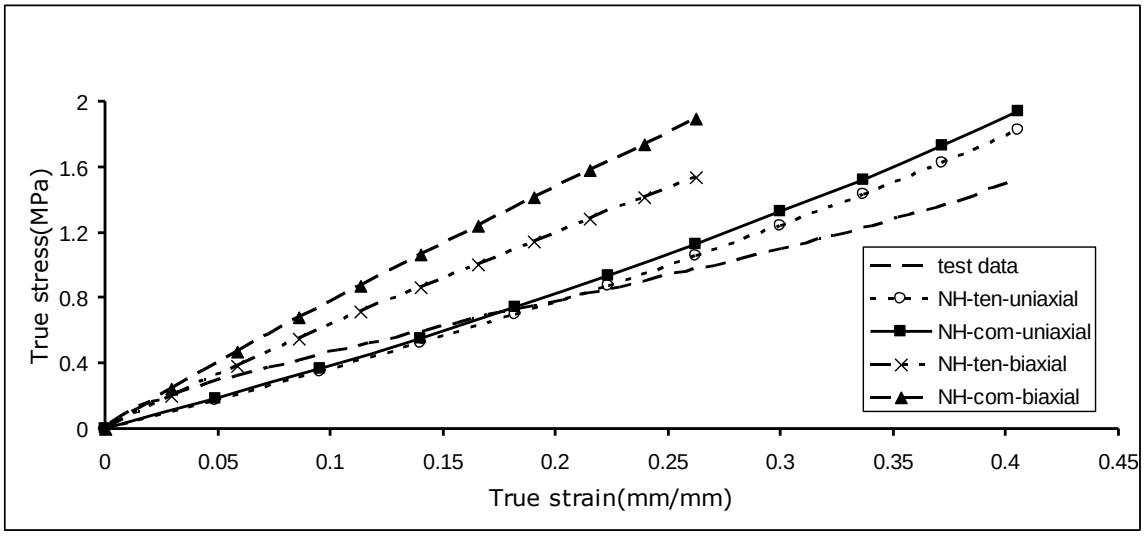

Fig.2.1. Fit of uniaxial and biaxial tension with neoHookean model

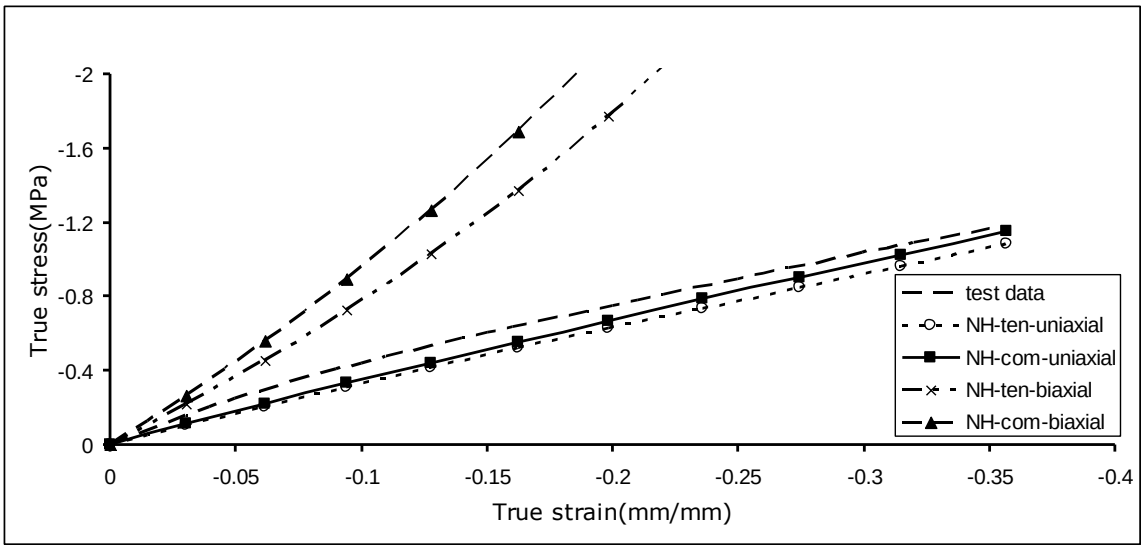

Fig.2.2. Fit of uniaxial and biaxial compression with neoHookean model

Note: In all figures names are given such that three words in between dashes. First one is represented by short form of model used example NeoHookean by NH, Mooney Rivlin by MR. second one represented type of test data used to fit the model , tension (ten) and compression (com) and third one represents the mode of deformation predicted. In this thesis biaxial means it is equibiaxial unless it is specified.

Though biaxial test data is not available, model behaviour is plotted to show how the model behaves in biaxial mode. From fig.2.1 and 2.2, it is observed that small variation in uniaxial mode while using uniaxial tension and compression data used fit the model magnifies in biaxial mode. The coefficients of all models are given in table.1,2,3 when coefficients are determined using uniaxial tension , uniaxial compression and both uniaxial tension and compression respectively.

2.5. Yeoh form:

Yeoh form of stored energy function is a function of the first invariant of right Cauchy Green deformation tensor (yeoh, 1993)

$$\psi = C_{10}(I_1 - 3) + C_{20}(I_1 - 3)^2 + C_{30}(I_1 - 3)^3 \qquad (2.18)$$

The Yeoh form clearly predicts the shape of the stress strain curve at higher strains. But it is interesting to point out from the fig.1a that even at lower strains, where experimentally the typical sigmoidal shape does not develop, there is a tendency to mimic the shape with Yeoh model. Fig.2.3 and 2.4 are shown the prediction of the Yeoh model for small strains in uniaxial and biaxial when the coefficients are used uniaxial tension and uniaxial compression used to fit the model. This model deviates in compression from the experimental values above 20 percent of strains. It can be observed that this model overestimates the uniaxial tension curve when uniaxial compression data is used to determine the coefficients. The model gives a better fit when both tension and compression data are used to determine the coefficients. Though the model behaves in uniaxial is similar, the results are quite different in biaxial mode. It can be seen from fig.2.3 the estimation of biaxial tension values are very close to uniaxial tension values when use uniaxial tension data used to fit the model. Estimation of biaxial compression is very high values when use uniaxial compression data to fit the model.

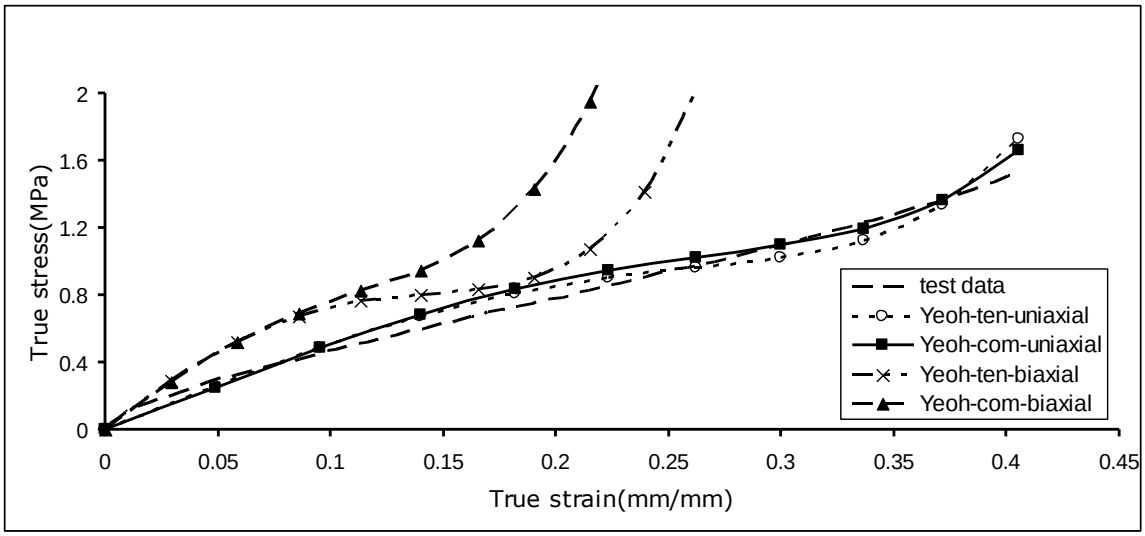

Fig.2.3. Fit of uniaxial and biaxial tension with Yeoh model

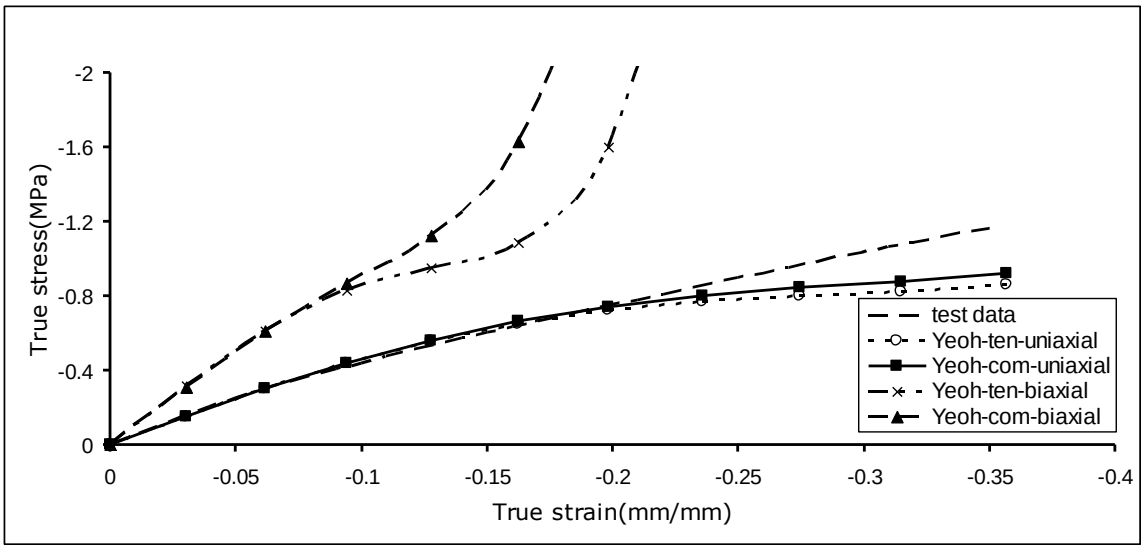

Fig.2.4. Fit of uniaxial and biaxial compression with Yeoh model

2.6. Arruda-Boyce form (AB):

This model is based on "eight-chain representation of the macromolecular network structure and non-Gaussian behaviour of the polymer chains" (Arruda and Boyce, 1993).The series expansion form the stored energy function is used. The first five terms are given as (ABAQUS)

$$\psi = \mu\left(\frac{1}{2}(\mathrm{I}_1-3)+\frac{1}{20\lambda_m^2}(\mathrm{I}_1^2-3^2)+\frac{11}{1050\lambda_m^2}(\mathrm{I}_1^3-3^3)+\frac{19}{7000\lambda_m^2}(\mathrm{I}_1^4-3^4)+\frac{519}{673750\lambda_m^2}(\mathrm{I}_1^5-3^5)\right) \quad (2.19)$$

$$\mu_0 = \mu\left(1+\frac{3}{5\lambda_m^2}+\frac{99}{175\lambda_m^4}+\frac{513}{875\lambda_m^6}+\frac{42039}{67375\lambda_m^8}\right) \quad (2.20)$$

For small strains the first term dominates and behaves exactly like NH model.

2.7. Mooney-Rivlin form (MR):

Mooney-Rivilin form of stored energy function depends on the first and second invariants of **C**. It can be expressed as (ABAQUS)

$$\psi = \mathrm{C}_{10}(\mathrm{I}_1-3)+\mathrm{C}_{01}(\mathrm{I}_2-3) \quad (2.21)$$

If only one test data (uniaxial tension or compression) is used to determine the coefficients, there is a possibility that either C_{10} or C_{01} is negative. In the first case the model becomes unstable in biaxial compression. When C_{01} is negative, the model becomes unstable in biaxial tension. If $C_{10} >> C_{01}$ it behaves like the neoHookean model and if C_{10} is equal to C_{01} the model becomes symmetric with respect to origin.

Fig.2.5 shows comparison of fit of this model in uniaxial and biaxial tension when the coefficients are used to fit the model uniaxial tension, uniaxial compression and both tension and compression. When the coefficients are determined from tension data. The fit is good in uniaxial tension. it is overestimating the biaxial tension. Fig.2.6 shows comparison of fit of this model in uniaxial and biaxial comparison when the coefficients are used to fit the model uniaxial tension, uniaxial compression and both tension and compression. It is very poor in compression prediction when tension data used. this model gives the good prediction is in tension and compression when coefficients are determined using both uniaxial tension and compression data .

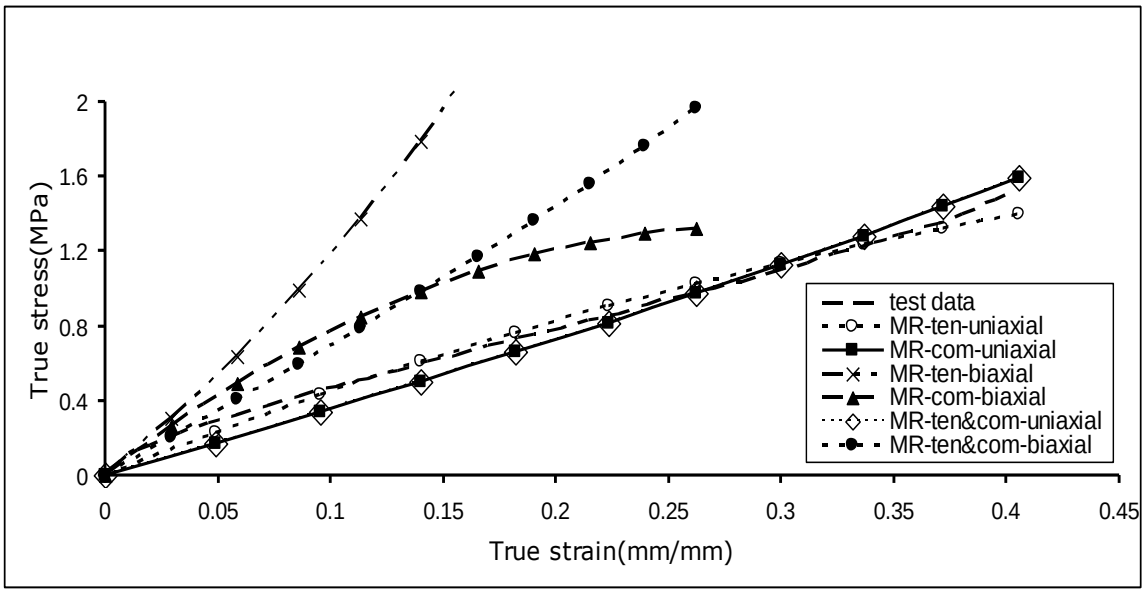

Fig.2.5. Fit of uniaxial and biaxial tension with Mooney Rivlin model

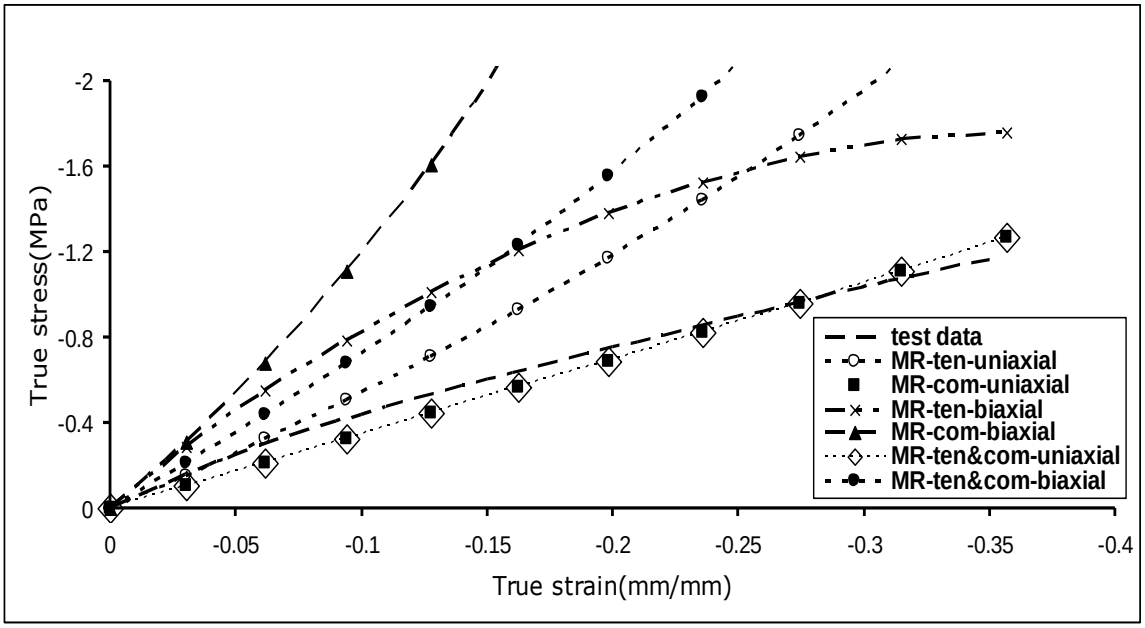

Fig.2.6. Fit of uniaxial and biaxial compression with Mooney Rivlin model

2.8. Vander Waals form:

This model was proposed by Kilian in 1981, based on concepts from ideal gas laws. It is based on an entropy elastic ideal polymer network.

$$\psi = \mu\left(-\left(\lambda_m^2 - 3\right)\left[\ln(1-\eta) + \eta\right] - \frac{2}{3}a\left(\frac{\tilde{I}-3}{2}\right)^{3/2}\right) \tag{2.22}$$

$$\tilde{I} = (1-\beta)I_1 + \beta I_2; \qquad \eta = \left(\frac{\tilde{I}-3}{\lambda_m^2 - 3}\right)^{1/2} \tag{2.23}$$

Where μ is Shear modules, λ_m is locking stretch, a is global interaction parameter and β is Invariant mixture parameter.

In fig.2.7 and fig.2.8 shows fit of this model when uniaxial tension and compression data is used to fit the model. The fit of this model is like that of Yeoh, when the coefficients are determined using uniaxial tension data. It gives excellent fit when uniaxial compression is used to determine the coefficients of the model.

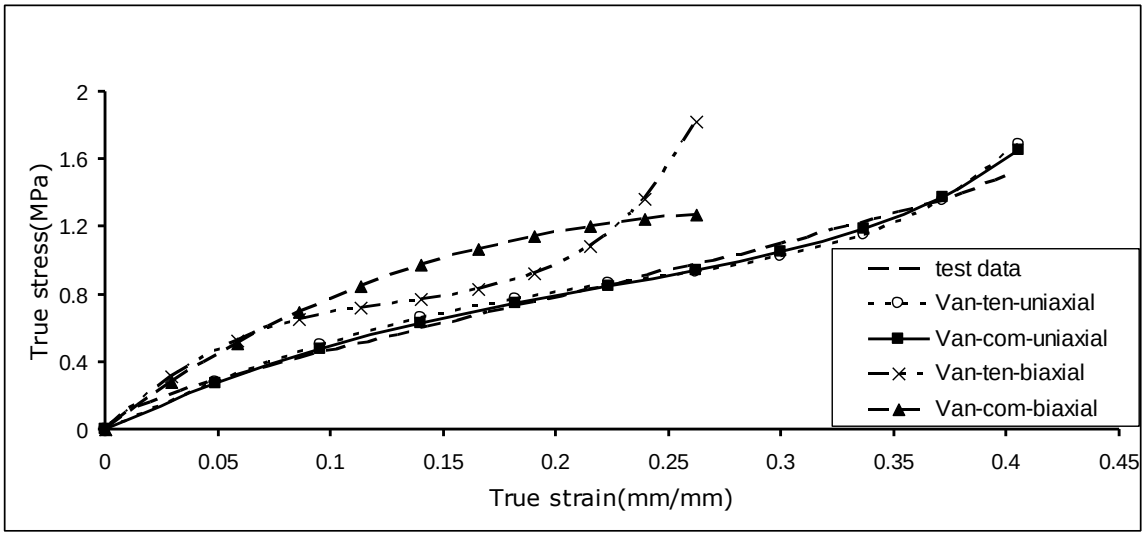

Fig.2.7. Fit of uniaxial and biaxial Tension with Vanderwaals model

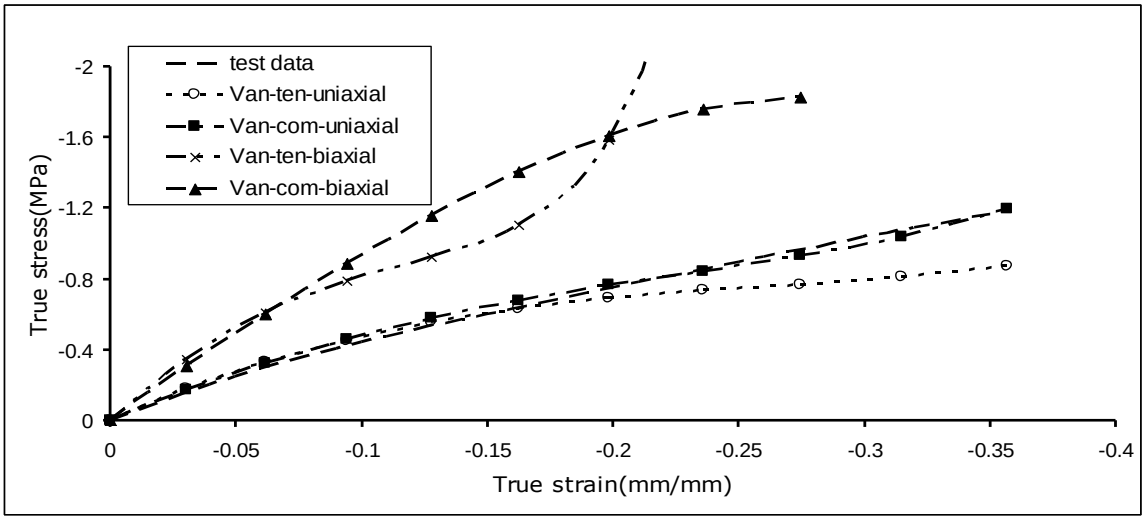

Fig.2.8. Fit of uniaxial and biaxial compression with Vanderwaals model

2.9. Ogden form:

Ogden stored energy function is written in terms of principal stretches instead of the invariants. Ogden form can be reduced into neoHookean and Mooney Rivlin by choosing particular values for α and N. Ogden form of stored energy function is given as (ABAQUS),

$$\psi = \sum_{r=1}^{N} \frac{2\mu_r}{\alpha_r}\left(\lambda_1^{\alpha_r} + \lambda_2^{\alpha_r} + \lambda_3^{\alpha_r} - 3\right) \qquad (2.24)$$

Where

μ_r, α_r are constants

In fig.2.9, 2.10 shows the fit for Ogden model, when n=1 by using uniaxial tension and compression data. This model predicts the uniaxial test data very well. It can be observed that the error is very high for compression data when tension data used to fit the model. As can be seen from fig.2.9 this model overestimates uniaxial tension when uniaxial compression is used to determine the coefficient. this model gives a better fit when the coefficients are determined using both uniaxial tension and uniaxial compression data.

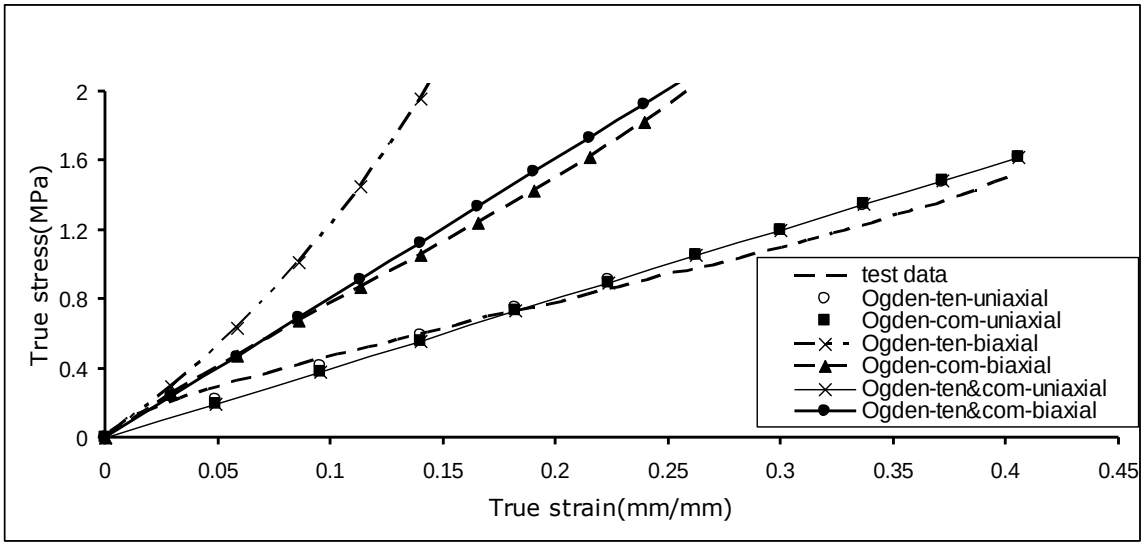

Fig.2.9. Fit of uniaxial and biaxial Tension with Ogden model

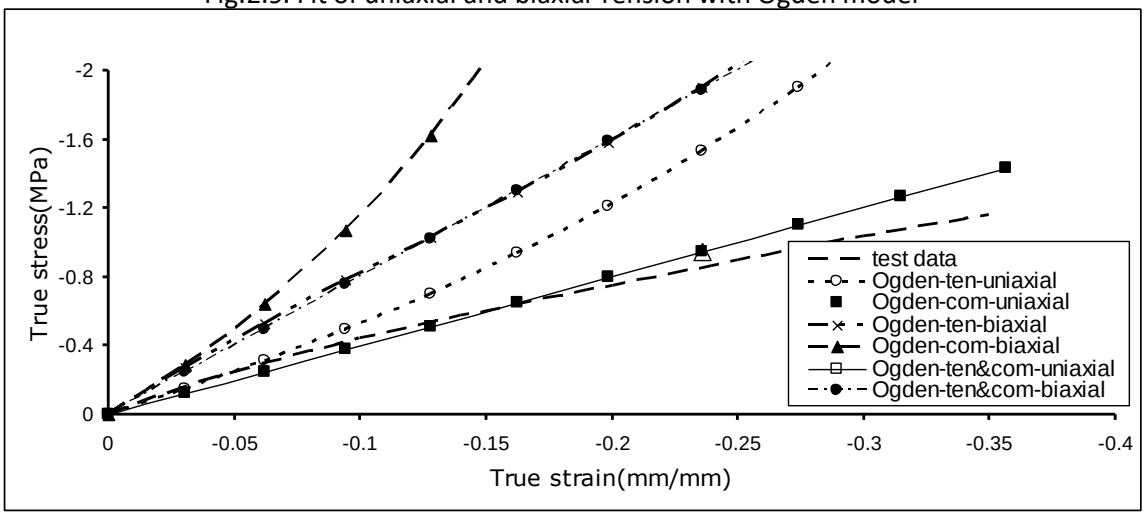

Fig.2.10. Fit of uniaxial and biaxial Tension with Ogden model

Table.1. Hyperelastic models coefficients are predicted using uniaxial tension data

Sl.No	MODEL	COEFFICIENTS
1	neoHookean	C_{10} =0.2876
2	Yeoh	C_{10} = 0.43; C_{20} = -0.52; C_{30}=0.44;
3	Arruda-Boyce	μ =0.575; μ_0 =0.575; λm=1645
4	Mooney-Rivlin	C_{10} = -0.159; C_{01}=0.57
5	Van der Waals	μ =1.072; λm =2.25; a=3.03; β=0.0
6	Ogden, n=1	μ=0.787; α=-3.99

Table. 2. Hyperelastic models coefficients are predicted using compression test data

Sl.No	MODEL	COEFFICIENTS
1	neoHookean	C_{10} =0.353
2	Yeoh	C_{10} = 0.422; C_{20} = -0.445; C_{30}=0.6164;
3	Mooney-Rivlin	C_{10} = 0.6324; C_{01}=-0.2238
4	Van der Waals	μ =1.0187; λm =2.23; a=2.846; β=0.406
5	Ogden, n=1	μ=0.742; α=4.012

Table.3. Hyperelastic models coefficients are predicted using uniaxial tension and compression test data

Sl.No	MODEL	COEFFICIENTS
1	neoHookean	C_{10} =0.3057
2	Yeoh	C_{10} = 0.423; C_{20} = -0.434; C_{30}=0.338;
3	Mooney-Rivlin	C_{10} = 0.117; C_{01}=0.1127
4	Van der Waals	μ =1.0187; λm =2.23; a=2.846; β=0.406
5	Ogden, n=1	μ=0.668; α=-2.078

2.10. Summary:

In this chapter popular models such as neoHookean, Mooney Rivlin, Yeoh, Ogden, Arruda-Boyce and Vander Waals models behaviour studied for the small strains (<50%). The Stored energy function when expressed in terms of the first invariant alone can fit compression data with a small error, using the uniaxial tension data. On the otherhand, the tension behaviour cannot be predicted accurately from compression data vanderwaals model captures tension behaviour from uniaxial compression with small error. it fails the predicting the compression data from tension. To fit Ogden and Mooney Rivlin model requires the both uniaxial tension and compression data.

Chapter 3

PROPOSED HYPERELASTIC MODEL

It is practice for many industries using uniaxial tension or uniaxial compression to fit the hyperelastic material models. Depending upon the curing process the material properties will change. It is may not possible to conduct the compression test every time and results will depend how the test has been conducted. It is discussed in chapter2, from uniaxial tension data neoHookean and yeoh models are predicting the uniaxial compression with error. Form uniaxial compression except vanderwaals none of the model is capturing the uniaxial tension. In this chapter a new stored energy function is proposed which captures accurately either from uniaxial tension or uniaxial compression.

3.1. Deformation Gradient:

Deformation gradient gives the relationship between an initial or reference configuration and the deformed configuration. If $\mathrm{d}X$ is the infinitesimal line element in the reference configuration and same line element is deformed to $\mathrm{d}x$ after the application of load**s**, the deformation gradient F gives the relation ship between $\mathrm{d}X$ and $\mathrm{d}x$

$$\mathrm{d}x_i = \frac{\partial x_i}{\partial X_J}\mathrm{d}X_J \qquad (3.1)$$

$$F_{iJ} = \frac{\partial x_i}{\partial X_J} \qquad (3.2)$$ From Equation 3.2 it can be observed that F is a two point tensor involving point in reference configuration as well as deformed configuration.

3.2. Polar decomposition of deformation gradient

The deformation gradient multiplicative decomposed into symmetry part and orthogonal part. Symmetry part represents the pure displacement and orthogonal part represents the rotation of material

F=RU=vR (3.3)

U is right stretch tensor, v is left stretch tensor. Both tensors have the same eigen values.

3.2 Deformation Tensors

There are two most important deformation tensors through which most of the strain measures are defined. The first one is called right Cauchy-Green deformation tensor or Green deformation tensor C defined through Equation 3.4 and the left Cauchy-Green deformation tensor or finger deformation tensor b defined through Equation 3.5.

$$C = F^T F = U^2 \quad (3.4)$$

$$b = FF^T = v^2 \quad (3.5)$$

One of the important features of both C and b is that they are symmetric have same eigen values and eigen vectors varies with rotation means if C has the e eigen vector b has the eigen vector is Re.

3.3. Hyperelastic material:

Elastic material is defined as current state of stress is dependents upon the current state of deformation. Constitutive equation reads as (Haupt,2000)

$$P = f(F) \quad (3.6)$$

Here, P is first poila stress tensor. f(.) is a symmetry tensor valued function of F.

A hyperelastic material are defined as, whose constitutive equations are defined based on stored energy function.

$$P = \frac{\partial \psi(F)}{\partial F} \tag{3.7}$$

3.4. **Conditions should satisfy the stored energy function:**

The stored energy function written in terms of deformation should satisfy the following conditions (Holzafel, 2000)

a) Normalization, The stored function should vanishes with respect to reference configuration and increases with deformation

$$\begin{aligned} \psi(F) &= 0 \quad \text{if } F = I \\ \psi(F) &\geq 0 \quad \text{if } F \neq I \end{aligned} \tag{3.8}$$

b) The ψ should satisfy the growth conditions. It implies that

$$\begin{aligned} \psi(F) &\to +\infty \quad \text{as def}(F) \to \infty \\ \psi(F) &\to +\infty \quad \text{as def}(F) \to 0+ \end{aligned} \tag{3.9}$$

c) Objectivity ψ is scalar valued function value completely independent of frame of reference. i.e. Translation and rotation of deformation should not change the energy.

$$\psi(F) = \psi(QF) = \psi(U) \tag{3.10}$$

Q can be any orthogonal tensor, for special case $Q=R^T$ implies QF=U

d) Isotropy hyperelastic materials strain energy function is isotropic function (independent of rotation of current configuration), it should satisfy

$$\psi(F) = \psi(FQ^T) = \psi(v) \tag{3.11}$$

e) U is unique positive square root of C and v is unique root of b. the function

$$\psi(U) = \psi(C) = \psi(b) = \psi(v) \tag{3.12}$$

f) Constitutive requirement of the stored energy function should be convex with respect to deformation gradient **F**. condition for convexity is given in eq(3.13) (Hartmann and Neff, 2003)

$$\psi\left(\mathrm{F}+(1-\lambda)\mathrm{a}\otimes\mathrm{b}\right)\leq\lambda\psi\left(\mathrm{F}\right)+(1-\lambda)\psi\left(\mathrm{F}+\mathrm{a}\otimes\mathrm{b}\right) \tag{3.13}$$

$\lambda \in [0,1]$, a, b are the vectors

Convexity condition with respect to derivative is

$$\psi(\mathrm{F}+\mathrm{a}\otimes\mathrm{b})\geq\psi(\mathrm{F})+\frac{\partial\psi(\mathrm{F})}{\partial\mathrm{F}}:(\mathrm{a}\otimes\mathrm{b})$$

or (3.14)

$$\frac{\partial^2\psi(\mathrm{F})}{\partial\mathrm{F}^2}>0$$

Convexity of strain energy density is important to study the uniqueness of solution in nonlinear problems. It gives the positive definiteness of elastic tensor. Full positive defineness would guarantee global uniqueness of solution in case where physical reason for such a uniqueness is not expected (Ball, 1977; Drozdov,1996).

g) Suitable condition for material instability is the quasiconvex proposed by Morrey (1952). The quasiconvexity condition is

$$\int_{\mathrm{D}}\psi\left(\mathrm{X},\mathrm{F}+\nabla\mathrm{u}(\mathrm{x})\right)\mathrm{dx}\geq\int_{\mathrm{D}}\psi\left(\mathrm{X},\mathrm{F}\right)=\mathrm{m}(\mathrm{D})\psi\left(\mathrm{X},\mathrm{F}\right) \tag{3.15}$$

Should hold for bounded open subset $\mathrm{D}\subseteq\mathrm{R}^3$, and for all u is subset of infinitely differentiable functions. Here m denotes the Lebesgue measure. Quasiconvexity condition stored energy function satisfies the Legendre-Hadamard or ellipticity condition.

$$\mathrm{H}:\frac{\partial^2\psi}{\partial\mathrm{F}^2}:\mathrm{H}\geq 0 \tag{3.16}$$

Here $\mathrm{H}=\mathrm{a}\otimes\mathrm{b}$. Quasiconvex condition of ψ ensures the quadratic convergence of solution in certain iteration techniques.

h) Polyconvex: ψ is Polyconvex, if there is function $\psi*(I_1, I_2, J)$ is convex in I_1, I_2 and **J** jointly. If the function additively decomposed, then the function is Polyconvex if and only individual terms are convex. Let stored energy ψ sufficiently smooth. Then, if ψ is Polyconvex, it is quasiconvex and elliptic.

3.5. Stored energy function

Nearly incompressible materials deformation gradient is decomposed into deviatoric part and volumetric part. It is assumed stored energy function is additively decomposed into deviatoric and volumetric part (Holzafel, 2000)

$$\psi = \psi_{dev}(F_{dev}) + \psi_{vol}(F_{vol}) \tag{3.17}$$

Or

$$\psi = \psi_{dev}(\bar{C}) + \psi_{vol}(J) = \psi_{dev}(\bar{I}_1, \bar{I}_2) + \psi_{vol}(J) \tag{3.18}$$

Where $F_{dev} = J^{-1/3}F$; $F_{vol} = J^{1/3}I$; $\bar{C} = F_{dev}^{T}F_{dev}$; J =det F and $\bar{I}_1, \bar{I}_2$ are first and second invariants of $\bar{C}$.

$$\bar{I}_1 = \frac{\|F\|^2}{J^{2/3}} = \frac{F_{ij}F_{ij}}{J^{2/3}} \tag{3.19}$$

$$\bar{I}_2 = \frac{\|\text{adj } F\|^2}{J^{4/3}} \tag{3.20}$$

Some deviatoric terms which are satisfy the Polyconvexity conditions are (Hartmann and Neff ,2003)

$$\varphi_1(\bar{I}_1) = \bar{I}_1^{k} \tag{3.21}$$

$$\varphi_2(\bar{I}_2) = \bar{I}_2^{3k/2} \tag{3.22}$$

$\bar{I}_2$ is not convex function and mixed term $\bar{I}_1^{k}\bar{I}_2^{3k/2}$ is not Polyconvex. Where, k is positive integer.

Some volumetric terms which satisfy the Polyconvex conditions are

$$\varphi_3(\mathbf{J}) = \left(\mathbf{J^k} + \mathbf{J^{-k}} - 2\right) \tag{3.23}$$

$$\varphi_4(\mathbf{J}) = \left(\mathbf{J} - 1\right)^k \tag{3.24}$$

3.6. Proposed Stored energy function:

The new stored energy function is assumed to be a function of first and second invariants of the right cauchy deformation tensor.

$$\psi = C_1 * \ln\left(\frac{\alpha \bar{I}_1^{3k} + (1-\alpha)\bar{I}_2^{3k}}{3^{3k}}\right) + \frac{1}{D}(J-1) \qquad (1 \le k \le \infty) \tag{3.25}$$

In the eq. (3.25) k can be any positive integer in this case k is considered as one, α can vary from zero to one and C_1 is a constant which can be determined from any one of the test data. α =0.5 yields the symmetry with respect to true stress-true strain condition, about the origin. The asymmetry of test data can be predicted by varying the α values. When α is greater than 0.9 the proposed model behaves like neoHookean model. If one test data available, it is better to keep the α value to be 0.5, and then determine the C_1 coefficient.

Fig.3.1, 3.2 shows prediction of proposed model in tension and compression. From fig.3.1 it can be seen this model gives better estimation than any other model in uniaxial tension when uniaxial compression data is used to determine the coefficients. From fig.3.2 shows that this model gives better estimation in uniaxial compression when the coefficients are determined from uniaxial tension. The coefficient are given table.3.1 coefficient are predicted using curve fitting technique in MATLAB. The procedure to fit model is given in section 3.9.

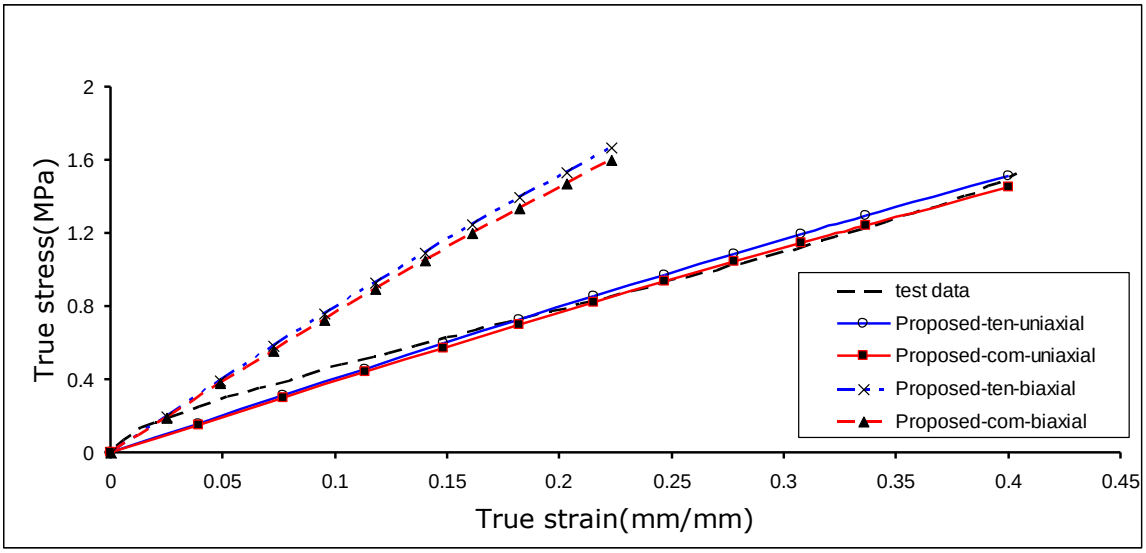

3.1. Fit of uniaxial and biaxial tension with prposed model

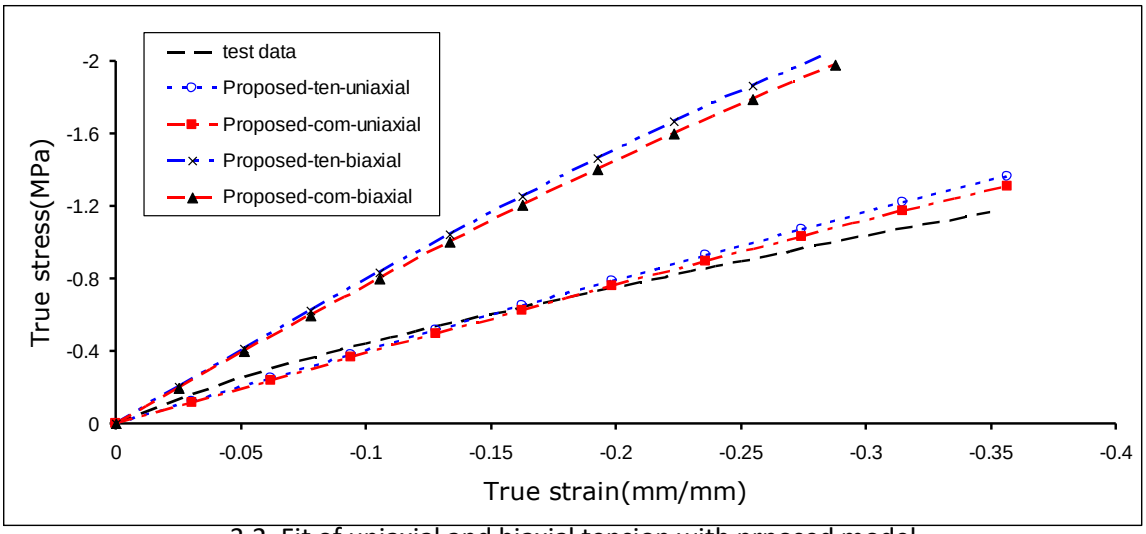

3.2. Fit of uniaxial and biaxial tension with prposed model

Table.3.2. Proposed models coefficients are predicted using different test data's

Sl.no	Test data used	Proposed model coefficients
1	Uniaxial tension	C_1 =0.025; α=0.5
2	Uniaxial compression	C_1 =0.0248; α=0.5
3	Both uniaxial tension and compression	C_1 =0.024; α=0.62

3.7. Finite element implementation:

Proposed stored energy function implemented in commercial package ABAQUS6.5.1 using user material (UMAT) option algorithm as follows (Holzafel,2000)

1. Initial deformation gradient input from ABAQUS (F)

2. determine the determent of deformation gradient

$$J = \det F \tag{3.26}$$

3. calculate the deviatoric part of deformation gradient

$$\bar{F} = J^{-1/3} F \tag{3.27}$$

4. calculate left cauchy deformation tensor

$$\bar{B} = \bar{F}\bar{F}^{T} \tag{3.28}$$

5. calculate eigen value and eigen vectors of $\bar{B}$

6. calculate the principal values of cauchy stress

$$\sigma_i = \lambda_i \frac{\partial \psi}{\partial \lambda_i} \tag{3.29}$$

7. rotate stress into 3-D space using eigen vectors of B

8. calculate the elastic tensor ($\square_{abcd}$)using following relations

$$J\square^{\sigma T}_{abcd} = \sum_{i=1}^{3}\sum_{j=1}^{3}\left(\square_{ij} - 2\sigma_i\delta_{ij}\right) q_a^i q_b^i q_c^j q_d^j + \frac{1}{2}\sum_{i=1}^{3}\sum_{j=1}^{3} g_{ij}\left(q_a^i q_b^j q_c^i q_d^j + q_a^i q_b^j q_c^j q_d^i\right) \tag{3.30}$$

Where

$$\square_{ij} = \lambda_j \frac{\partial \sigma_i}{\partial \lambda_j} \tag{3.31}$$

$$g_{ij} = \begin{cases} = \dfrac{\sigma_i \lambda_j^2 - \sigma_j \lambda_i^2}{\lambda_i^2 - \lambda_j^2} & \text{if} \quad \lambda_i \neq \lambda_j \\ = \square_{ii} - \square_{ij} & \text{if} \quad \lambda_i = \lambda_j \end{cases} \tag{3.32}$$

9. Update the stress and elastic tensor to ABAQUS

10. detailed derivation of elastic tensor given in Appendix

3.8. Comparison between the proposed model with the existing models:

Fig 3.3 summarizes the R^2 values for different models. Coefficients of all the models are determined using uniaxial tension data. It can be seen that R^2 in tension of all the models are almost the same in tension except NH model. But in compression, the proposed model has the highest R^2 value. Fig.3.4 shows the R^2 values when compression data is used to predict these models. It can be observed that only Vander Waals and proposed models are able to capture the tension data. Among these two, the proposed model has the highest R^2 value. Fig.3.5 summarizes the R^2 values when both uniaxial tension and compression data are used to predict the models. It can be seen that vanderwaals has the highest correlation along with the proposed models.

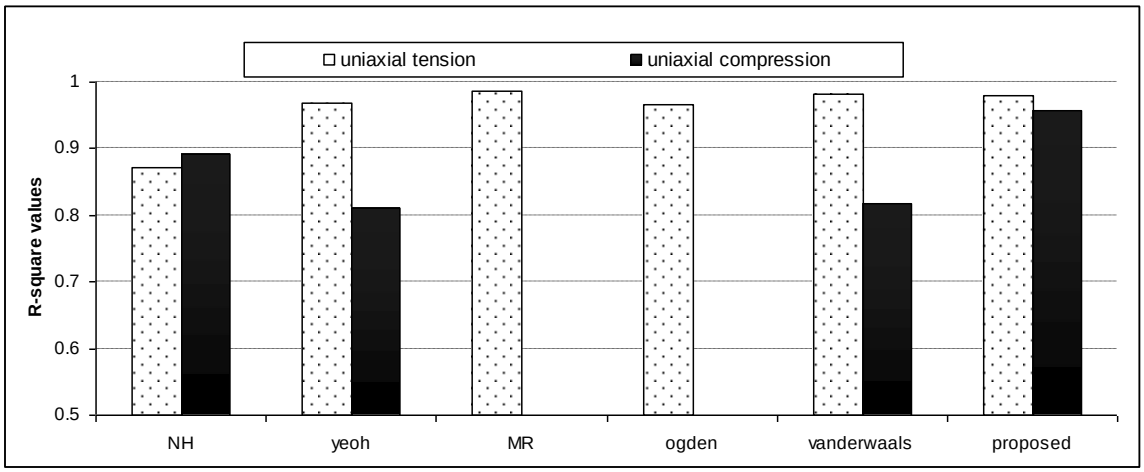

Fig.3.3. Comparison of R^2 value of NH, Yeoh, MR, Ogden, Vander Waals and proposed models in uniaxial tension and compression. Models coefficients are determined using uniaxial tension data

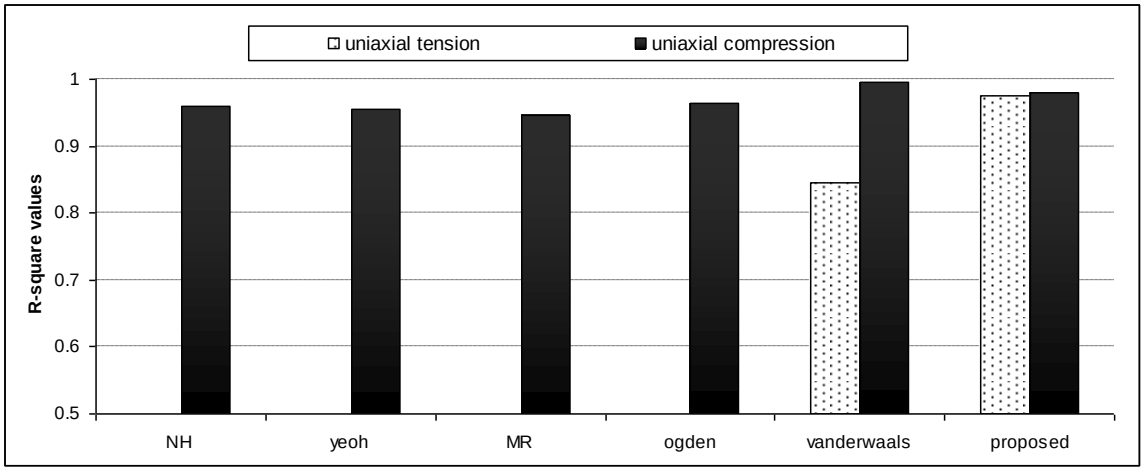

Fig.3.4 Comparison of R^2 value of NH, Yeoh, MR, Ogden, Vander Waals and proposed models in uniaxial tension and compression. Models coefficients are determined using uniaxial compression data

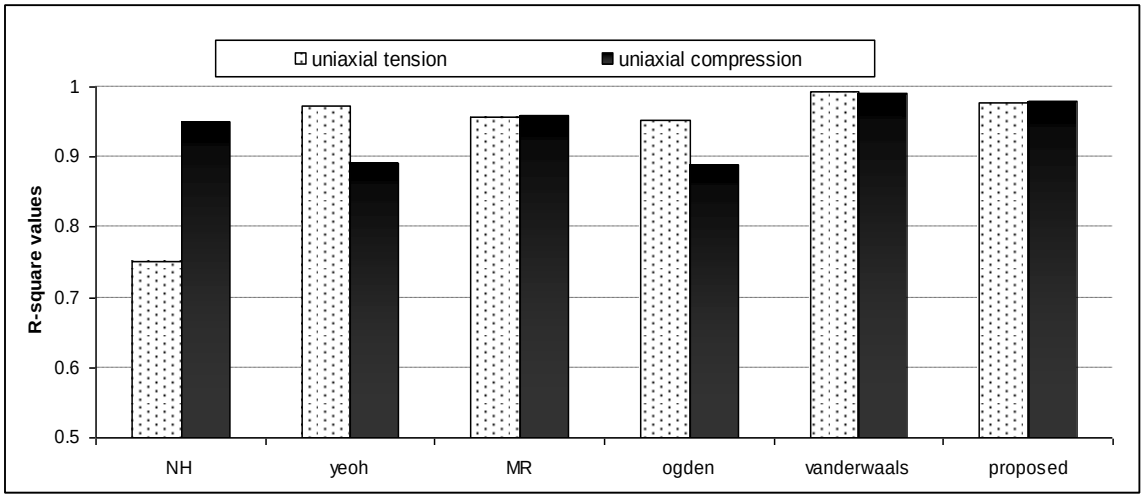

Fig.3.5 Comparison of R^2 value NH, Yeoh, MR, Ogden, Vander Waals and proposed models in uniaxial tension and compression. Models coefficients are determined using both uniaxial tension and compression test data.

3.9. The coefficients of proposed model using uniaxial test data

Eq. (3.25) reduced in case of uniaxial tension (or compression) using eq. (2.4) to eq.(2.6)

$$\sigma_u = \frac{162C_1}{\alpha I_1^3 + (1-\alpha) I_2^3}\left\{\alpha I_1^2\left(\lambda^2 - \frac{1}{\lambda}\right) + (1-\alpha) I_2^2\left(\lambda - \frac{1}{\lambda^2}\right)\right\} \qquad (3.33)$$

If one test data (uniaxial tension or uniaxial compression) is available convert the data into stretch verses true stress (or nominal stress) keep the α value is 0.5 and curve fit in matlab determine the constant C_1 value.

If uniaxial tension and uniaxial compression both data are available convert the data into stretch verses true stress (or nominal stress) keep the α value limits as zero to one and the fit the eq. (3.13) using curve fit in matlab determine the C_1 and α values.

3.10. Conditions satisfied by proposed stored energy function:

The volumetric part of stored energy function well known term. The proposed deviatoric part of stored energy function is checking the necessary conditions to be satisfied.

a) Normality condition, in reference configuration (F=I) deviatoric part first and second invariants are given by

$$\bar{I}_1 = 3 \quad \text{if } F = I \tag{3.34a}$$

$$\bar{I}_1 > 3 \quad \text{if } F \neq I \tag{3.34b}$$

$$\bar{I}_2 = 3 \quad \text{if } F = I \tag{3.35a}$$

$$\bar{I}_2 > 3 \quad \text{if } F \neq I \tag{3.35b}$$

First and second invariants (3.34a), (3.35a) substitute in equation (3.25).

$$\psi_{dev} = C_1 * \ln\left(\frac{\alpha 3^{3k} + (1-\alpha)3^{3k}}{3^{3k}}\right) = \ln(1) = 0 \tag{3.36}$$

So the proposed deviatoric function is satisfies the normality condition

b) Growth condition, in eq(3.9) the first and second condition

If $\det(F) \to \infty \Rightarrow \lambda_1\lambda_2\lambda_3 \to \infty \Rightarrow \lambda_1 \text{ or } \lambda_2 \text{ or } \lambda_3 \to \infty \Rightarrow \bar{\lambda}_1 \text{ or } \bar{\lambda}_2 \text{ or } \bar{\lambda}_3 \to \infty$

If $\det(F) \to 0 \Rightarrow \lambda_1\lambda_2\lambda_3 \to 0 \Rightarrow \lambda_1 \text{ or } \lambda_2 \text{ or } \lambda_3 \to 0 \Rightarrow \bar{\lambda}_1 \text{ or } \bar{\lambda}_2 \text{ or } \bar{\lambda}_3 \to 0$

For $\bar{\lambda}_1 \to 0 \text{ or } \infty$, the invariants are tends to infinite

$$\bar{I}_1 = \bar{\lambda}_1^2 + \bar{\lambda}_2^2 + \frac{1}{\bar{\lambda}_1^2 \bar{\lambda}_2^2} \to +\infty \qquad (3.37a)$$

$$\bar{I}_2 = \frac{1}{\bar{\lambda}_1^2} + \frac{1}{\bar{\lambda}_2^2} + \bar{\lambda}_1^2 \bar{\lambda}_2^2 \to +\infty \qquad (3.37b)$$

The stored energy function tends to infinite

$$\psi_{dev} \to C_1 * \ln(+\infty) = +\infty \qquad (3.38)$$

So the proposed deviatoric function is satisfies the growth condition

c) Convexity condition, as we understood stored energy function is not convex function. It is **locally convex** by defining the quasiconvexity.

$$\Phi = \frac{\alpha \bar{I}_1^{3k} + (1-\alpha)\bar{I}_2^{3k}}{3^{3k}} \qquad (1 \le k \le \infty)$$

For $\alpha \in (0,1)$ the function Φ is satisfies the Polyconvex condition (Hartmann and Neff, 2003). If Φ is convex, it is may or may not be a logarithmic convex. Because of more number of parameters involved in elastic tensor (detailed derivation of elastic tensor given in appendix) it is difficult to prove the function is quasiconvex. Depending upon properties of $\Phi\ (\ge 1 \text{ and convex})$ a simple equallent function is assumed as

$$\Phi' = 1 + a * x^{2n}$$

It is easy to prove Φ' is log-convex in domain of ($1 \le 1 + a * x^{2n} \le 2n$).

Similarly the function Φ is log-convex in domain of $1 \le \Phi = \frac{\alpha \bar{I}_1^{3k} + (1-\alpha)\bar{I}_2^{3k}}{3^{3k}} \le 3k$.

For small strains **(** $\leq 50\%$), all possible deformations Φ value less than 3k. So the proposed function ψ_{dev} is quasiconvex. Quasiconvexity condition of ψ_{dev} automatically satisfies the elastic tensor to positive define in that range.

3.11. Summary:

In this chapter a new stored energy function is proposed and compared with existing models by calculating the r-square values. The proposed model checked for necessary condition to be satisfied by stored energy function. Proposed model implemented in ABAQUS/standard using UMAT option. Detailed steps are given for finite element implementation.

CHAPTER 4

FINITE STRAIN VISCOELASTIC MODELS

4.1. Introduction:

Viscoelastic constitutive models are used to define the rate dependent behaviour. As per Haupt (2000) rate dependent behaviour can be defined using functional with fading memory and representing by means of the internal variables. In two cases total stress is spilt into elastic part and inelastic part. In this work we are only concentrating only internal variables concepts.

4.2. Representing by means of internal variables:

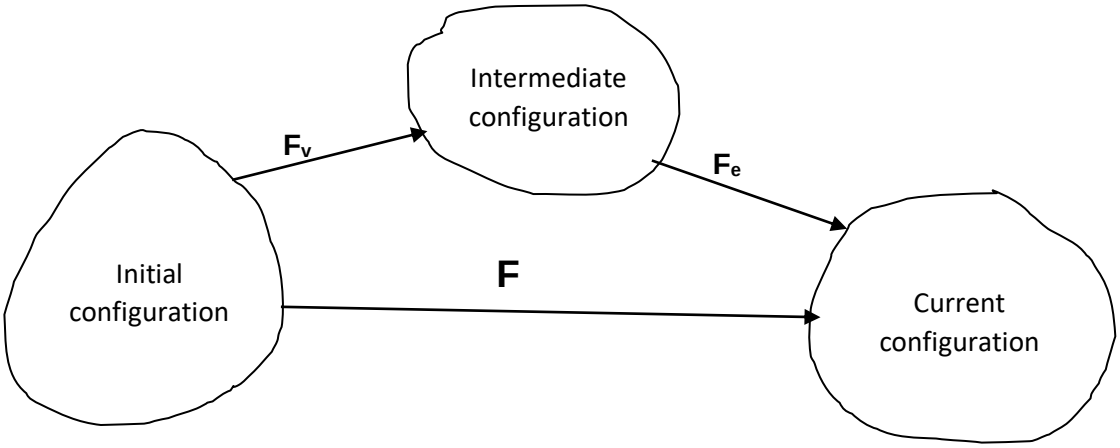

Fig.3.1. Pictorial representation of multiplicative decomposion of deformation gradient

In this total strain additively decomposed into elastic part and viscoelastic (inelastic) part. In 3-D Equallent to this is multiplicative decomposion of deformation gradient ($\mathbf{F}$) to elastic part ($\mathbf{F}_e$) and viscoelastic part ($\mathbf{F}_v$) by introducing intermediate configuration (Lion, 1997b; Lin and Schomburg, 2003).schematic representation of multiplicative deformation shown in fig.3.1.

$$\mathbf{F} = \mathbf{F}_e \mathbf{F}_v \tag{4.1a}$$

4.2.1. Strain tensors:

Introduction intermediate configuration is purely imaginary. The decomposition of deformation gives rise to other deformation tensors which are defined with respect reference, intermediate and current configuration and $\mathbf{N}_a$, $\hat{\mathbf{N}}_a$, $\mathbf{n}_a$ are the eigen vectors.

Right cauchy Green of deformation tensor

$$\mathbf{C} = \mathbf{F}^T\mathbf{F} = \sum_{a=1}^{3} \lambda_a^2 \, \mathbf{N}_a \otimes \mathbf{N}_a \tag{4.1b}$$

Elastic part of right cauchy Green deformation tensor

$$\mathbf{C}_e = \mathbf{F}_e^T\mathbf{F}_e = \sum_{a=1}^{3} \lambda_{ae}^2 \, \hat{\mathbf{N}}_a \otimes \hat{\mathbf{N}}_a \tag{4.2}$$

Inelastic part of right cauchy Green deformation tensor

$$\mathbf{C}_v = \mathbf{F}_v^T\mathbf{F}_v = \sum_{a=1}^{3} \lambda_{av}^2 \, \mathbf{N}_a \otimes \mathbf{N}_a \tag{4.3}$$

Left cauchy Green of deformation tensor

$$\mathbf{b} = \mathbf{F}\mathbf{F}^T = \sum_{a=1}^{3} \lambda_a^2 \, \mathbf{n}_a \otimes \mathbf{n}_a \tag{4.4}$$

Elastic part of left cauchy Green deformation tensor

$$\mathbf{b}_e = \mathbf{F}_e\mathbf{F}_e^T = \sum_{a=1}^{3} \lambda_{ae}^2 \, \mathbf{n}_a \otimes \mathbf{n}_a \tag{4.5}$$

Inelastic part of left cauchy Green deformation tensor

$$\mathbf{b}_v = \mathbf{F}_v\mathbf{F}_v^T = \sum_{a=1}^{3} \lambda_{av}^2 \, \hat{\mathbf{N}}_a \otimes \hat{\mathbf{N}}_a \tag{4.6}$$

Where, λ_a^2, λ_{ae}^2 and λ_{av}^2 are the eigen values of total ,elastic and viscoelastic part cauchy deformation tensors. It is well known that left and right cauchy deformation tensors have the same eigen vectors. Subscript a represents the 1, 2, 3.

True strain

$$\varepsilon_a = \ln(\lambda_a) \tag{4.7}$$

Elastic part

$$\varepsilon_{ae} = \ln(\lambda_{ae}) \tag{4.8}$$

Inelastic part

$$\varepsilon_{av} = \ln(\lambda_{av}) \tag{4.9}$$

Solid like viscoelastic materials can be represented using generalized Maxwell element or generalized Kelvin element though, these models behaviour is same in loading, they are different in unloading. In this chapter detailed development of finite strain Maxwell and Kelvin models are described. Finite strain Maxwell model well developed in literature (Reese and Govindjee, 1998), Kelvin model is not been proposed for finite strain using internal variables concept upto the date. For sake of completeness development of Maxwell model given briefly.

4.3. Maxwell model (Generalized Maxwell model):

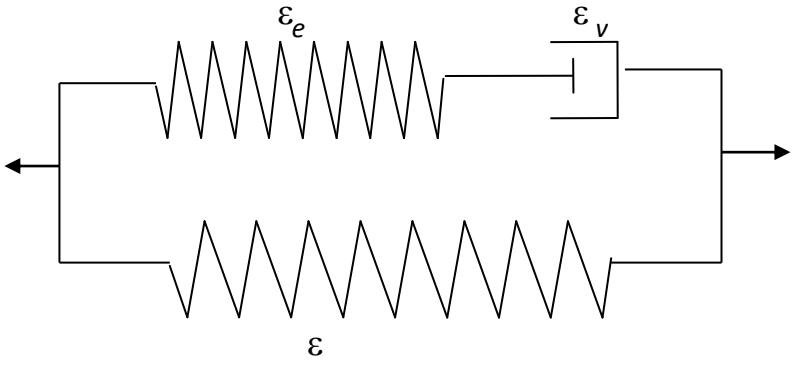

Fig.3b 1-D Representation of the Generalised Maxwell model

Maxwell model starts with assuming the stored energy can be additively decomposed into elastic and inelastic part. Elastic part is function of $\mathbf{C}$, and inelastic part is function of $\mathbf{C}_e$

$$\psi = \psi_e(\mathbf{C}) + \psi_m(\mathbf{C}_e) \tag{4.10}$$

Where ψ represents total energy of model $\psi_e(\mathbf{C})$ represents stored energy of spring which is parallel to Maxwell element and the $\psi_m(\mathbf{C}_e)$ represents the stored energy of spring in Maxwell element. Thermomechanical behaviour of metal are based on energy concept where as solid polymers is based on an entropy concept. So the constitutive equations are consistent with the second law of Thermodynamics which is also known as entropy inequality. Which states the entropy production for all thermodynamic process is never negative. The global formulation of 2nd law of thermodynamics merges into the Clausius-Duhem inequality, neglecting the temperature effects, inequality written as,

$$\mathbf{S}:\frac{1}{2}\dot{\mathbf{C}}-\dot{\psi}\geq 0 \tag{4.11}$$

Eq.(4.10) substituted in the eq.(4.11)

$$\left(\mathbf{S}-2\frac{\partial\psi_e(\mathbf{C})}{\partial\mathbf{C}}-2\mathbf{F}_v^{-1}\frac{\partial\psi_m(\mathbf{C}_e)}{\partial\mathbf{C}_e}\mathbf{F}_v^{-T}\right):\frac{1}{2}\dot{\mathbf{C}}+\frac{\partial\psi_m(\mathbf{C}_e)}{\partial\mathbf{C}_e}:\left(\mathbf{C}_e\mathbf{l}_v+\mathbf{l}_v^T\mathbf{C}_e\right)\geq 0 \tag{4.12}$$

Using Coll & Gurtin (1967) argument

$$\mathbf{S}=2\frac{\partial\psi_e(\mathbf{C})}{\partial\mathbf{C}}+2\mathbf{F}_v^{-1}\frac{\partial\psi_m(\mathbf{C}_e)}{\partial\mathbf{C}_e}\mathbf{F}_v^{-T} \tag{4.13}$$

In Maxwell model stress is additively decomposed into elastic and inelastic part .using the eq.(4.13) in eq.(4.12) residual terms is,

$$2\frac{\partial\psi_m(\mathbf{C}_e)}{\partial\mathbf{C}_e}:\left(\mathbf{C}_e\mathbf{l}_v+\mathbf{l}_v^T\mathbf{C}_e\right)\geq 0 \tag{4.14}$$

eq. (4.14) further reduced into

$$\tau_m:\left(-\frac{1}{2}\mathbf{L}_v(\mathbf{b}_e)\right)\mathbf{b}_e^{-1}\geq 0 \tag{4.15}$$

Where

$$\tau_m=\mathbf{F}_e\frac{\partial\psi_m}{\partial\mathbf{C}_e}\mathbf{F}_e^T \tag{4.16}$$

Eq.(4.15) is represents the dissipation inequality, should satisfy for any arbitrary deformation process. One way of doing eq. (4.15) positive definite is assuming the $\mathbf{L}_v(\mathbf{b}_e)\mathbf{b}_e^{-1}$ is function of τ_m given as

$$-\frac{1}{2}\mathbf{L}_v(\mathbf{b}_e)\mathbf{b}_e^{-1} = \gamma_v^{-1} : \boldsymbol{\tau}_m \tag{4.17}$$

Where γ_v^{-1} is fourth order isotropic tensor defined as

$$\gamma_v^{-1} = \frac{1}{2\eta_d}\left(\mathrm{II} - \frac{1}{3}\mathrm{I}\otimes\mathrm{I}\right) + \frac{1}{9\eta_v}\mathrm{I}\otimes\mathrm{I} \tag{4.18}$$

Eq.(4.17) is evolution equation of Maxwell model, this implicit equation is solved using numerical techniques. It starts with assuming the trail $\mathbf{b_e}$ in elastic predictor step, and spatial velocity gradient (l) is zero inelastic corrector step (Reese and Govindjee ,1998a).

$$\mathbf{L}_v(\mathbf{b}_e) = \dot{\mathbf{b}}_e \tag{4.19}$$

Eq. (3.44) substitute in the eq. (3.43) and integrated equation gives

$$\mathbf{b}_e = \exp\left(-\int_{t_n}^{t_{n+1}}\left(\frac{1}{\eta_d}\mathbf{dev}(\boldsymbol{\tau}_m) + \frac{2}{9\eta_v}\boldsymbol{\tau}_m : \mathbf{I}\right)\mathbf{dt}\right)(\mathbf{b}_e)_{\mathbf{trial}} \tag{4.20}$$

Elastic tensor in reference configuration

$$\square_{\mathbf{ABCD}} = \frac{\partial^2\psi_e}{\partial\mathbf{C}_{\mathbf{AB}}\partial\mathbf{C}_{\mathbf{CD}}} + \left(\mathbf{F}_v^{-1}\right)_{\mathbf{AP}}\left(\mathbf{F}_v^{-1}\right)_{\mathbf{BQ}}\left(\mathbf{F}_v^{-1}\right)_{\mathbf{CR}}\left(\mathbf{F}_v^{-1}\right)_{\mathbf{DS}}\frac{\partial^2\psi_m}{\partial(\mathbf{C}_e)_{\mathbf{PQ}}\,\partial(\mathbf{C}_e)_{\mathbf{RS}}} \tag{4.21}$$

4.4. Kelvin model (Generalized kelvin model):

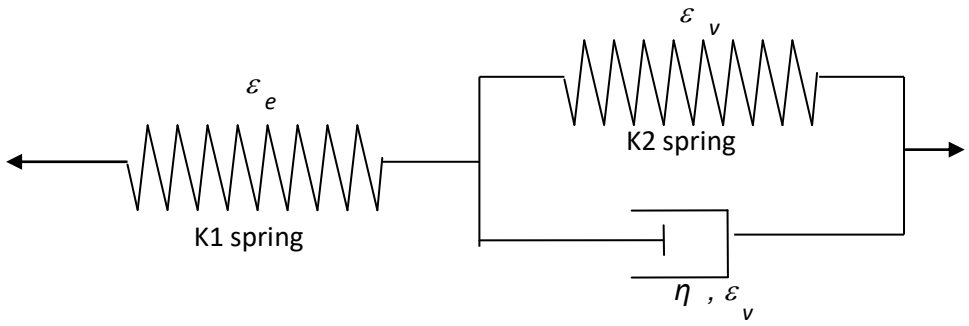

Fig.3c 1-D Representation of the Generalised Kelvin model

In the Kelvin model, as with the Maxwell model, the stored energy can be additively decomposed into elastic and an inelastic part. Unlike Maxwell model , Elastic part is a function of the elastic part of right Cauchy green deformation gradient ($\mathbf{C}_e$), and inelastic part is function of inelastic part of right Cauchy green deformation gradient **($\mathbf{C}_v$)**

$$\psi = \psi_{ke}(\mathbf{C}_e) + \psi_{kv}(\mathbf{C}_v) \tag{4.22}$$

Where ψ represents the total stored energy of the Kelvin model, $\psi_{ke}(\mathbf{C}_e)$ the stored energy of K_1spring, which is in series with the Kelvin element, and $\psi_{kv}(\mathbf{C}_v)$ the stored energy function of K_2spring, which is parallel to the dashpot in the Kelvin element. At the thermodynamic equilibrium dashpot velocity is zero, and the model acts like two springs in parallel. Constitutive equations further should satisfy the second law of thermodynamics. For an isothermal process the second law of thermodynamics can be given in eq (4.10) and substituting the eq.(4.22) into eq.(4.10),

$$\mathbf{S} : \frac{1}{2}\dot{\mathbf{C}} - \frac{\partial \psi_{ke}(\mathbf{C}_e)}{\partial \mathbf{C}_e} : \dot{\mathbf{C}}_e - \frac{\partial \psi_{kv}(\mathbf{C}_e)}{\partial \mathbf{C}_v} : \dot{\mathbf{C}}_v \geq 0 \tag{4.33}$$

Using the equations (1.6) and (1.7) further reduced into

$$\left(\mathbf{S} - 2\mathbf{F}_v^{-1} \frac{\partial \psi_{ke}(\mathbf{C}_e)}{\partial \mathbf{C}_e} \mathbf{F}_v^{-T} \right) : \frac{1}{2}\dot{\mathbf{C}} + \frac{\partial \psi_{ke}(\mathbf{C}_e)}{\partial \mathbf{C}_e} : \left(\mathbf{C}_e \mathbf{l}_v + \mathbf{l}_v^T \mathbf{C}_e \right) - \frac{\partial \psi_{kv}(\mathbf{C}_v)}{\partial \mathbf{C}_v} : \dot{\mathbf{C}}_v \geq 0 \tag{4.34}$$

Using the Coleman and Gurtin (1967) argument it can be concluded from the eq. (4.34) is

$$\mathbf{S} = 2\mathbf{F}_{\mathbf{v}}^{-1}\frac{\partial \psi_{\mathbf{ke}}}{\partial \mathbf{C}_{\mathbf{e}}}\mathbf{F}_{\mathbf{v}}^{-\mathbf{T}} \tag{4.35}$$

Using eq. (4.34) in (4.35) dissipation inequality is

$$2\frac{\partial \psi_{\mathbf{ke}}}{\partial \mathbf{C}_{\mathbf{e}}} : \left(\mathbf{C}_{\mathbf{e}}\mathbf{l}_{\mathbf{v}} + \mathbf{l}_{\mathbf{v}}^{\mathbf{T}}\mathbf{C}_{\mathbf{e}}\right) - \frac{\partial \psi_{\mathbf{kv}}}{\partial \mathbf{C}_{\mathbf{v}}} : \dot{\mathbf{C}}_{\mathbf{v}} \geq 0 \tag{4.36}$$

Using the property that the stress and strain have the same eigen vectors, one can see that $\hat{\mathbf{S}}_{\mathbf{ke}}\mathbf{C}_{\mathbf{e}} = \mathbf{C}_{\mathbf{e}}\hat{\mathbf{S}}_{\mathbf{ke}}$ and thus the symmetry property of $\mathbf{C}_{\mathrm{e}}$. Introducing $\mathbf{C}_{\mathrm{v}}$ $\hat{\mathbf{S}}_{\mathbf{ke}}, \hat{\boldsymbol{\tau}}_{\mathbf{kv}}$ and $\dot{\mathbf{C}}_{\mathrm{v}}$ in eq.(4.36) further reduced into (Reese and Govindgee ,1998a)

$$\left(\hat{\mathbf{S}}_{\mathbf{ke}}\mathbf{C}_{\mathbf{e}} - \hat{\boldsymbol{\tau}}_{\mathbf{kv}}\right) : \mathbf{l}_{\mathbf{v}} \geq 0 \tag{4.37}$$

where, $\hat{\mathbf{S}}_{\mathbf{e}}$ is 2nd PK type and $\hat{\boldsymbol{\tau}}_{\mathbf{kv}}$ is Cauchy type stresses with respect to an intermediate configuration, defined as

$$\hat{\mathbf{S}}_{\mathbf{ke}} = 2\frac{\partial \psi_{\mathbf{ke}}(\mathbf{C}_{\mathbf{e}})}{\partial \mathbf{C}_{\mathbf{e}}} \tag{4.38}$$

$$\hat{\boldsymbol{\tau}}_{\mathbf{kv}} = 2\mathbf{F}_{\mathrm{v}}\frac{\partial \boldsymbol{\psi}_{\mathbf{kv}}(\mathbf{C}_{\mathrm{v}})}{\partial \mathbf{C}_{\mathrm{v}}}\mathbf{F}_{\mathrm{v}}^{\mathrm{T}} \tag{4.39}$$

Utilizing the symmetry property of $\hat{\boldsymbol{\tau}}_{\mathrm{v}}$, rewriting the eq.(2.4)

$$\left(\mathbf{F}_{\mathbf{e}}\hat{\mathbf{S}}_{\mathbf{ke}}\mathbf{F}_{\mathbf{e}}^{\mathbf{T}} - \mathbf{F}_{\mathbf{e}}\hat{\boldsymbol{\tau}}_{\mathbf{kv}}\mathbf{F}_{\mathbf{e}}^{-1}\right) : \mathbf{F}_{\mathbf{e}}\mathbf{l}_{\mathbf{v}}\mathbf{F}_{\mathbf{e}}^{-1} \geq 0 \tag{4.40}$$

$\mathbf{F}_{\mathbf{e}}\mathbf{l}_{\mathbf{v}}\mathbf{F}_{\mathbf{e}}^{-1}$ can be divided into a symmetric part and a skew symmetric part. Because stress is symmetry, skew symmetry part of $\mathbf{F}_{\mathbf{e}}\mathbf{l}_{\mathbf{v}}\mathbf{F}_{\mathbf{e}}^{-1}$ do not play role in the equation (4.40) and symmetry part of $\mathbf{F}_{\mathbf{e}}\mathbf{l}_{\mathbf{v}}\mathbf{F}_{\mathbf{e}}^{-1}$ can be written as $-\frac{1}{2}\mathbf{L}_{\mathrm{v}}(\mathbf{b}_{\mathbf{e}})\mathbf{b}_{\mathbf{e}}^{-1}$ is substitute in the eq.(4.40), it will be reduces into

$$\left(\boldsymbol{\tau}_{ke}-\boldsymbol{\tau}_{kv}\mathbf{b}_e^{-1}\right):\left(-\frac{1}{2}\mathbf{L}_v(\mathbf{b}_e)\mathbf{b}_e^{-1}\right)\geq 0 \tag{4.41}$$

Where $\boldsymbol{\tau}_e$, $\boldsymbol{\tau}_v$ are the weighted Cauchy stresses in the current configuration, defined as

$$\boldsymbol{\tau}_e=\mathbf{F}_e\hat{\mathbf{S}}_e\mathbf{F}_e^T \tag{4.42}$$

$$\boldsymbol{\tau}_v=\mathbf{F}_e\hat{\boldsymbol{\tau}}_{kv}\mathbf{F}_e^T \tag{4.43}$$

The rate of deformation tensor, D represents the total strain rate, decomposed into, elastic $\mathbf{D}_e$ and inelastic strain rate $-\frac{1}{2}\mathbf{L}_v(\mathbf{b}_e)\mathbf{b}_e^{-1}$

$$\mathbf{D}=\mathbf{D}_e+\left(-\frac{1}{2}\mathbf{L}_v(\mathbf{b}_e)\mathbf{b}_e^{-1}\right) \tag{4.44}$$

Assuming positive definiteness, $-\frac{1}{2}\mathbf{L}_v(\mathbf{b}_e)\mathbf{b}_e^{-1}$ can be treated as a function of $\left(\boldsymbol{\tau}_{ke}-\boldsymbol{\tau}_{kv}\mathbf{b}_e^{-1}\right)$, let

$$-\frac{1}{2}\mathbf{L}_v(\mathbf{b}_e)\mathbf{b}_e^{-1}=\boldsymbol{\gamma}_v^{-1}:\left(\boldsymbol{\tau}_{ke}-\boldsymbol{\tau}_{kv}\mathbf{b}_e^{-1}\right) \tag{4.45}$$

where

$$\gamma_v^{-1}=\frac{1}{2\eta_d}\left(\mathrm{II}-\frac{1}{3}\mathrm{I}\otimes\mathrm{I}\right)+\frac{1}{9\eta_v}\mathrm{I}\otimes\mathrm{I} \tag{4.46}$$

Where η_d, η_v represents the coefficients of viscosity, if are constants η_d , η_v in Equation (4.46), then there is a linear relation between inelastic stress and inelastic strain rate and the model is called finite strain linear Maxwell model. Nonlinearity can be introduced by assuming the η_d, η_v and as function of inelastic strain and strain rate.

Eq (4.45) is an evolution equation and the numerical integration of eq.(4.45) starts with the elastic corrector step, with the trail elastic left Cauchy deformation tensor assumed as

$$\left(\mathbf{b}_e\right)^{trial}=\mathbf{F}_{n+1}\left(\mathbf{C}_v^{-1}\right)_n\mathbf{F}_{n+1}^T \tag{4.47}$$

And assuming the spatial velocity gradient to be zero in the inelastic corrector step,

$$\frac{1}{2}\mathbf{L}_{\mathbf{v}}(\mathbf{b}_{\mathbf{e}}) = \dot{\mathbf{b}}_{\mathbf{e}} \tag{4.48}$$

Using the eq. (4.48), the eq. (4.45) can be rewritten as,

$$\dot{\mathbf{b}}_{\mathbf{e}}\,\mathbf{b}_{\mathbf{e}}^{-1} = -2\boldsymbol{\gamma}_{\mathbf{v}}^{-1} : \left(\boldsymbol{\tau}_{\mathbf{ke}} - \boldsymbol{\tau}_{\mathbf{kv}}\mathbf{b}_{\mathbf{e}}^{-1}\right) \tag{4.49}$$

Solving the differential eq. (4.49)

$$\mathbf{b}_{\mathbf{e}} = \exp\left(-2\int_{\mathbf{t}=\mathbf{t}_{\mathbf{n}}}^{\mathbf{t}=\mathbf{t}_{\mathbf{n+1}}} \gamma_{\mathbf{v}}^{-1} : \left(\tau_{\mathbf{ke}} - \tau_{\mathbf{kv}}\mathbf{b}_{\mathbf{e}}^{-1}\right)\mathbf{dt}\right)\mathbf{b}_{\mathbf{e}}^{\mathbf{trial}} \tag{4.50}$$

Assuming $\gamma_{\mathbf{v}}^{-1}$ to be isotropic and the first order approximation of the above eq.(4.50) can be given as

$$\mathbf{b}_{\mathbf{e}} = \exp\left(-\Delta\mathbf{t}\left(\frac{1}{\eta_{\mathbf{d}}}\mathbf{dev}\left(\tau_{\mathbf{ke}} - \tau_{\mathbf{kv}}\mathbf{b}_{\mathbf{e}}^{-1}\right) + \frac{2}{9\eta_{\mathbf{v}}}\mathbf{vol}\left(\tau_{\mathbf{ke}} - \tau_{\mathbf{kv}}\mathbf{b}_{\mathbf{e}}^{-1}\right)\right)\right)\mathbf{b}_{\mathbf{e}}^{\mathbf{trial}} \tag{4.51}$$

It is easy to work with the principal coordinate system, where shear components of stress and strain disappear. Eq.(4.51) in the principal coordinate system is given as

$$\lambda_{\mathrm{ae}}^{2} = \exp\left(-\Delta\mathrm{t}\left(\frac{1}{\eta_{\mathrm{d}}}\mathrm{dev}\left(\tau_{\mathrm{ke}} - \tau_{\mathrm{kv}}\right)_{\mathrm{a}} + \frac{2}{9\eta_{\mathrm{v}}}\mathrm{vol}\left(\tau_{\mathrm{ke}} - \tau_{\mathrm{kv}}\right)\right)\right)\left(\lambda_{\mathrm{ae}}^{2}\right)_{\mathrm{trial}} \tag{4.52}$$

Where

$$\mathbf{b}_{\mathbf{e}} == \sum_{\mathbf{a}=1}^{3} \lambda_{\mathbf{ae}}^{2}\,\mathbf{n}_{\mathbf{a}} \otimes \mathbf{n}_{\mathbf{a}} \tag{4.53}$$

$$\tau_{\mathbf{ke}} == \sum_{\mathbf{a}=1}^{3} \underbrace{\lambda_{\mathbf{ae}}\frac{\partial\psi_{\mathbf{ke}}}{\partial\lambda_{\mathbf{ae}}}}_{\tau_{\mathbf{ke}}}\mathbf{n}_{\mathbf{a}} \otimes \mathbf{n}_{\mathbf{a}} \tag{4.54}$$

$$\tau_{\mathbf{kv}}\mathbf{b}_{\mathbf{e}}^{-1} = \sum_{\mathbf{a}=1}^{3} \underbrace{\lambda_{\mathbf{av}}\frac{\partial\psi_{\mathbf{kv}}}{\partial\lambda_{\mathbf{av}}}}_{\tau_{\mathbf{kv}}}\mathbf{n}_{\mathbf{a}} \otimes \mathbf{n}_{\mathbf{a}} \tag{4.55}$$

The evolution eq. (4.45) can be rewritten in terms of true stress and true strain by applying the logarithm to both sides which is given as,

$$\varepsilon_{ae} = -\Delta t\left(\frac{1}{2\eta_d}\left(\mathrm{dev}\left(\tau_{ke}\right)_a - \mathrm{dev}\left(\tau_{kv}\right)_a\right) + \frac{1}{9\eta_v}\mathrm{vol}\left(\tau_{ke} - \tau_{kv}\right)\right) + \left(\varepsilon_{ae}\right)_{trial} \tag{4.56}$$

This is an implicit equation, and can be solved using Newton Rapson method given in next section. Elastic tensor in the reference configuration can be given as

$$\square_{ABCD} = \left(\mathbf{F}_v^{-1}\right)_{AP}\left(\mathbf{F}_v^{-1}\right)_{BQ}\left(\mathbf{F}_v^{-1}\right)_{CR}\left(\mathbf{F}_v^{-1}\right)_{DS}\frac{\partial^2\psi_{ke}}{\partial\left(\mathbf{C}_e\right)_{PQ}\partial\left(\mathbf{C}_e\right)_{RS}} \tag{4.57}$$

4.5. Finite element implementation of Maxwell model:

Maxwell model is implemented in ABAQUS using UMAT option. The algorithm as follows

Global iteration starts with assuming trial $\mathbf{F}_{n+1}$ which is input from ABAQUS

1. Calculate the deviatoric part of $\mathbf{F}_{n+1}$ and **b**

$$\bar{\mathbf{F}}_{n+1} = \mathbf{J}^{-1/3}\mathbf{F}_{n+1} \tag{4.58}$$

$$\bar{\mathbf{b}}_{n+1} = \bar{\mathbf{F}}_{n+1}\bar{\mathbf{F}}_{n+1}^{T} \tag{4.59}$$

2. Calculate the eigen values $\bar{\lambda}^2$ and eigen vectors **n** of $\bar{\mathbf{b}}_{n+1}$

3. Calculate the stress

$$\left(\bar{\tau}\right)_a^i = \frac{\partial\left(\psi\right)_{dev}}{\partial\left(\varepsilon_{ae}\right)_i} = \left(\bar{\lambda}_a\right)_i\frac{\partial\left(\psi\right)_{dev}}{\partial\left(\bar{\lambda}_a\right)_i} \tag{4.60}$$

4. Calculate the $\left(\bar{\mathbf{b}}_e\right)_{trial}$ using following equation

$$\left(\bar{\mathbf{b}}_e\right)_{trial} = \bar{\mathbf{F}}_{n+1}\left(\bar{\mathbf{C}}_v^{-1}\right)_n\bar{\mathbf{F}}_{n+1} \tag{4.61}$$

5. Calculate the eigen values $(\bar{\lambda}_e^2)_{trial}$ and eigen vectors **n**a of $\left(\bar{\mathbf{b}}_e\right)_{\mathbf{trial}}$

6. Calculate the trail true strain $\left(\varepsilon_{ae}\right)_{trial}$ using following equation

$$\left(\varepsilon_{ae}\right)_{trial} = \ln(\bar{\lambda}_{ae})_{trial} \tag{4.62}$$

7. To Calculate $\left(\mathbf{F_e}\right)_{\mathbf{n}+1}$ and $\left(\mathbf{F_v}\right)_{\mathbf{n}+1}$ using the local Newton Rapson method, we start with initial gauss values as

$$\left(\bar{\lambda}_{ae}\right)_i = (\bar{\lambda}_{ae})_{trial} \tag{4.63}$$

$$\left(\varepsilon_e\right)_a^i = \left(\varepsilon_{ae}\right)_{trial} \tag{4.64}$$

Initial gauss value is equallent to trail value, these values changes in loop. Where as trail values will not change in local N-R loop

8. Local Newton Rapson method loop starts here, Calculate the $\tau_{\mathbf{m}}$ using the following equations

$$\left(\bar{\tau}_m\right)_a^i = \frac{\partial\left(\psi_m\right)_{dev}}{\partial\left(\varepsilon_{ae}\right)_i} = \left(\bar{\lambda}_{ae}\right)_i \frac{\partial\psi_m}{\partial\left(\bar{\lambda}_{ae}\right)_i} \tag{4.65}$$

Calculate the error value $\mathbf{r_v}$ using following equation

$$\left(r_v\right)_a^i = \left(\varepsilon_e\right)_a^i + \frac{\Delta t}{\eta_d}\left(\bar{\tau}_m\right)_a^i - \left(\varepsilon_{ae}\right)_{trial} \tag{4.66}$$

9. Check for convergence $\mathbf{r_v}$ < tolerarance, if it is converged go to step 13 , not continue the next steps

10. Calculate the local stiffness matrix using following equation

$$\left(\frac{\partial\left(r_v\right)_a}{\partial\left(\varepsilon_e\right)_b}\right)_i = I + \frac{\Delta t}{\eta_d}\left[\frac{\partial\left(\bar{\tau}_{ke}\right)_a}{\partial\left(\varepsilon_e\right)_b}\right]_i \tag{4.67}$$

11. Calculate the corrected $\left(\varepsilon_e\right)$ and $\left(\varepsilon_v\right)$ using following equation

$$\left(\varepsilon_e\right)_a^{i+1} = \left(\varepsilon_e\right)_a^i + \left(\frac{\partial\left(r_v\right)_a}{\partial\left(\varepsilon_e\right)_b}\right)_i^{-1} \left(\varepsilon_e\right)_b^i \tag{4.68}$$

$$\left(\varepsilon_v\right)_a^{i+1} = \left(\varepsilon\right)_n - \left(\varepsilon_e\right)_a^{i+1} \tag{4.69}$$

12. Calculate the starches from updated true strain using following equations and go to step8

$$\left(\lambda_{ae}\right)_{i+1} = \exp\left(\varepsilon_e\right)_a^{i+1} \tag{4.70}$$

$$\left(\lambda_{av}\right)_{i+1} = \exp\left(\varepsilon_v\right)_a^{i+1} \tag{4.71}$$

13. Calculate the elastic tensor in principal coordinate system

$$\square_{ab} = \square = \frac{\partial^2\left(\psi\right)_{dev}}{\partial\varepsilon_a\partial\varepsilon_b} + \frac{\partial^2\left(\psi_m\right)_{dev}}{\partial\varepsilon_{ae}\partial\varepsilon_{be}} + \frac{2}{D}\left(2J-1\right)J\delta_{ab} \tag{4.72}$$

14. Update the stress and elastic tensor to ABAQUS

Stress components (σ_{ij})

$$\sigma_{ij} = \frac{1}{J}\sum_{a=1}^{3}\left(\overline{\tau} + \overline{\tau}_m\right)_a n_a^i n_a^j + p\delta_{ij} \tag{4.73}$$

where $p = \frac{2}{D}\left(J-1\right)J$

Elastic tensor ($\square_{ijkl}$)

$$\left(\square_{ijkl}^{\sigma T}\right)_{dev} = \sum_{a=1}^{3}\sum_{b=1}^{3}\left(\square_{ab} - 2\left(\overline{\tau} + \overline{\tau}_m\right)_a \delta_{ab}\right) n_a^i n_a^j n_b^k n_b^l + \frac{1}{2}\sum_{a=1}^{3}\sum_{b=1}^{3} g_{ab}\left(n_i^a n_j^b n_k^a n_l^b + n_i^a n_j^b n_k^b n_l^a\right) \tag{4.74}$$

4.6. Finite element implementation of finite strain kelvin model:

Proposed Kelvin model Implemented in ABAQUS using UMAT option. The algorithm as follows

Global iteration starts with assuming trial $\mathbf{F}_{n+1}$ which is input from ABAQUS

1. Calculate the deviatoric part of $\mathbf{F}_{n+1}$ and **C**

$$\bar{\mathbf{F}}_{n+1} = \mathbf{J}^{-1/3}\mathbf{F}_{n+1} \tag{4.75}$$

$$\bar{\mathbf{C}}_{n+1} = \bar{\mathbf{F}}_{n+1}^{T}\bar{\mathbf{F}}_{n+1} \tag{4.76}$$

2. Calculate the eigen values $\bar{\lambda}^2$ and eigen vectors **n** of $\bar{\mathbf{C}}_{n+1}$

3. Calculate the $\left(\bar{\mathbf{b}}_e\right)_{trial}$ using following equation

$$\left(\bar{\mathbf{b}}_e\right)_{trial} = \bar{\mathbf{F}}_{n+1}\left(\bar{\mathbf{C}}_v^{-1}\right)_n \bar{\mathbf{F}}_{n+1} \tag{4.77}$$

4. Calculate the eigen values $(\bar{\lambda}_e^2)_{trial}$ and eigen vectors of $\left(\bar{\mathbf{b}}_e\right)_{trial}$

5. Calculate the trail true strain $\left(\varepsilon_{ae}\right)_{trial}$ using following equation

$$\left(\varepsilon_{ae}\right)_{trial} = \ln(\bar{\lambda}_{ae})_{trial} \tag{4.78}$$

6. To Calculate $\left(\mathbf{F}_e\right)_{n+1}$ and $\left(\mathbf{F}_v\right)_{n+1}$ using the local Newton Rapson method, we start with initial gauss values as

$$\left(\bar{\lambda}_{ae}\right)_i = (\bar{\lambda}_{ae})_{trial} \tag{4.79}$$

$$\left(\bar{\lambda}_{av}\right)_i = (\bar{\lambda}_{av})_n \tag{4.80}$$

7. Local Newton Rapson method loop starts here, Calculatethe τ_{ke} and τ_{kv} using the following equations

$$\left(\bar{\tau}_{ke}\right)_a^i = \frac{\partial\left(\psi_{ke}\right)_{dev}}{\partial\left(\varepsilon_{ae}\right)_i} = \left(\bar{\lambda}_{ae}\right)_i \frac{\partial\psi_{ke}}{\partial\left(\bar{\lambda}_{ae}\right)_i} \tag{4.81}$$

$$\left(\bar{\tau}_{kv}\right)_a^i = \frac{\partial\left(\psi_{kv}\right)_{dev}}{\partial\left(\varepsilon_{av}\right)_i} = \left(\bar{\lambda}_{av}\right)_i \frac{\partial\psi_{kv}}{\partial\left(\bar{\lambda}_{av}\right)_i} \tag{4.82}$$

8. Calculate the error value $\mathbf{r}_v$ using following equation

$$\left(r_v\right)_a^i=\left(\varepsilon_e\right)_a^i+\frac{\Delta t}{\eta_d}\left[\left(\bar{\tau}_{ke}\right)_a^i-\left(\bar{\tau}_{kv}\right)_a^i\right]-\left(\varepsilon_e\right)_{trial} \tag{4.83}$$

9. Check for convergence $\mathbf{r}_v$ < tolerarance, if it is converged go to step 13 , not continue the next steps

10. Calculate the local stiffness matrix using following equation

$$\left(\frac{\partial\left(r_v\right)_a}{\partial\left(\varepsilon_e\right)_b}\right)_i=I+\frac{\Delta t}{\eta_d}\left[\frac{\partial\left(\bar{\tau}_{ke}\right)_a}{\partial\left(\varepsilon_e\right)_b}+\frac{\partial\left(\bar{\tau}_{kv}\right)_a}{\partial\left(\varepsilon_v\right)_b}\right]_i \tag{4.84}$$

11. Calculate the corrected $\left(\varepsilon_e\right)$ and $\left(\varepsilon_v\right)$ using following equation

$$\left(\varepsilon_e\right)_a^{i+1}=\left(\varepsilon_e\right)_a^i+\left(\frac{\partial\left(r_v\right)_a}{\partial\left(\varepsilon_e\right)_b}\right)_i^{-1}\left(\varepsilon_e\right)_b^i \tag{4.85}$$

$$\left(\varepsilon_v\right)_a^{i+1}=\left(\varepsilon\right)_n-\left(\varepsilon_e\right)_a^{i+1} \tag{4.86}$$

12. Calculate the starches from updated true strain using following equations and go to step7

$$\left(\lambda_{ae}\right)_{i+1}=\exp\left(\varepsilon_e\right)_a^{i+1} \tag{4.87}$$

$$\left(\lambda_{av}\right)_{i+1}=\exp\left(\varepsilon_v\right)_a^{i+1} \tag{4.88}$$

13. Calculate the elastic tensor in principal coordinate system

$$\square_{ab}=\frac{\partial^2\left(\psi_{ke}\right)_{dev}}{\partial\varepsilon_{ae}\partial\varepsilon_{be}}+\frac{2}{D}\left(2J-1\right)J\delta_{ab} \tag{4.89}$$

14. Update the following terms to ABAQUS

Stress components (σ_{ij})

$$\sigma_{ij}=\frac{1}{J}\sum_{a=1}^{3}\left(\bar{\tau}_{ke}\right)_a n_a^i n_a^j+p\delta_{ij} \tag{4.90}$$

where $p=\frac{2}{D}\left(J-1\right)J$

Elastic tensor ($\square_{ijkl}$)

$$\left(\square_{ijkl}^{\sigma T}\right)_{dev} = \sum_{a=1}^{3}\sum_{b=1}^{3}\left(\square_{ab} - 2\left(\overline{\tau}_{ke}\right)_a \delta_{ab}\right) n_a^i n_a^j n_b^k n_b^l + \frac{1}{2}\sum_{a=1}^{3}\sum_{b=1}^{3} g_{ab}\left(n_i^a n_j^b n_k^a n_l^b + n_i^a n_j^b n_k^b n_l^a\right) \quad (4.91)$$

4.7. Summary

In this chapter constitutive equations for finite strain Maxwell and Kelvin model are developed using concept of internal variables. Step by step procedure is given to implement the Finite element for these models in ABAQUS using UMAT option. Jacobi iteration method used to adopt the eigen values and eigen vectors.

Chapter 5

RESULTS AND DISCUSSION

5.1. Study on viscoelastic material models

In this section Maxwell and kelvin model behaviour discussed while predicting the loading and unloading behaviour of rubber. Linear Maxwell model developed in Reese and Govindjee (1998a) implemented and fitted with experimental data. Nonlinearity introduced in Maxwell model using Lion function (1996). The result of Kelvin model formulation for finite strain has developed part of thesis. Nonlinearity used in kelvin is similar to Lion (1996). In fig.5.1 shows the experimental data of rubber in loading and unloading with different strain rates 0.000667, 0.00667 and 0.0667 sec^{-1}, the experimental data has been discussed in chapter.1. Fig. 5.2 is experimental data of rubber for large strains with strain rates 0.00667, 0.033 sec^{-1}. The variation and issues while fitting the experimental data with finite strain Maxwell and kelvin model has brought out clearly.

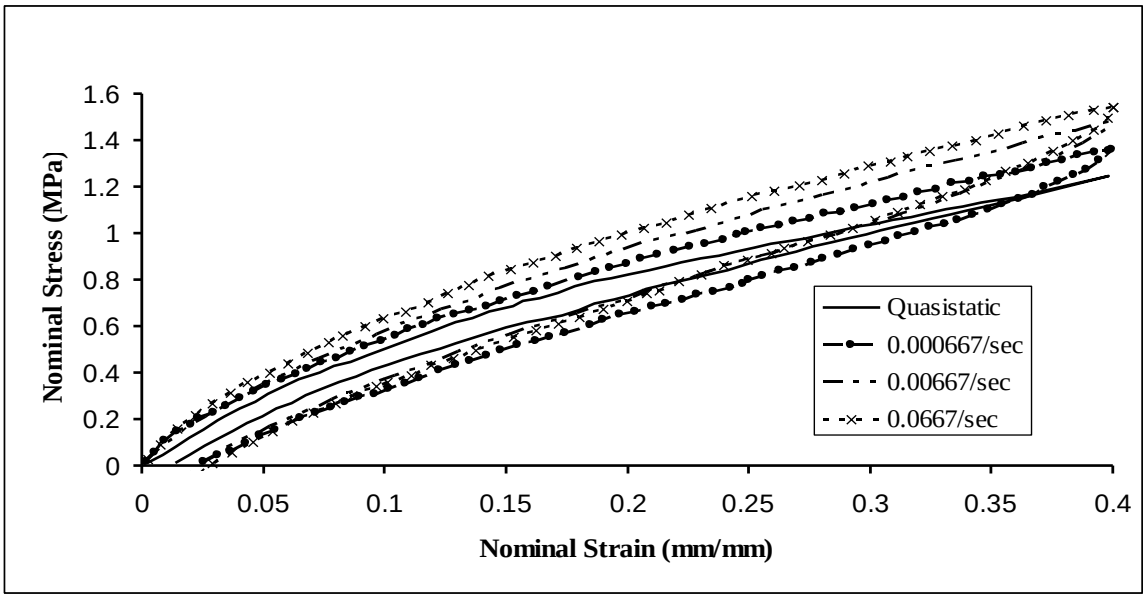

Fig. 5.1. Experimental data of rubber in loading and unloading with different strain rates.

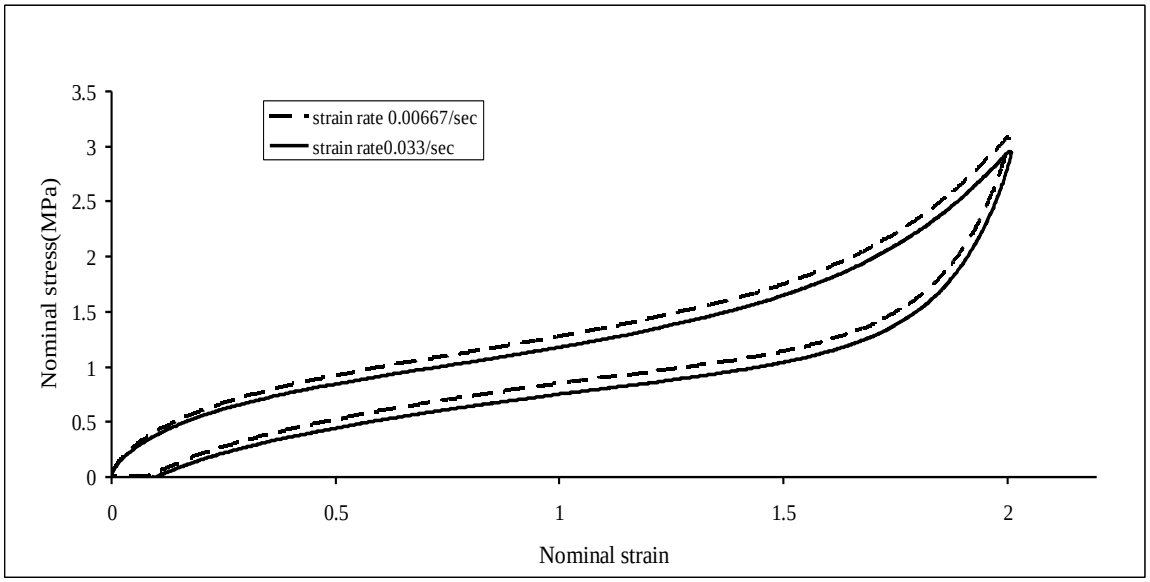

Fig.5.2. Experimental data of rubber in loading and unloading with different strain rates.

5.2. Finite strain linear Maxwell model:

In linear model as discussed in chapter.4 evolution equation (4.36) the viscoelastic coefficients are constants. The coefficients of elastic part are determined using the experimental data of quasistatic test loading data using curve fitting. Other spring coefficient is determined using different strain rate loading paths and a viscous coefficient is determined using loading and unloading data (hysteresis). The experimental data of loading and unloading with different strain rates 0.000667, 0.00667 and 0.0667 sec^{-1} is fitted with a linear model is shown in Fig.5.3-5.5. It can be observed that this model is poor prediction in the loading and unloading behavior because of the linear relation between viscoelastic part of stress and stain. Maxwell model at low strain rate, stress in dashpot zero and effect of Maxwell element is zero. At higher strain rate strain in dashpot zero, total strain strains are taken by spring in Maxwell element it behaves like two elastic springs are in parallel. It means at low and high strain rates Maxwell model behaves like purely elastic. In between strain rates Maxwell model gives the rate dependent behaviour. From fig.5.6, it is shown that rate dependent hysteresis increases with strain rate and then decreases. This kind of decaying with strain rate behaviour not observed in real material. The coefficients are given in table.5.1.

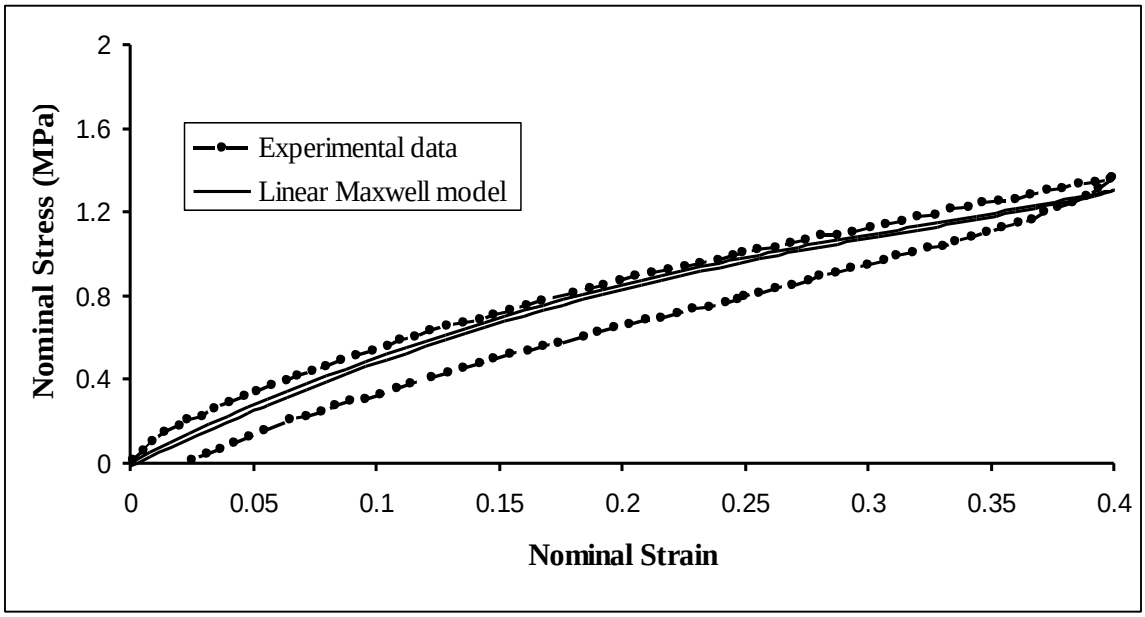

Fig.5.3. Comparison of linear Maxwell model prediction with experimental data at strain rate 0.000667 sec^{-1}.

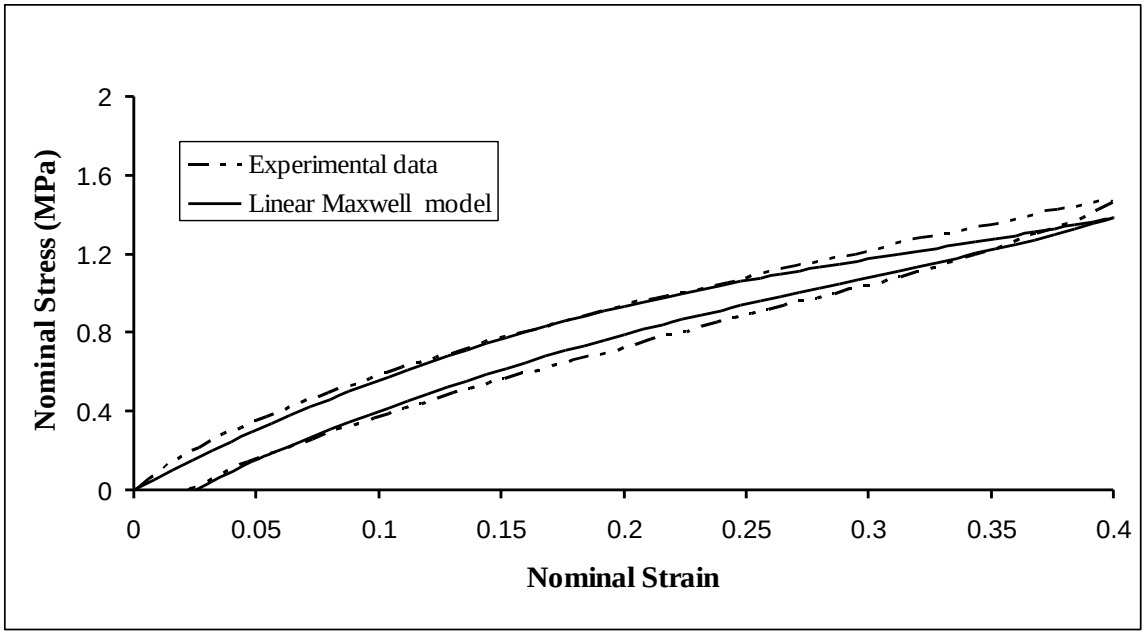

Fig.5.4. Comparison of linear Maxwell model prediction with experimental data at strain rate 0.00667 sec^{-1}

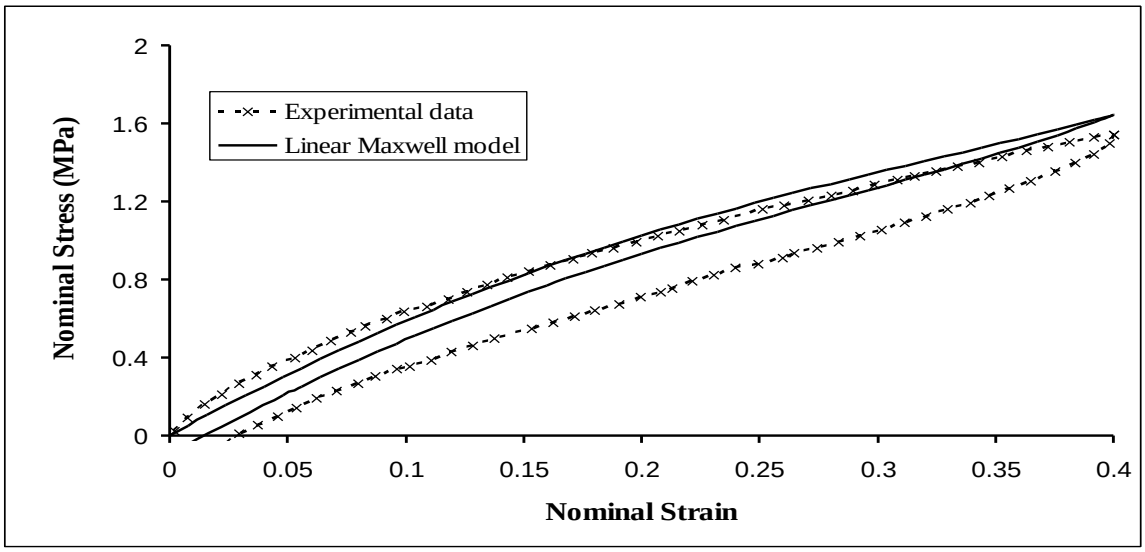

Fig.5.5. Comparison of linear Maxwell model prediction with experimental data at strain rate 0.0667 sec^{-1}

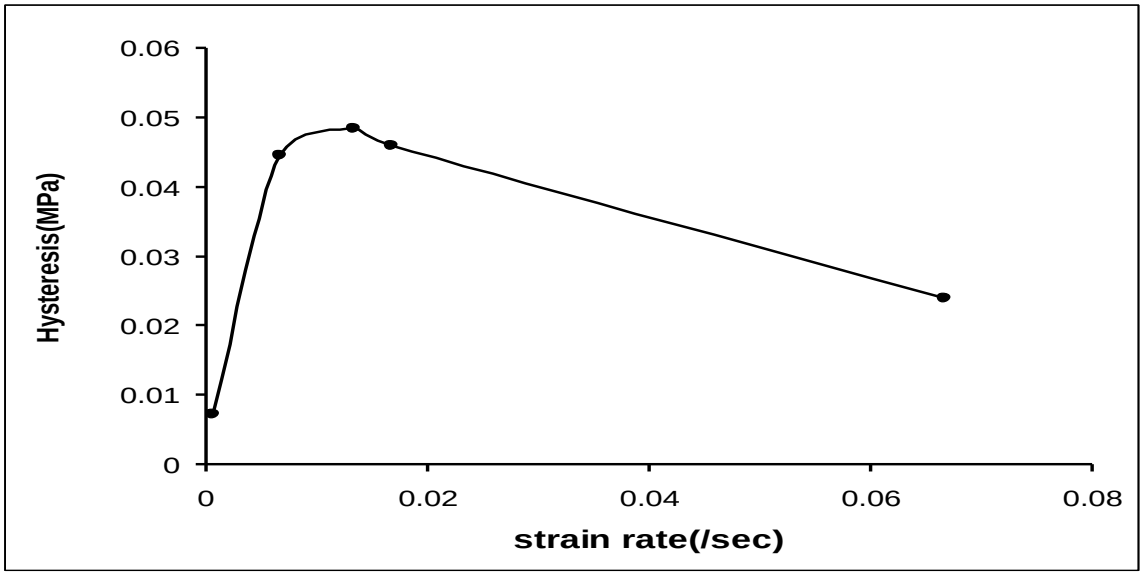

Fig.5.6. Hysteresis varies with strain rate using finite strain linear Maxwell model

In Maxwell model hysteresis is totally controlled by the Maxwell element. The distribution of applied strain into elastic and inelastic strains with different strain rates 0.000667, 0.00667 and 0.0667 sec^{-1} are shown in fig.5.7-5.9. It can be observed that in loading, applied strain rate is positive (in tensile test) correspondingly strain rate in dashpot is positive and increases with applied strain rate. To get the stress equilibrium in Maxwell element elastic strains are positive and increases with strain applied strain rate. In unloading though, the applied strain rate is negative, strain rate in dashpot is positive s because elastic strain existed in Maxwell element (spring) during loading is positive. It takes some time to become negative strain rate in dashpot. The strain at which the negative strain rate in unloading occurs in dashpot increases with applied strain rate. Because of the positive strain rates in the dashpot, the hysteresis loop has a sharp edge at the tip and bulges when the elastic strains become negative. Because of delay in negative strain rate response this model cannot be used to fit the unloading behaviour for large strains (greater than 100% strain). Prediction of experimental data for large strains is shown in fig.5.10.

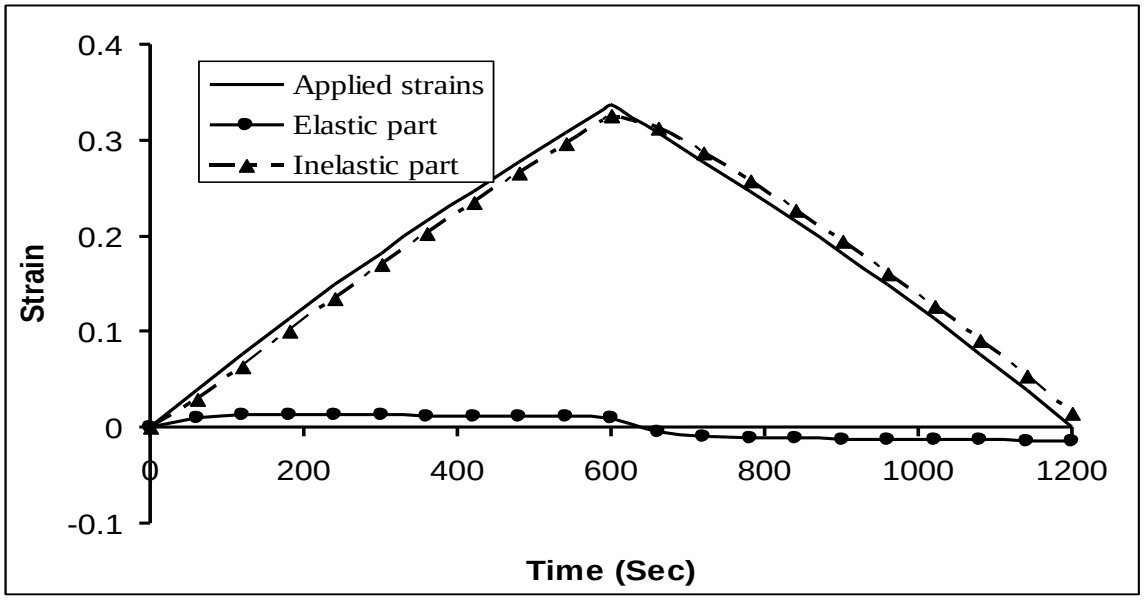

Fig.5.7. The variation in applied strain, elastic and inelastic strains linear Maxwell model at strain rate 0.000667 sec^{-1}

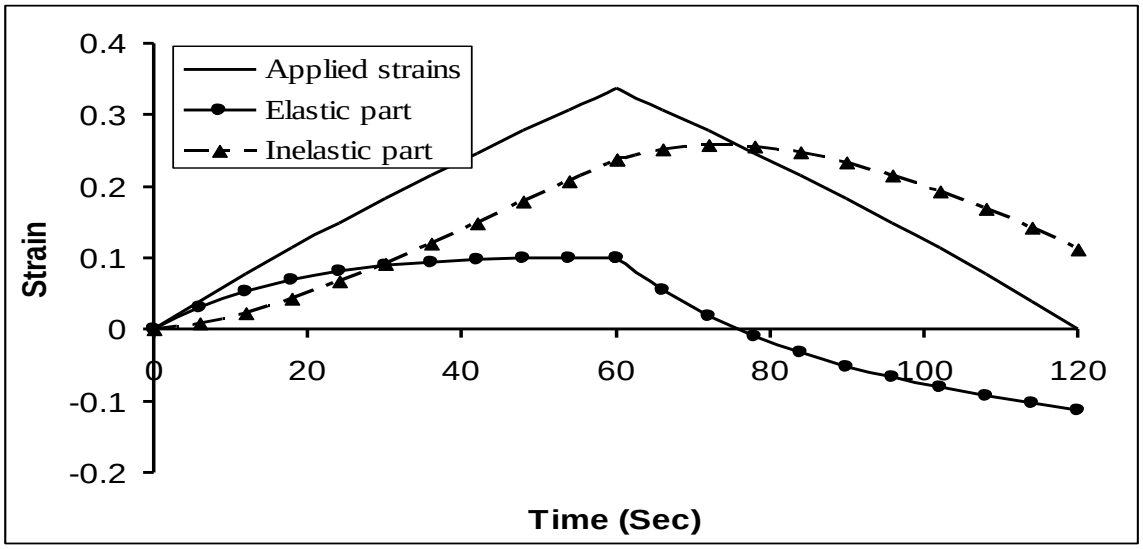

Fig.5.8. The variation in applied strain, elastic and inelastic strains linear Maxwell model at strain rate 0.00667 sec^{-1}

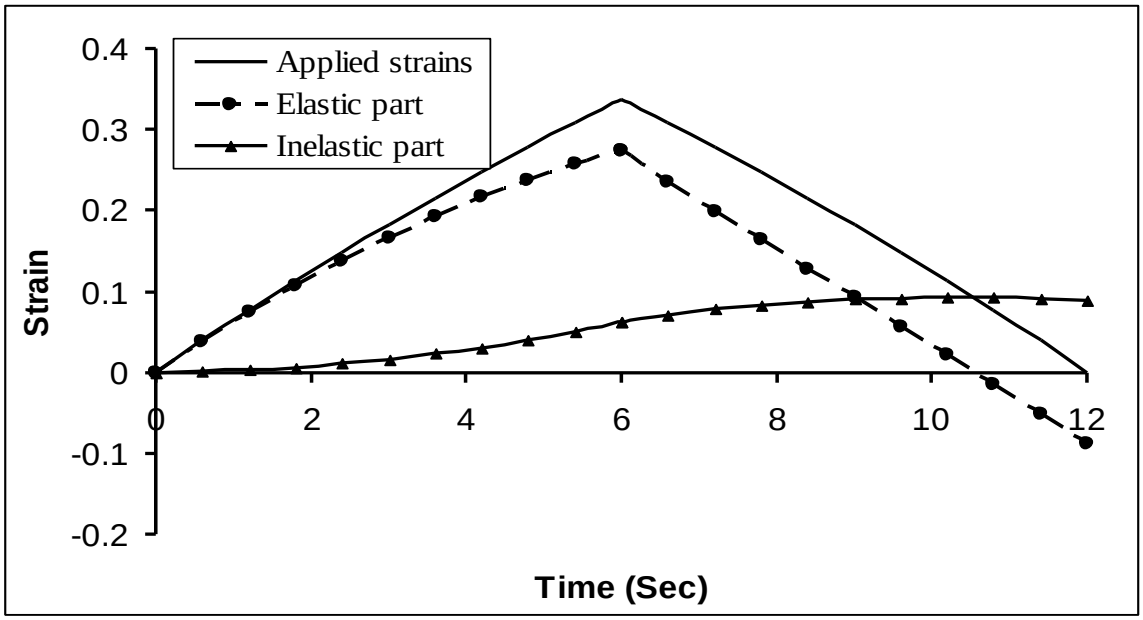

Fig.5.9. The variation in applied strain, elastic and inelastic strains linear Maxwell model at strain rate 0.0667 sec^{-1}

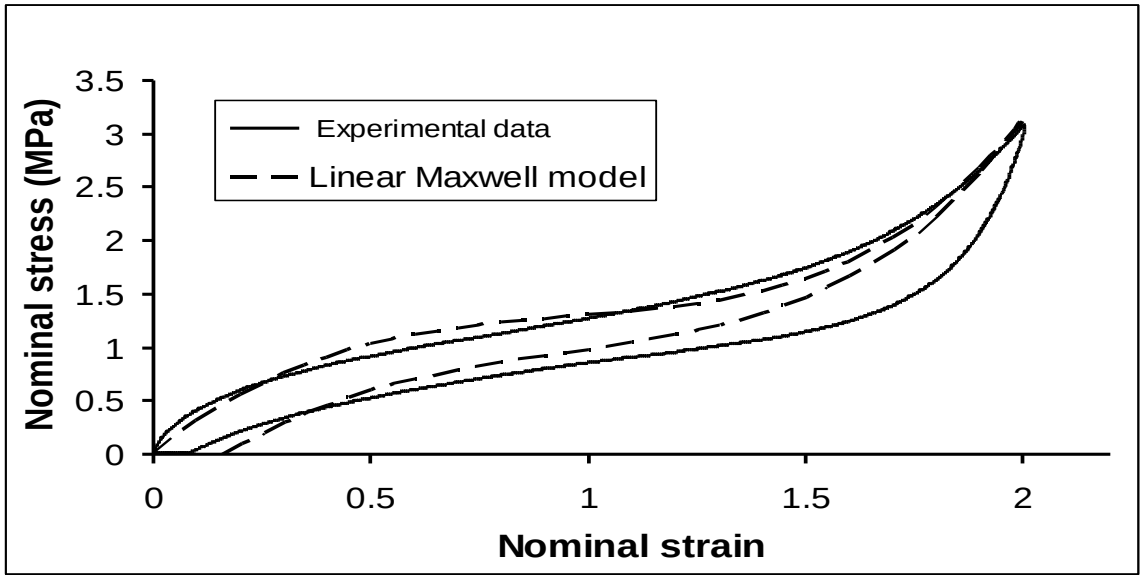

Fig.5.10. Comparison of linear Maxwell model prediction with experimental data at strain rate 0.0667 sec^{-1}

5.3. Finite strain Nonlinear Maxwell model:

As discussed in chapter4, the difference between the linear and nonlinear models is the stress and strain rate relations in the dashpot of the Maxwell element. In linear model, inelastic stress is assumed to vary linearly with strain rate, using a viscoelastic coefficient. In the nonlinear model the viscoelastic coefficient is assumed to be of an exponential from given as: (Lion, 1996)

$$\eta_d = \eta_0 \exp\left(-\frac{\|\tau_m\|}{s_0 \left|C_v^{-1}\right|^3} \right) \qquad (5.1)$$

Where η_0, S_0 are constants. Physical meaning of this function is that the viscoelastic coefficient decays exponentially with strain rate (strain rate represented through stress in the Maxwell element) and increases with strain (strain represented by $\mathbf{C_v}$). Exponential function has chosen to satisfy the second law of Thermodynamics.

Nonlinear model fitted with available experimental data with different strain rates in loading and unloading is shown in fig. 5.11-5.13. It can be observed that nonlinear model predicts the loading behaviour accurately than the linear model. Because the control parameters in case of linear model is

one, where as in nonlinear model the number of control parameters are two. So it is quite possible that nonlinear model predicts the loading behaviour better than linear model. Unloading behaviour is not captured accurately. As discussed in linear model, nonlinear model can be fitted large range of strain rates than linear model. As it can be seen from the fig.5.11 to 5.13 the hysteresis are increasing, where as for same range of strain rate in linear model hysteresis started increasing and decreasing.

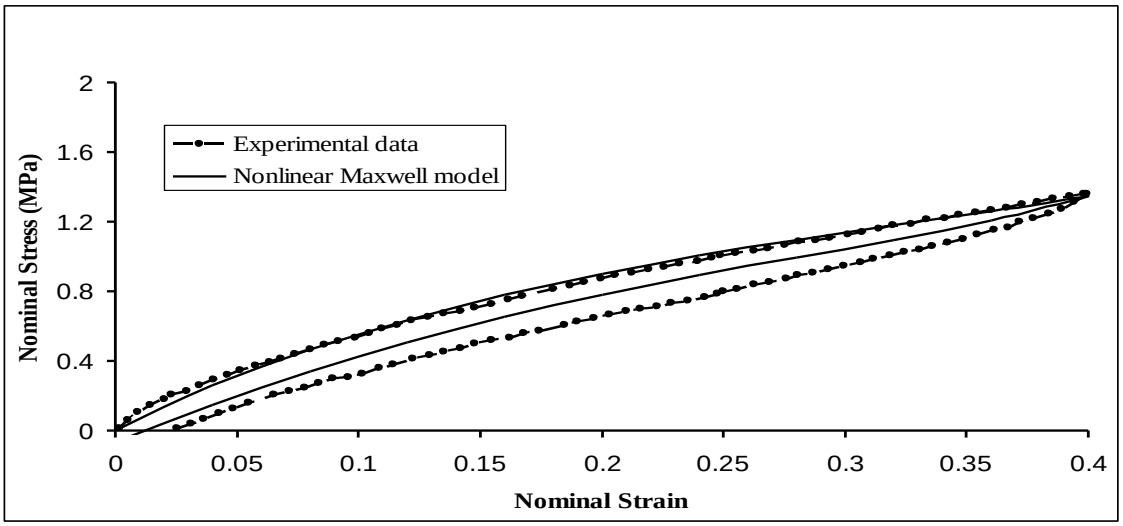

Fig.5.11. Comparison of nonlinear Maxwell model prediction with experimental data at strain rate 0.000667 sec^{-1}

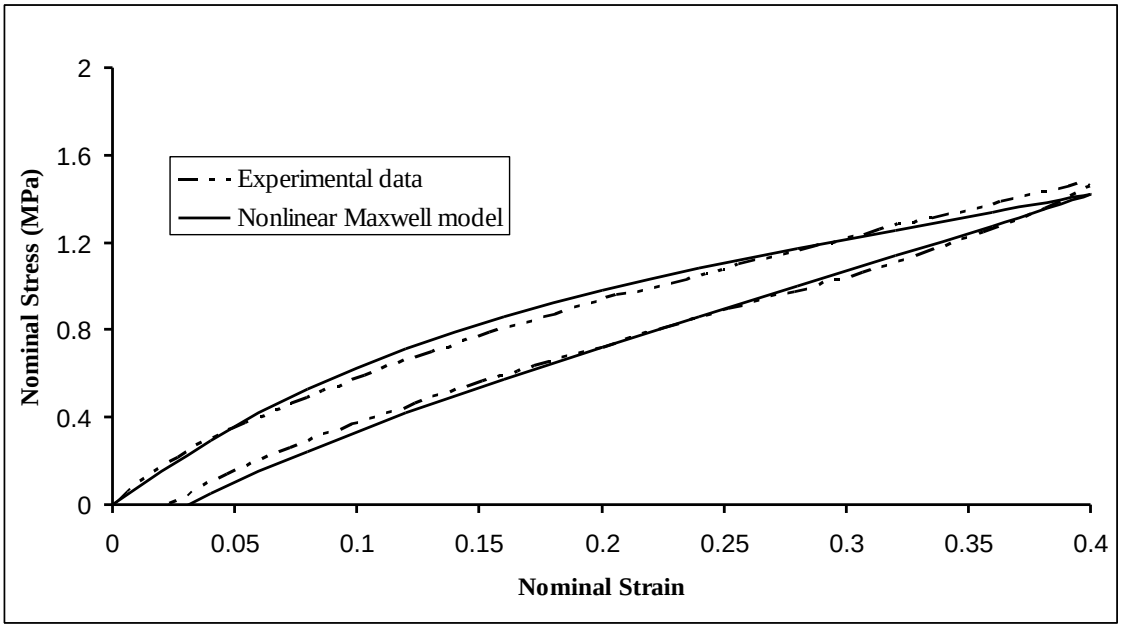

Fig.5.12. Comparison of nonlinear Maxwell model prediction with experimental data at strain rate 0.00667 sec^{-1}

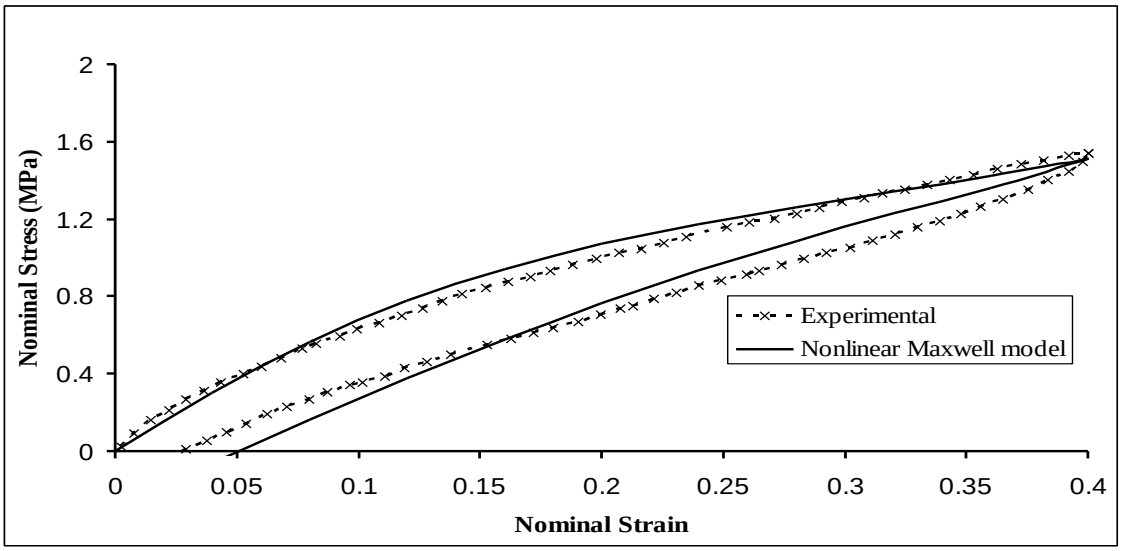

Fig.5.13. Comparison of nonlinear Maxwell model prediction with experimental data at strain rate 0.0667 sec^{-1}

The decomposition of applied strain into elastic and inelastic strains with respect to strain rates 0.000667, 0.00667 and 0.0667 sec^{-1} are shown in fig.5.14-5.16. It can be noticed that the elastic strains and applied strain rates are positive in loading. With strain rate increases, elastic strains are increasing similar to linear model. In unloading, strain rate in the dashpot is positive, though the applied strain rate is negative. The strain at which negative inelastic strains occurs increases with strain rate. Because of that, the model results in a sharp edge at the tip of the hysteresis loop and a bulge as the elastic strains become negative. It can be understood, Maxwell model don't have the ability to obtain negative strain rate in tension and positive strain rates in compression. Existed negative strain rate in tension are virtual. In Linear and nonlinear Maxwell models hysteresis starts increasing initially upto a certain strain rate after which there is a decrease.

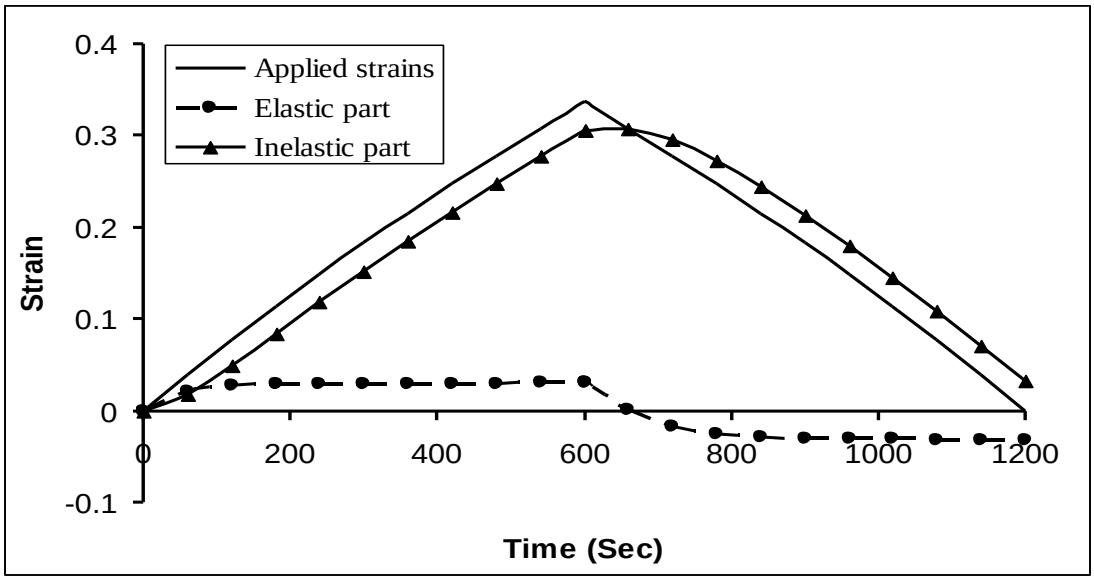

Fig.5.14. The variation in applied strain, elastic and inelastic strains nonlinear Maxwell model at strain rate 0.000667 sec^{-1}

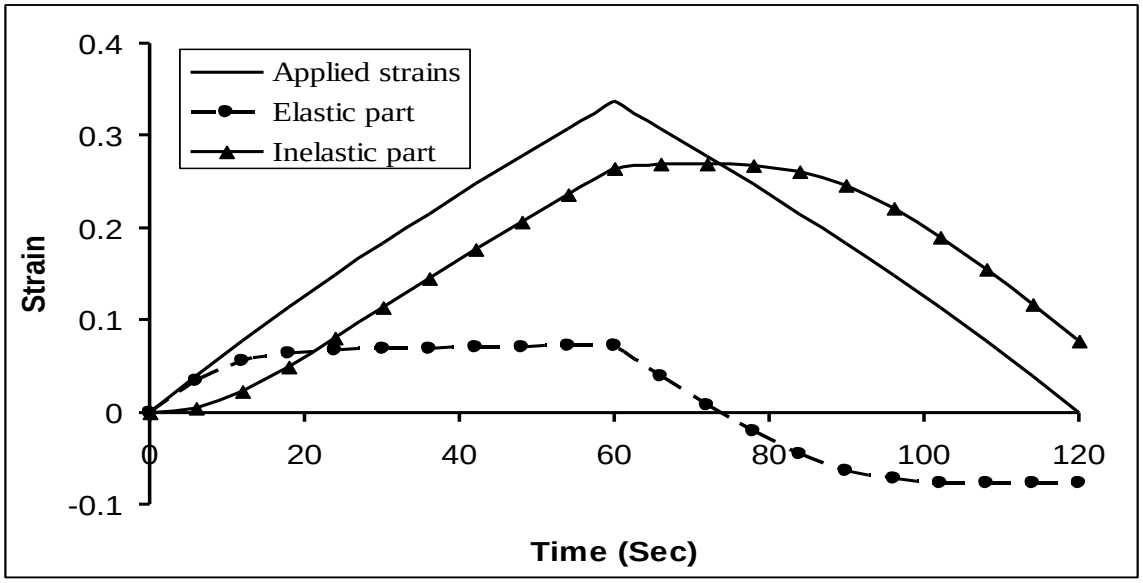

Fig.5.15. The variation in applied strain, elastic and inelastic strains nonlinear Maxwell model at strain rate 0.00667 sec^{-1}

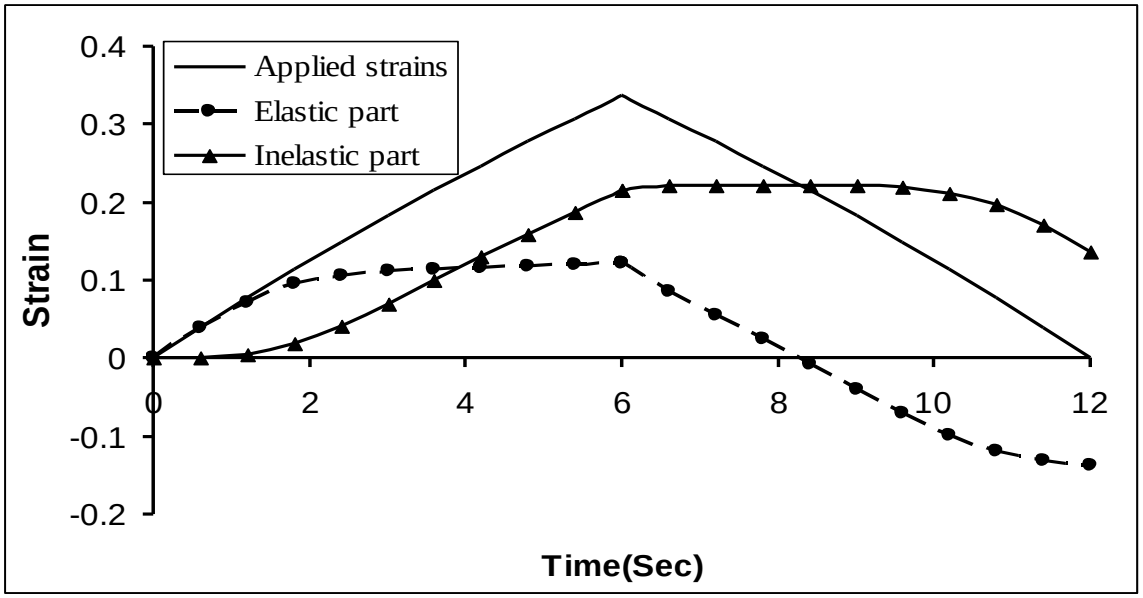

Fig.5.16. The variation in applied strain, elastic and inelastic strains nonlinear Maxwell model at strain rate 0.0667 sec^{-1}

5.4. Finite strain linear Kelvin model:

In this section describes the developed finite strain linear kelvin model, the evolution equation (4.45) represents the relation between stress and strain rate in the dashpot of kelvin model, by assuming the η_d constant in eq. (4.46) linear relation adopted in model. Fig.5.17-5.19 shows the prediction of the loading and unloading behaviour using linear model with strain rates 0.000667, 0.00667, 0.0667 sec^{-1}. It can be observed that the model results in a poor prediction in loading and unloading. The linear Kelvin model behaves similar to the linear Maxwell model in loading. The result is different in unloading, the shape of unloading curve takes different from Maxwell model, and hysteresis loop is expanding the both side of quasistatic loop. Unlike the Maxwell model the hysteresis loop do not have the sharp edges at unloading initiates and bulging is not occurring in loop.

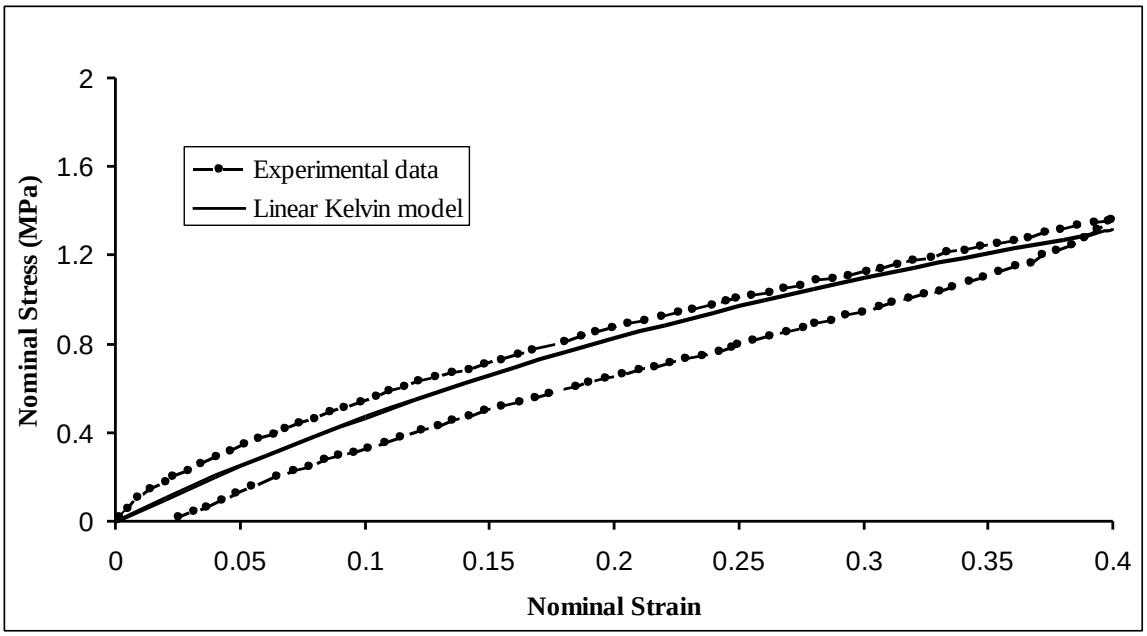

Fig.5.17. Comparison of linear Kelvin model prediction with experimental data at strain rate 0.000667 sec^{-1}

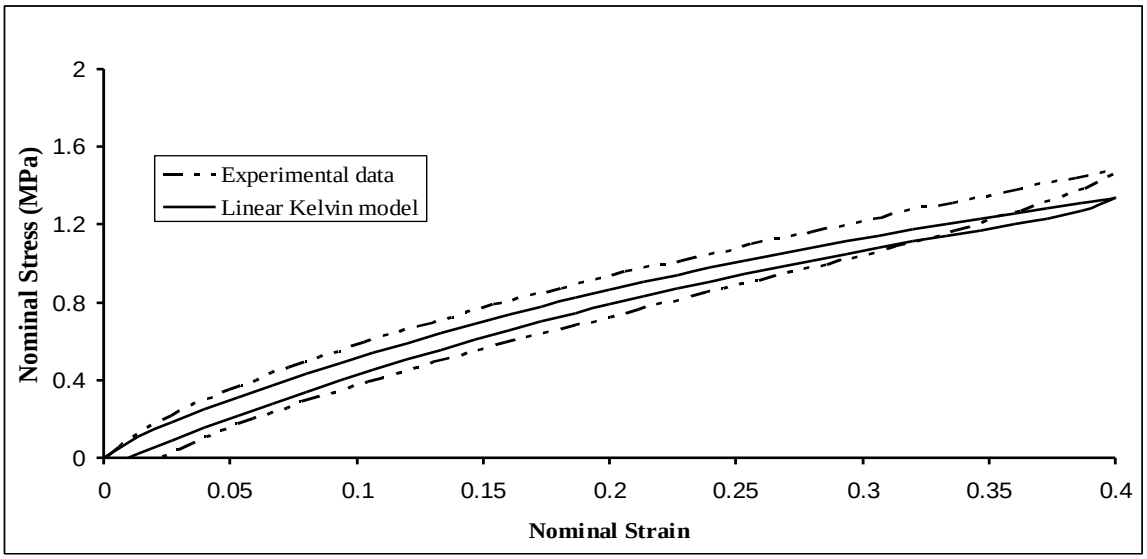

Fig.5.18. Comparison of linear Kelvin model prediction with experimental data at strain rate 0.00667 sec^{-1}

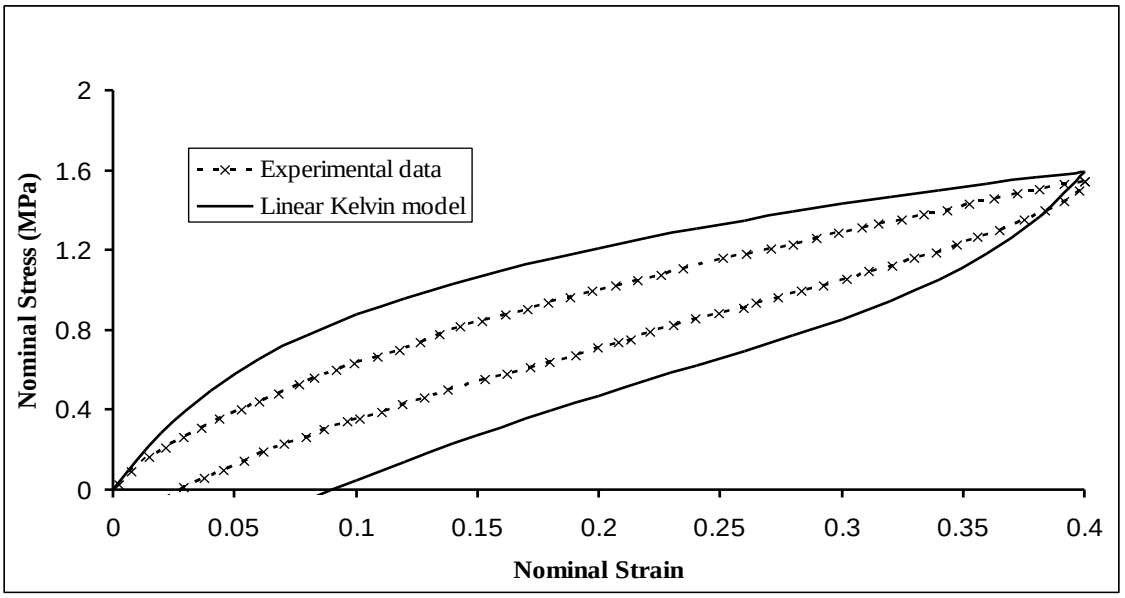

Fig.5.19. Comparison of linear Kelvin model prediction with experimental data at strain rate 0.0667 sec^{-1}

Fig.5.20, 5.21 shows the variation of elastic and inelastic strains in Kelvin model. The difference between Maxwell and Kelvin models is in unloading the elastic and inelastic strains are less then applied strains whereas in Maxwell model elastic strains are negative in tension and inelastic strains are greater than the applied strains (see fig.5.16). In unloading applied strain rate is negative, the strain rate in dash pot follows applied strain rate faithfully. Because of unloading negative strain rates exist in dashpot hysteresis loop don't have the sharp edges and bulging behaviour.

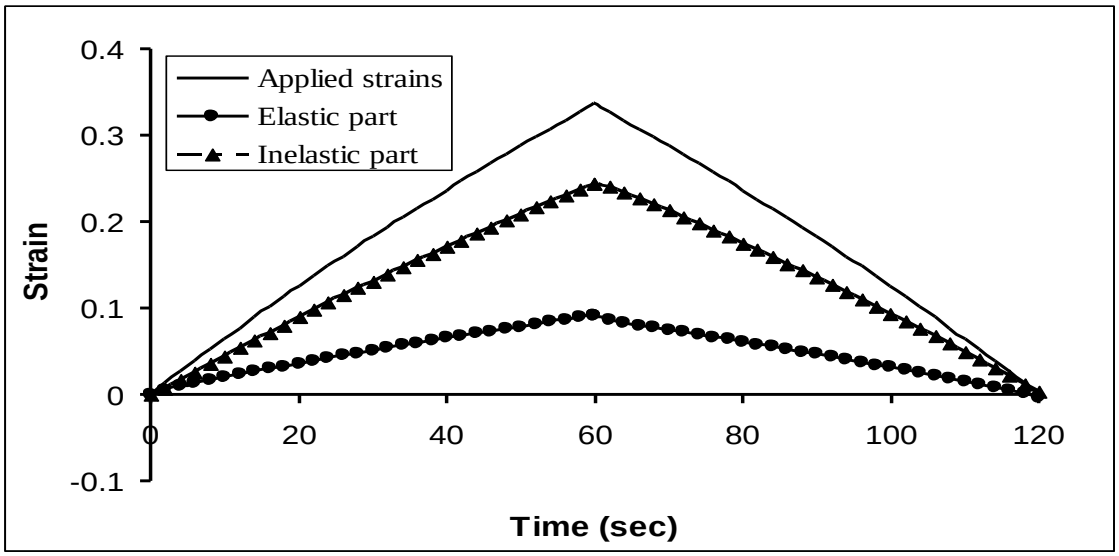

Fig.5.20. The variation in applied strain, elastic and inelastic strains linear Kelvin model at strain rate 0.00667 sec^{-1}

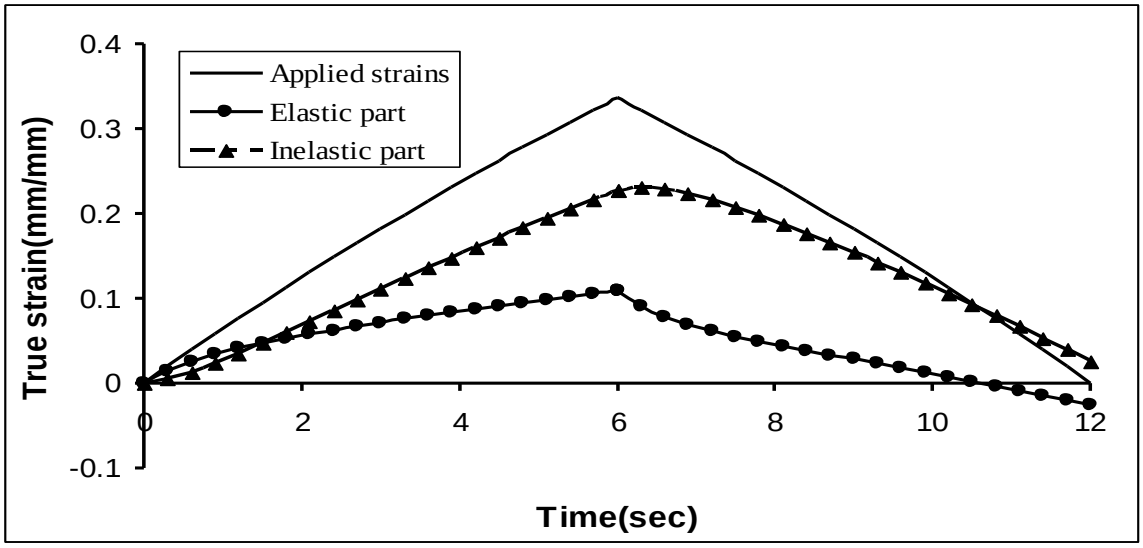

Fig.5.21. The variation in applied strain, elastic and inelastic strains linear Maxwell model at strain rate 0.0667 sec^{-1}

If the spring coefficients in Kelvin model are chosen such that K_2 spring stiffness is much grater than K_1 spring stiffness in that case the strain rate increases, strains in K_1 spring increase, accompanied by a drop in strain in the Kelvin element, in order to achieve the force equilibrium. Because of strain drop in the Kelvin element, the effect of k_2 spring drops with strain rate and in an overall sense the model behaves like the Maxwell model.

5.5. Finite strain nonlinear Kelvin model

Nonlinearity is introduced in the Kelvin model by assuming the viscosity coefficient (η) to be a function of strain and strain rate. Strain in the dashpot is represented using the inelastic part of right Cauchy deformation tensor, C_v and the strain rate is represented through the stress in the dashpot.

$$\eta_v = \eta_0 \exp\left(-\frac{\left\| \tau_e - \tau_v b_e^{-1} \right\|}{s_0 \left| C_v^{-1} \right|^3} \right) \tag{3.3}$$

Where η_0, S_0 are constants. Fig.5.22,5.23 and 5.24 shows the prediction of Kelvin model in loading and unloading with strain rates 0.000667, 0.00667, 0.0667 sec^{-1} when both the springs stiffness is equal.

It predicts the loading path well. It can be observed that the loading and unloading curves of the Kelvin model hysteresis loop expand equally on both sides of the quasistatic curve.

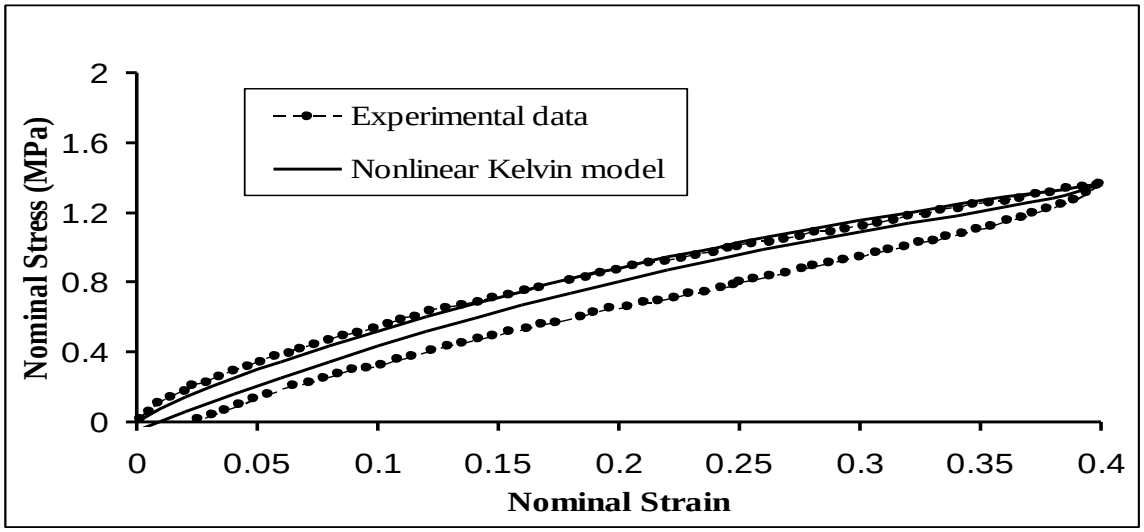

Fig.5.22. Comparison of nonlinear Kelvin model prediction with experimental data at strain rate 0.000667 sec^{-1}

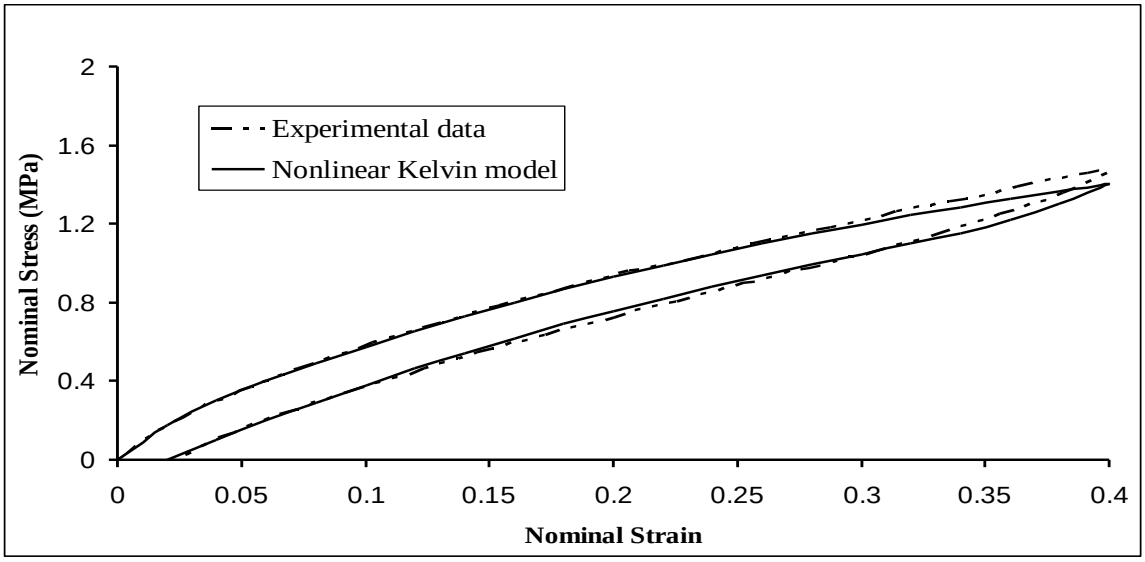

5.23. Comparison of nonlinear Kelvin model prediction with experimental data at strain rate 0.00667 sec^{-1}

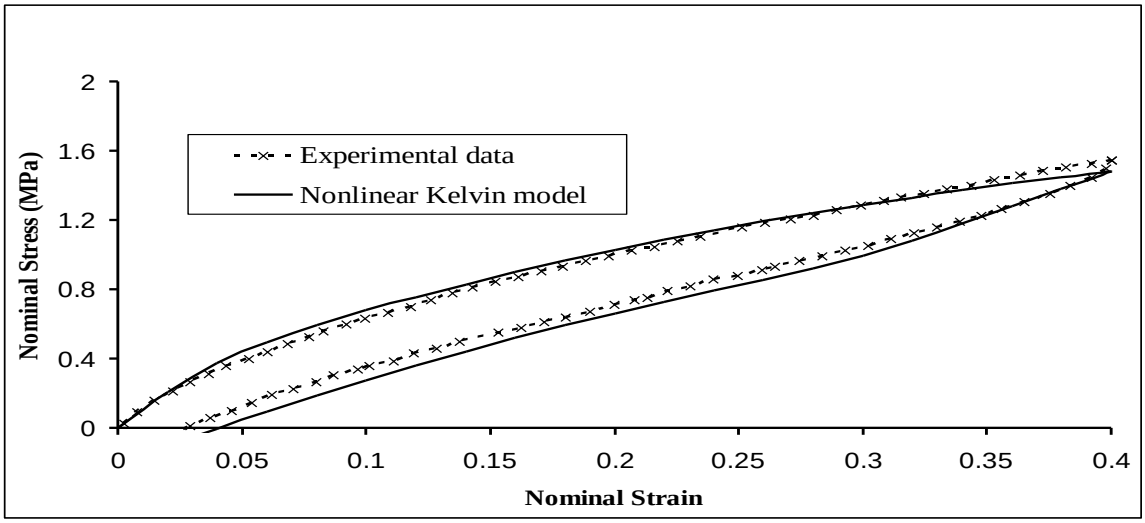

Fig.5.24. Comparison of nonlinear Kelvin model prediction with experimental data at strain rate 0.0667 sec^{-1}

Fig.5.25, 5.26 show the elastic and inelastic strain variations in Kelvin element at strain rates 0.00667, 0.0667 sec^{-1}. It can be observed that as the transition takes place from loading to unloading, dash pot takes time to reach a negative strain rate in the dashpot because of the negative strain rate in the dashpot, This results in sharp edges to be formed at the tip of the loading and unloading transition. Loop expansion about the quasistatic curve is not observed in the rubber test data. This model is also not suitable to predict the rubber unloading behaviour.

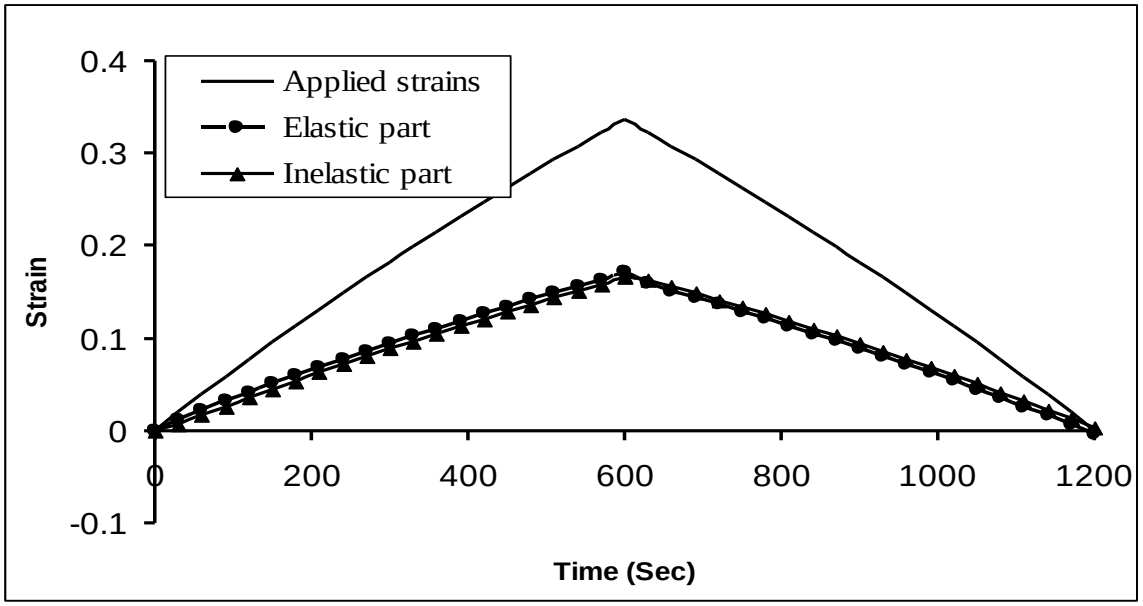

Fig.5.25. The variation in applied strain, elastic and inelastic strains nonlinear Kelvin model at strain rate 0.00667 sec^{-1}

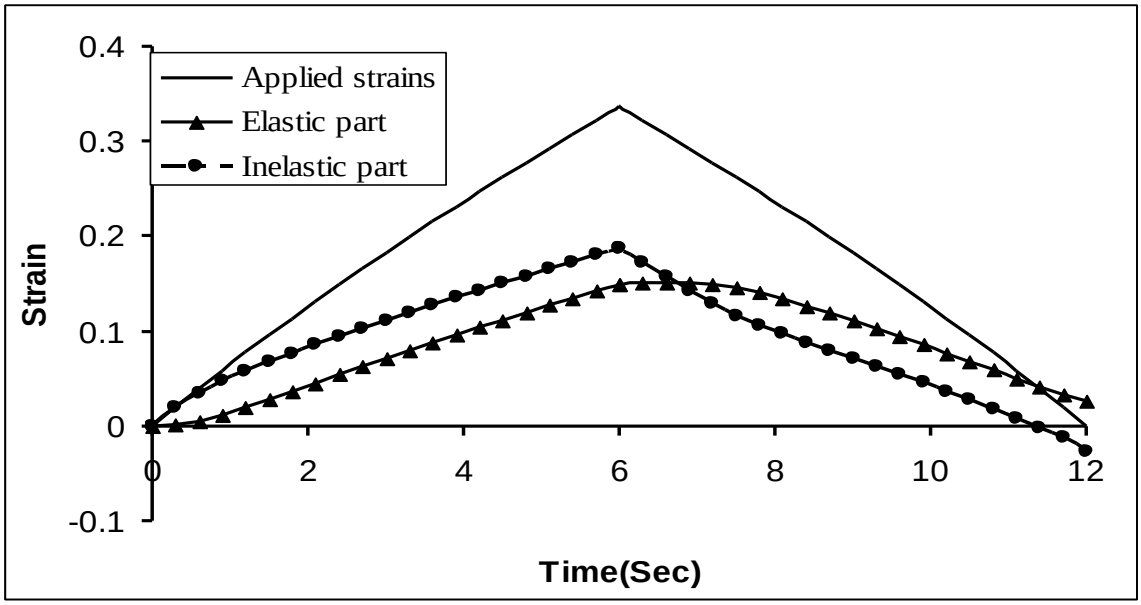

Fig.5.26. The variation in applied strain, elastic and inelastic strains nonlinear kelvin model at strain rate 0.0667 sec^{-1}

Table 3. Coefficients used in different models

model	coefficients
Finite stain linear Maxwell model	**C_1=0.054, α=0.5 ; C_{1m}=0.16; η_d=4**
Finite stain linear Maxwell model (large strains fig.1h)	**C_{10}=0.454, C_{20}=-0.048, C_{30}=0.004 ; C_{10m}=0.22, C_{20m}=-0.022, C_{30m}=0.0025 ; η_d=6**
Finite strain nonlinear Maxwell model	**C_1=0.054, α=0.5; C_{1m}=0.18 ; η_0=120, S_0=500**
Finite strain linear Kelvin model	**C_{1ke}=0.19, α=0.5 ; C_{1kv}=0.07 ; η_d=5**
Finite strain nonlinear Kelvin model	**C_{10ke}=0.105, α=0.5; C_{10kv}=0.105 ; η_0=100,S_0=2000**

5.6. Summary:

The finite strain linear Maxwell model is poor predicting the loading behaviour, and the nonlinear model gives a good prediction in loading behaviour. Both models are not able to capture the unloading behaviour. In the Maxwell model, hysteresis increases initially with strain rate and then decreases. The developed finite strain Kelvin model also predicts well the loading behaviour in the range of strain rates tested, the hysteresis increases with a Kelvin model.

Chapter 6

CONCLUSIONS

Experiments like uniaxial tension, uniaxial compression and quasistatic test conducted on rubber. Study illustrates Mullins effect and the importance of constitutive model for small strain. The popular hyperelastic models evaluated for small strains. A new hyperelastic model has been proposed to capture the tension and compression once. Proposed model implemented in finite element software ABAQUS.

Experimental data of rubber explain Rate dependent and rate independent hysteresis. Finite strain Maxwell model is implemented in ABAQUS to capture the loading and unloading behaviour of rubber. Inefficiency of Maxwell capturing the hysteresis and unloading behaviour, a new formulation has developed for kelvin model using internal variable concept. Finite element implementation of developed kelvin model has done in ABAQUS. Based on this work following conclusion are with drawn

1. The Stored energy function which is expressed in terms of the first invariant alone like NeoHookean, Arruda Boyce and Yeoh can fit compression data with a small error, using the uniaxial tension data. The tension behaviour cannot be predicted accurately from compression data.
2. The models which are function of first and second invariants like Mooney Rivlin and Vanderwaals require both tension and compression data.
3. To fit the Ogden model both uniaxial tension and compression required.
4. Proposed model can be predicted using either tension or compression data more accurately.
5. The finite strain linear Maxwell model is poor predicting the loading behaviour, and the nonlinear model gives a good prediction in loading behaviour. In the Maxwell model, hysteresis increases initially with strain rate and then decreases.

6. The developed finite strain Kelvin model also predicts well the loading behaviour in the range of strain rates tested, the hysteresis increases with a Kelvin model.
7. Both Maxwell and kelvin models are not able to capture the unloading behaviour rubber. Further research is required to develop model to fit the unloading behaviour accurately.

Appendix

Detailed derivation of elastic tensor for proposed stored energy function

Proposed Stored energy function

$$\psi = C_1 * \ln\left(\frac{\alpha \bar{I}_1^3 + (1-\alpha)\bar{I}_2^3}{3^3}\right) + \frac{1}{D}(J-1)^2 \tag{A.1}$$

Stored energy function can be additively decomposed into deviatoric part (ψ_{dev}) and volumetric part (ψ_{vol}) written as

$$\psi_{dev} = C_1 * \ln\left(\frac{\alpha \bar{I}_1^3 + (1-\alpha)\bar{I}_2^3}{3^3}\right) \tag{A.2}$$

$$\psi_{vol} = \frac{1}{D}(J-1)^2 \tag{A.3}$$

Let $\Upsilon = \alpha \bar{I}_1^3 + (1-\alpha)\bar{I}_2^3$ (A.4)

$$\lambda_i \frac{\partial \bar{I}_1}{\partial \lambda_i} = 2\left(\bar{\lambda}_i^2 - \frac{1}{3}\bar{I}_1\right) \tag{A.5}$$

$$\lambda_i \frac{\partial \bar{I}_2}{\partial \lambda_i} = 2\left(\bar{\lambda}_i^2\left(\bar{I}_1 - \bar{\lambda}_i^2\right) - \frac{2}{3}\bar{I}_2\right) \tag{A.6}$$

$$\frac{\partial \psi_{dev}}{\partial \bar{I}_1} = \frac{81 C_1 \alpha \bar{I}_1^2}{\Upsilon} \tag{A.7}$$

$$\frac{\partial \psi_{dev}}{\partial \bar{I}_2} = \frac{81 C_1 (1-\alpha)\bar{I}_2^2}{\Upsilon} \tag{A.8}$$

$$\frac{\partial^2 \psi_{dev}}{\partial \bar{I}_1^2} = 81 C_1\left(\frac{2\alpha \bar{I}_1}{\Upsilon} - \frac{3\alpha^2 \bar{I}_1^4}{\Upsilon^2}\right) \tag{A.9}$$

$$\frac{\partial^2 \psi_{dev}}{\partial \bar{I}_2^2} = 81 C_1 \left(\frac{2(1-\alpha)\bar{I}_2}{\Upsilon} - \frac{3(1-\alpha)^2 \bar{I}_2^4}{\Upsilon^2} \right) \tag{A.10}$$

$$\frac{\partial^2 \psi_{dev}}{\partial \bar{I}_1 \partial \bar{I}_2} = 81 C_1 \alpha (1-\alpha) \left(-\frac{3\bar{I}_1^2 \bar{I}_2^2}{\Upsilon^2} \right) \tag{A.11}$$

Deviatoric part of cauchy stress (σ^{dev})

$$\sigma_i^{dev} = \lambda_i \frac{\partial \psi_{dev}}{\partial \lambda_i} = \frac{\partial \psi_{dev}}{\partial \bar{I}_1} \left(\lambda_i \frac{\partial \bar{I}_1}{\partial \lambda_i} \right) + \frac{\partial \psi_{dev}}{\partial \bar{I}_2} \left(\lambda_i \frac{\partial \bar{I}_2}{\partial \lambda_i} \right) \tag{A.12}$$

Volumetric part of cauchy stress (σ^{vol})

$$\sigma_i^{vol} = \lambda_i \frac{\partial \psi_{vol}}{\partial J} \frac{\partial J}{\partial \lambda_i} = \frac{2}{D}(J-1)J \tag{A.13}$$

Total stress (σ)

$$\sigma_i = \sigma_i^{dev} + \sigma_i^{vol} \tag{A.14}$$

$$\begin{aligned} \frac{\partial \sigma_i^{dev}}{\partial \bar{I}_1} = {} & \frac{\partial^2 \psi_{dev}}{\partial \bar{I}_1^2} \left(\lambda_i \frac{\partial \bar{I}_1}{\partial \lambda_i} \right) + \frac{\partial \psi_{dev}}{\partial \bar{I}_1} \frac{\partial}{\partial \bar{I}_1} \left(\lambda_i \frac{\partial \bar{I}_1}{\partial \lambda_i} \right) \\ & + \frac{\partial^2 \psi_{dev}}{\partial \bar{I}_1 \partial \bar{I}_2} \left(\lambda_i \frac{\partial \bar{I}_2}{\partial \lambda_i} \right) + \frac{\partial \psi_{dev}}{\partial \bar{I}_2} \frac{\partial}{\partial \bar{I}_1} \left(\lambda_i \frac{\partial \bar{I}_2}{\partial \lambda_i} \right) \end{aligned} \tag{A.15}$$

$$\frac{\partial \sigma_i^{dev}}{\partial \bar{I}_1} = \begin{bmatrix} \left(\frac{2\alpha \bar{I}_1^1}{\Upsilon} - \frac{3\alpha^2 \bar{I}_1^4}{\Upsilon^2} \right) 2 \left(\bar{\lambda}_i^2 - \frac{1}{3} \bar{I}_1 \right) - \frac{2}{3} \frac{\alpha \bar{I}_1^2}{\Upsilon} + \frac{(1-\alpha)\bar{I}_2^2}{\Upsilon} 2\bar{\lambda}_i^2 \\ - \frac{3\alpha(1-\alpha)\bar{I}_2^2 \bar{I}_1^2}{\Upsilon^2} 2 \left(\bar{\lambda}_i^2 \left(\bar{I}_1 - \bar{\lambda}_i^2 \right) - \frac{2}{3} \bar{I}_2 \right) \end{bmatrix} \tag{A.16}$$

$$\frac{\partial \sigma_i^{dev}}{\partial \bar{I}_2} = \frac{\partial^2 \psi_{dev}}{\partial \bar{I}_1 \partial \bar{I}_2}\left(\lambda_i \frac{\partial \bar{I}_1}{\partial \lambda_i}\right) + \frac{\partial \psi_{dev}}{\partial \bar{I}_1}\frac{\partial}{\partial \bar{I}_2}\left(\lambda_i \frac{\partial \bar{I}_1}{\partial \lambda_i}\right) + \frac{\partial \psi_{dev}}{\partial \bar{I}_2}\frac{\partial}{\partial \bar{I}_2}\left(\lambda_i \frac{\partial \bar{I}_2}{\partial \lambda_i}\right) + \frac{\partial^2 \psi_{dev}}{\partial \bar{I}_2^2}\left(\lambda_i \frac{\partial \bar{I}_2}{\partial \lambda_i}\right) \quad \text{(A.17)}$$

$$\frac{\partial \sigma_i^{dev}}{\partial \bar{I}_2} = \left[-\frac{3\alpha(1-\alpha)\bar{I}_1^2 \bar{I}_2^2}{\Upsilon^2} 2\left(\bar{\lambda}_i^2 - \frac{1}{3}\bar{I}_1\right) - \frac{2}{3}\frac{(1-\alpha)\bar{I}_2^2}{\Upsilon} + \left(\frac{2(1-\alpha)\bar{I}_2^1}{\Upsilon} - \frac{3(1-\alpha)^2 \bar{I}_2^4}{\Upsilon^2}\right) 2\left(\bar{\lambda}_i^2\left(\bar{I}_1 - \bar{\lambda}_i^2\right) - \frac{2}{3}\bar{I}_2\right) \right] \quad \text{(A.18)}$$

Deviatoric part of elastic tensor ($\square^{dev}$)

$$\square_{ij}^{dev} = \frac{\partial \sigma_i^{dev}}{\partial \bar{I}_1}\left(\lambda_j \frac{\partial \bar{I}_1}{\partial \lambda_j}\right) + \frac{\partial \sigma_i^{dev}}{\partial \bar{I}_2}\left(\lambda_j \frac{\partial \bar{I}_2}{\partial \lambda_j}\right) + \frac{81 C_1 \alpha \bar{I}_1^2}{\Upsilon} 4\left(\bar{\lambda}_i \bar{\lambda}_j \delta_{ij} - \frac{1}{3}\bar{\lambda}_i^2\right) + \frac{81 C_1 \alpha \bar{I}_2^2}{\Upsilon} 4\left[\bar{\lambda}_i \bar{\lambda}_j \left(\bar{I}_1 - 2\bar{\lambda}_i^2\right)\delta_{ij} - \frac{2}{3}\bar{\lambda}_i^2\left(\bar{I}_1 - \bar{\lambda}_i^2\right)\right] \quad \text{(A.19)}$$

Volumetric part of elastic tensor ($\square^{vol}$)

$$\square_{ij}^{vol} = \lambda_j \frac{\partial \sigma_i^{vol}}{\partial \lambda_j} = \frac{2}{D}\left(2J - 1\right)J \quad \text{(A.20)}$$

Elastic tensor ($\square$)

$$\square_{ij} = \square_{ij}^{dev} + \square_{ij}^{vol} \quad \text{(A.21)}$$

REFERENCES

1. **ABAUQS,** *ABAQUS Version 6.5 Documentation*. ABQUS INC., Providence, RI, 2005.

2. **Arruda, E. M. and M. C. Boyce** (1993), A three-dimensional constitutive model for the large stretch behavior of rubber elastic materials. *Journal of the mechanics and physics of solids,* **41**, 389-412.

3. **Ball, J.M (1977),** Convexity conditions and existence theorems in nonlinear elasticity. Arch. Rational Mech. Anal, 63, 337-155.

4. **Boyce, M.C., and E.M. Arruda** (2000), Constitutive models of rubber elasticity: a review. *rubber chem. technol.* , **73**, 504-523.

5. **Bergstrom, J.S. and M. C. Boyce** (1998), Constitutive modeling of the large strain time dependent behavior of elastomers. *Journal of the mechanics and physics of solids,* **46**, 931-954.

6. **Bergstrom, J.S**., Constitutive Modeling of Elastomers – Accuracy of Predictions and Numerical Efficiency , *polymerFEM.com*

7. **Bonet, J.** (2001), Large strain viscoelastic constitutive models, *International journal of solids and structures.* **38**, 2953-2968.

8. **Coleman, B.D., and M. E. Gurtin** (1967), Thermodynamics with internal state variables. *The journal of chemical physics*, **47**, 597-613.

9. **Dalrymple, T., Jaehwan Choi and Kurt Miller** (2007), Elastomer rate- dependence: a testing and material modeling methodology, Axel Products,inc.

10. **Drozdov,A.D** (1997), Fractional differential models in finite viscoelasticity. *Acta Mechanica*, 124, 155-180.

11. **Drozdov,A.D**, *Finite elasticity and viscoelasticity : a course in nonlinear mechanics of solids.* World Scientific Publishing Co.Pte.Ltd. Singapore,1996.

12. **Hartmann, S. and P.Neff** (2003), Polyconvexity of generalized polynomial-type hyperelastic strain energy functions for near-incompressibility. *International Journal of Solids and Structures*, 40, 2767-2791.

13. **Haupt, P**, *Continuum Mechanics and Theory of Materials*, Springer-Verlag Berlin Heidelberg New York, 2000.

14. **Haupt, P. and A. Lion** (2002), On finite linear viscoelasticity of incompressible isotropic materials. *Acta mechanica*, **159**, 87-124.

15. **Haupt, P. and K. Sedlan** (2001), Viscoplasticity of elastomeric materials: experimental facts and constitutive modeling. *Archive of applied mechanics*, **71**, 89-109.

16. **Holzapfel G.A.** *Nonlinear Solid Mechanics*. John wiley & sons, Ltd., 2000.

17. **Holzapfel G.A.** (1996), On large strain vicoelasticity: continuum formulation and finite element applications to elastomeric structures. *International journal of numerical methods in engineering,* **39**, 3903-3926.

18. **Holzpfel, G. A. and J. C. Simo** (1996), A new viscoelastic constitutive model for continuous media at finite thermomechanical changes. *International journal of solids and structures,* **33**, 3019-3034.

19. **Kaliske, M. and H.Rothert** (1997), On the finite element implementation of rubber-like materials at finite strains, *Engineering Computations*, Vol. 14 No. 2, 216-232.

20. **Kaliske, M.** (2000), A formulation of elasticity and viscoelasticity for fibre reinforced material at small and finite strains. *Computer methods in applied mechanics and engineering,* **85**, 225-243.

21. Kilian, H.G., (1981), Equation of state of real networks, *Polymer*, 22, 209-17.

22. **Kurt Miller** (2000), Testing Elastomers for Hyperelastic Material Models in Finite Element Analysis, rept. Axel Products, Inc. testing for hyperelastic.

23. **Lee, E.H.** (1969), Elastic-plastic deformation at finite strain. *Journal of applied mechanics*, **36**, 1-6.

24. **Le Tallec, P., A. Kaiss, and C. Rahier** (1993), Three dimensional incompressible viscoelasticity in large strains: Formulation and numerical approximation. *Computer methods in applied mechanics and engineering*, **109**, 233-258.

25. **Lin, R.C. and U. Schomburg** (2003), A finite elastic-viscoelastic-elastoplastic material law with damage: theoretical and numerical aspects. *Computer methods in applied mechanics and engineering*, **192**, 1591-1627.

26. **Lion, A.** (1996), A constitutive model for carbon black filled rubber: Experimental investigations and mathematical representation. C*ontinuum mechanics and thermodynamics*, **l8**, 153-169.

27. **Lion, A.** (1997), A physically based method to represent the thermo-mechanical behaviour of elastomers. *Acta mechanica*, **123**, 1-25.

28. **Lubliner, J.** (1985), A model of rubber viscoelasticity. *Mechanics research communications*, **12**, 93-99.

29. **Morrey,C.**B.Jr (1952), Quasiconvexity and lower semicontinuity of multiple integrals, *Pacific J. Math*, 2, 25-53.

30. **Mullins,L and Tobin,N.R** (1957),Theoretical model for the elastic behaviour of filler reinforced vulcanized rubber. *Rubber Chem. Techol*, 30, 555-571.

31. **Nedjar, B.** (2002a), Frameworks for finite strain viscoelastic-plasticity based on multiplicative decompositions part I: Continuum formulations. C*omputer methods in applied mechanics and engineering*, **l91**, 1541-1562.

32. **Nedjar, B.** (2002b), Frameworks for finite strain viscoelastic-plasticity based on multiplicative decompositions part II: Computational aspects. C*omputer methods in applied mechanics and engineering*, **l91**, 1541-1562.

33. **Ogden, R. W.** (1972), Large deformation isotropic elasticity-On the correlation of theory and experiment for incompressible rubberlike solids. *Proceedings of royal society of London, series A, Mathematical and physical sciences*, **326**, 565-584.

34. Ogden ,R. W. and D. G. Roxburgh (1999), A Pseudo-Elastic Model for the Mullins Effect in Filled Rubber. *Proc. R. Soc. Lond. A*, 455, 2861-2877.

35. Qi, H. J. and M. C.Boyce (2004), Constitutive Model for Stretch-Induced Softening of the Stress-Strain Behavior of Elastomeric Materials. *J. Mech. Physics Solids*, 52, 2187-2205.

36. **Reese, S. and P. Wriggers** (1997), a material model for rubber-like polymers exhibiting plastic deformation: Computational aspects and a comparison with experimental results. C*omputer methods in applied mechanics and engineering*, **l48**, 279-298.

37. **Reese, S. and S. Govindjee** (1998a), A theory of finite viscoelasticity and numerical aspects. *International journal of solids and structures*, **35**, 3455-3482.

38. **Reese, S. and S. Govindjee** (1998b), Theoritical and numerical aspects in the thermo-viscoelastic material behaviour of rubber-like polymers. *Mechanics of time-dependent materials*, **1**, 357-396.

39. **Simo, J.C.** (1992), Algorithms for static and dynamic multiplicative plasticity that preserve the classical return mapping schemes of infinitesimal theory. C*omputer methods in applied mechanics and engineering*, **l99**, 61-112.

40. **Treloar, L.R.G.** *ThePphysics of Rubber Elasticity*. Third Edition, Clarendon press. Oxford, 1975.

41. **Valanis, K.C**. (1980) Fundamental consequences of a new intrinsic time measure plasticity as a limit of the endochronic theory. *Archives of mechanics,* **32**, 171-191.

42. **Yeoh, O. H.** (1993), some forms of strain energy function for rubber. *Rubber chemistry and technology,* **66**, 754-771.

LIST OF PUBLICATIONS BASED ON THE RESEARCH WORK

1. **Maboo Subhani, P. and R.Krishna Kumar,** A new stored energy function for rubber like materials for small strains, *Mechanics of Advanced Materials and Structures* (accepted for publication).

2. **Maboo Subhani, P. and R.Krishna Kumar,** A study of finite strain viscoelastic models for filled rubbers (To be communicated)